AD-A198 077

ADVANCED MODELING FOR FATIGUE GROWTH OF SMALL SURFACE CRACKS

Prepared By

T. A. Cruse
S. T. Raveendra

FINAL REPORT
AFOSR Contract F49620-86-C-0048
SwRI Project No. 06-1069

Prepared For
Air Force Office of Scientific Research
Washington, DC 20332

May 31, 1988

SOUTHWEST RESEARCH INSTITUTE
SAN ANTONIO   HOUSTON

ADA198077

REPORT DOCUMENTATION PAGE

1a. REPORT SECURITY CLASSIFICATION UNCLASSIFIED	1b. RESTRICTIVE MARKINGS
2a. SECURITY CLASSIFICATION AUTHORITY	3. DISTRIBUTION / AVAILABILITY OF REPORT Unlimited Distribution
2b. DECLASSIFICATION / DOWNGRADING SCHEDULE	
4. PERFORMING ORGANIZATION REPORT NUMBER(S) 06-1069	5. MONITORING ORGANIZATION REPORT NUMBER(S) AFOSR-TR- 88- 0 8 0 3

6a. NAME OF PERFORMING ORGANIZATION Southwest Research Inst.	6b. OFFICE SYMBOL (If applicable)	7a. NAME OF MONITORING ORGANIZATION Air Force Office of Scientific Research
6c. ADDRESS (City, State, and ZIP Code) PO Drawer 28510 San Antonio, TX 78284		7b. ADDRESS (City, State, and ZIP Code) same as 8C.

8a. NAME OF FUNDING / SPONSORING ORGANIZATION AFOSR	8b. OFFICE SYMBOL (If applicable) NA	9. PROCUREMENT INSTRUMENT IDENTIFICATION NUMBER F49620- 86- C- 0048
8c. ADDRESS (City, State, and ZIP Code) AFOSR/NA Bldg 410 Bolling AFB, DC 20332-6448		10 SOURCE OF FUNDING NUMBERS

PROGRAM ELEMENT NO. 61102F	PROJECT NO. 2302	TASK NO. B2	WORK UNIT ACCESSION NO.

11. TITLE (Include Security Classification)
"Advanced Modeling of Fatigue Growth of Small Surface Cracks" (U)

12. PERSONAL AUTHOR(S)
T.A. Cruse and S.T. Raveendra

13a. TYPE OF REPORT FINAL	13b. TIME COVERED FROM 01Apr86 TO 31Mar88	14. DATE OF REPORT (Year, Month, Day) 1988, May 31	15. PAGE COUNT 107

16. SUPPLEMENTARY NOTATION

17 COSATI CODES			18. SUBJECT TERMS (Continue on reverse if necessary and identify by block number)
FIELD	GROUP	SUB-GROUP	Fracture mechanics, fatigue crack growth, crack retardation, crack closure, crack opening displacement, boundary element method. (Jt3)

19. ABSTRACT (Continue on reverse if necessary and identify by block number)

The primary result of the sponsored research is the development and application of the boundary element method for two- and three-dimensional fatigue crack growth analysis. The two-dimensional formulation developed previously (AFOSR Contract No. F49620-84-C-0042) was extended to investigate the crack tip behavior of long and short cracks under cyclic loading. The influence of residual plasticity on stress intensity factor was used to obtain an unambiguous estimate of the plastic zone size. It was demonstrated that the effect of the plastic wake on the stress intensity factor for crack opening (closure) and the effect of the residual stress on the retardation are identical manifestations of the same plasticity process. The boundary integral equations also provide insight to the mathematical equivalence of these two effects. Key words.

The correlating role of crack closure in predicting crack propagation was studied extensively and the results indicate that while crack closure suggests excess crack tip plastic damage, it is the amount of plasticity with loss of constraint that leads to the breakdown of linear

20. DISTRIBUTION / AVAILABILITY OF ABSTRACT ☑ UNCLASSIFIED/UNLIMITED ☑ SAME AS RPT. ☐ DTIC USERS	21. ABSTRACT SECURITY CLASSIFICATION UNCLASSIFIED
22a. NAME OF RESPONSIBLE INDIVIDUAL LTC George K. Haritos	22b. TELEPHONE (Include Area Code) (202) 767 0463	22c. OFFICE SYMBOL NA

DD FORM 1473, 84 MAR
83 APR edition may be used until exhausted.
All other editions are obsolete.

SECURITY CLASSIFICATION OF THIS PAGE
UNCLASSIFIED

88 8 25 133

19.   (Continued)

elastic fracture mechanics for short cracks.

It was demonstrated that the elastoplastic boundary element procedure can be applied for the investigation of crack propagation in three-dimensional bodies, however, the numerical computation is rather cumbersome and requires further refinement in the procedure.

Accession For		
NTIS CRA&I	✓	
DTIC TAB	☐	
Unannounced	☐	
Justification		
By		
Distribution/		
Availability Codes		
Dist	Avail and/or Special	
A-1		

TABLE OF CONTENTS

ii

iii

LIST OF FIGURES
(Cont'd)

1.0 OVERVIEW

1.1 Introduction

The goal of the current research effort is to develop a boundary element method (BEM) analysis to study the effect of plasticity on the growth rate of fatigue cracks. The investigation mainly focuses on the crack tip behavior of two- and three-dimensional crack propagation and closure effects under cyclic loading for cracks where the plastic zone size is large relative to the crack size. This problem, known as small crack or small flaw problem, stems from the rapid growth of small surface cracks, hence, the deviation from linear elastic fracture mechanics (LEFM) predictions.

The United States Air Force has recognized the importance of the small flaw modeling problem and is currently funding an experimental study of turbine engine materials at SwRI. The analytical study reported here supplements this effort to provide a most complete utility of the work for the Air Force.

Because of many unresolved issues related to the two-dimensional analysis, a major portion of the current study is focused on two-dimensional modeling issues. A significant issue in the study of fatigue crack growth is the realization of crack closure phenomenon, first proposed by Elber [1,2], where the residual plastic stretch left in the wake of an advancing crack causes the crack surfaces to close during some portion of loading cycle. He proposed that crack growth is effected by the portion of loading cycle over which the crack remains open. This concept has been widely advocated in explaining the behavior of short crack acceleration phenomenon. The two-dimensional results, however, indicate that large amount of plasticity with loss of constraint rather than residual or crack closure effects, leads to the breakdown in LEFM conditions near the crack tip. The short crack effects grow with increasing ratios of applied stress to yield stress, and for decreasing crack tip constraint.

The growth of the surface or through crack is three-dimensional, where the region near the free surface is governed by plane stress conditions, and at the interior, the behavior is governed by plane strain conditions. The small flaw acceleration problem may be due to the influence of three-dimensional surface flaw plasticity effects, an influence that is not modeled by two-dimensional approaches. However, the task of modeling the three-dimensional propagating crack is substantial. The only numerical study reported to date is the limited investigation of Chermahini [3] using the finite element method. Unlike the two-dimensional boundary element modeling, where the presence of the crack is taken care of by a fundamental solution and, therefore, does not require the modeling of crack, the three-dimensional modeling requires modeling of the crack surface. The elastic problems solved by using the BEM as reported here substantiates the advantage of the method for this class of problems. However, the need to have small plastic cells to model the yielded region near the surface in an elastoplastic crack problem imposes a very high numerical constraint. While this limitation has been overcome to a certain extent in this study, a complete investigation requires further research effort. Some numerical results of the three-dimensional elastoplastic propagating crack are presented at the end of this report.

2.0 TWO-DIMENSIONAL ELASTOPLASTIC FRACTURE MECHANICS MODELING

2.1 Problem Statement

Figure 1 illustrates the correlating role of the elastic stress intensity factor (K) for fatigue crack growth problems. Three different fatigue specimens (A, B, C) were used to obtain baseline crack growth data: a standard ASTM modified compact tension specimen, plus two center-cracked specimens of different crack sizes and thicknesses. Two sets of surface crack growth data, taken from replicas of the surface cracks on a full-size component, are plotted in Figure 1 for smooth sections (D) and for notches (E).

The fact that the data are correlated for a wide range of crack size, crack shape and local stress field confirms the usual applicability of linear elastic fracture mechanics (LEFM) for many problems. Other data, e.g., [4-7] clearly indicate that the elastic stress intensity factor from LEFM does not correlate all crack data for problems with high applied stress, relative to the material yield stress. The crack sizes for these data are quite small compared to the crack sizes used for laboratory characterization of crack growth.

Thus, there is a clear indication from the experimental data, that LEFM may apply over a wide range of geometric conditions but not over all geometries. A recent review by Leis, et al. [4] attributes the so-called small flaw modeling problem to a lack of crack tip similitude. Stated somewhat more broadly, the damage process in the critically stressed (or strained) volume of material ahead of the crack is no longer independent of scaling below a certain size, which will be seen to depend on the applied stress level. Those who argue for the loss of similitude as the reason for the loss of correlation in the small flaw regime must seek a new measure of damage within the critical material volume, a measure that reduces to LEFM for the appropriate class of conditions.

$$da/dN = 2.11 \times 10^{-8}(K_{max} - 6)^{2.00}$$

LEGEND

- ○ Specimen A
- □ Specimen B
- ◇ Specimen C
- ◮ Component Location D
- △ Component Location E

Crack Growth Rate da/dN (inches/cycle)

10^{-4}

10^{-5}

10^{-6}

10^{-7}

5   10   100

Stress Intensity Factor K_{max} (ksi$\sqrt{\text{in}}$)
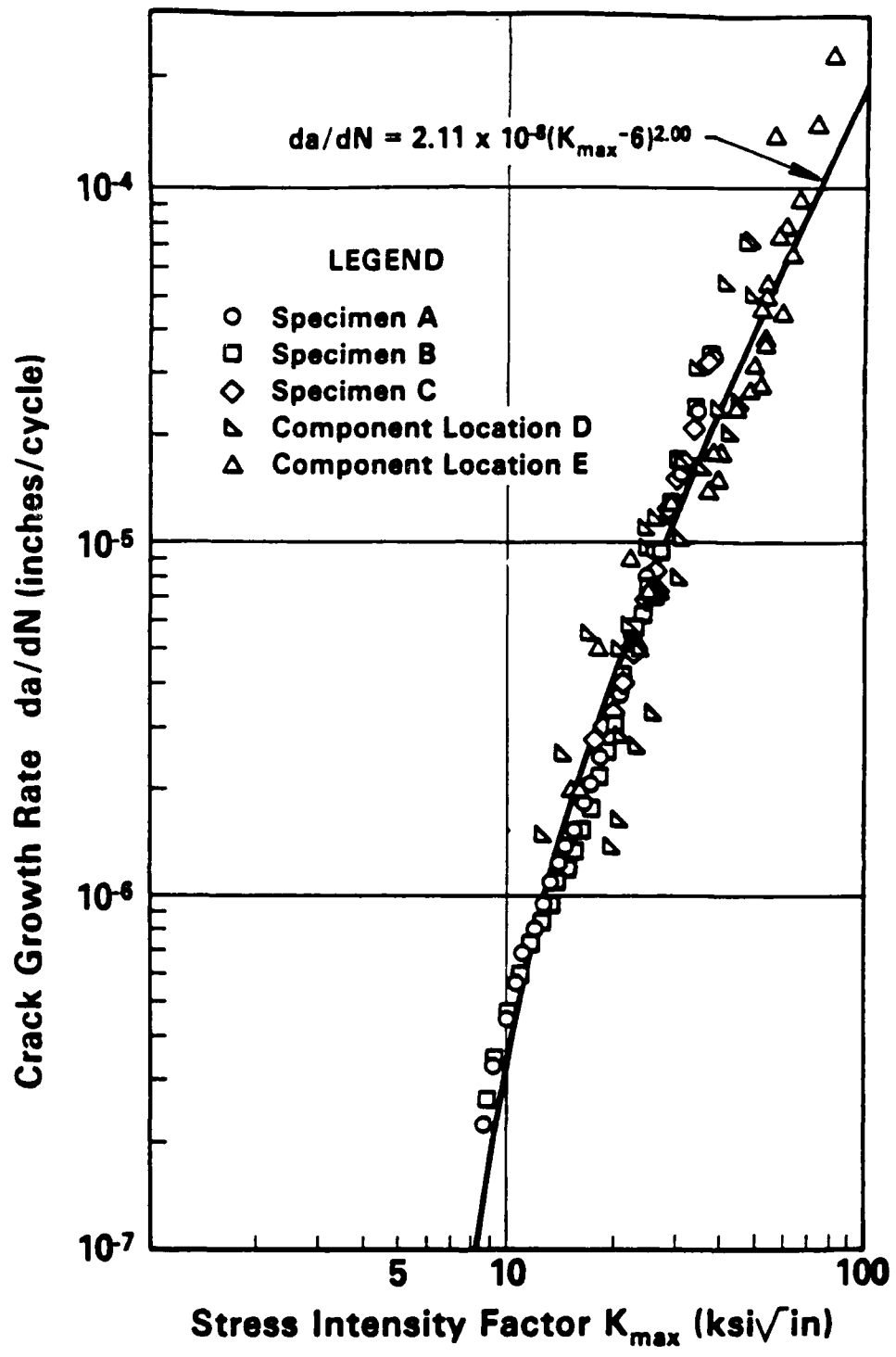
Figure 1. Crack Growth Rate Data for Surface Cracked
Components Compared to Baseline Data

2.1.1 Closure vs. Retardation

The presence of a plastic zone ahead of all fatigue cracks is generally ignored except for problems of overload and load ratio (R) effects. Baseline fatigue crack growth (FCG) data is usually generated at low load ratios (R = 0.1); this data intrinsically contains any effects of the plastic zone. Generally, for LEFM applicability, the strain field surrounding the plastic zone is controlled by the elastic strain field, and is not a separable influence.

The plastic zone becomes dominant for fatigue crack growth problems where load history effects are important [8]. An overload is sometimes seen as a modification of the residual stresses due to plasticity ahead of the crack which changes the cyclic stress intensity factor range, or a change in the range of loading for which the crack tip is closed (no fatigue damage) [9-11]. The actual solutions reported herein will demonstrate the complete duality of the residual stress and crack closure arguments.

The plastic zone, which remains along the crack surfaces after the crack tip advances, is referred to as the plastic wake. Under cyclic conditions, the tensile stretch of the material ahead of the crack tip exceeds the amount of reversed plastic strain as the load is released. The excess of plastic strain acts as an interference at the original crack plane, resulting in crack surface closure, even at positive loading. If there is an additional effect on the crack surface of interference due to mechanical locking of irregular crack surfaces, or due to significant oxidation, then the crack tip may be wedged open under zero load.

The actual fatigue process in the near crack tip region is, of course, quite complex. Cyclic plasticity may be distributed (wavy slip) or may be concentrated (planar slip). The structure of the material may play a key role in the crack growth kinetics through grain size or grain boundary resistance to crack extension. The conditions at the crack tip vicinity in regard to these phenomena may include cyclic strain and mean stress effects.

Thus, an understanding of the kinematics of the deformation and the state of stress are likely to be es.ential to an understanding of the large crack versus short crack growth rate data.

2.2 Crack Tip Singular Fields

2.2.1 Review of BIE for Elastoplastic Cracks

The elastoplastic boundary-integral equation (BIE) method is used for the current study. The formulation of the BIE uses the elastic Green's function to represent a planar body with a straight line, stress free crack [12]. The plasticity is a classical von Mises plasticity formulation, as recently reported [13,14]. The resulting elastoplastic BIE formulation for the fracture mechanics problem has yielded some new and important insight into the physical problem and will be briefly reviewed.

Figure 2 shows a finite plate with a central or edge crack which is taken to be stress free. The plastic strains are assumed to be contained within the discrete element region around the end of the crack; the elastoplastic strains are taken to be piecewise constant within each of the domain elements. Using the fundamental solution for a point load in an infinite elastic plate containing a single straight crack of length 2a, the Somigliana identity for the interior strain increment $\dot{\epsilon}_{ij}$ for the elastoplastic problem is given from [13]:

$$\dot{\epsilon}_{ij} = \int_S D_{ijk}\dot{u}_k dS + \int_S S_{ijk}\dot{t}_k dS + \int_{<A>} G_{iklj}\dot{\epsilon}^P_{kl} dA + E_{iklj}\dot{\epsilon}^P_{kl} \quad (1)$$

In Eq. (1), D_{ijk} and S_{ijk} are the symmetric parts of the gradients of the boundary tractions (on the uncracked surface S) and boundary displacements due to a unit load at an arbitrary interior point. The tensor G_{iklj} are generally the symmetric part of the gradient of the interior stress tensor due to the elastic load.* This tensor kernel is highly singular and has been

---

* This is true for three-dimensional elastoplasticity and for the plane stress kernel. The plane strain kernel is of a different form [13].

L = 1000 in
a = 10 in (long crack)
  = 0.1 in (short crack)
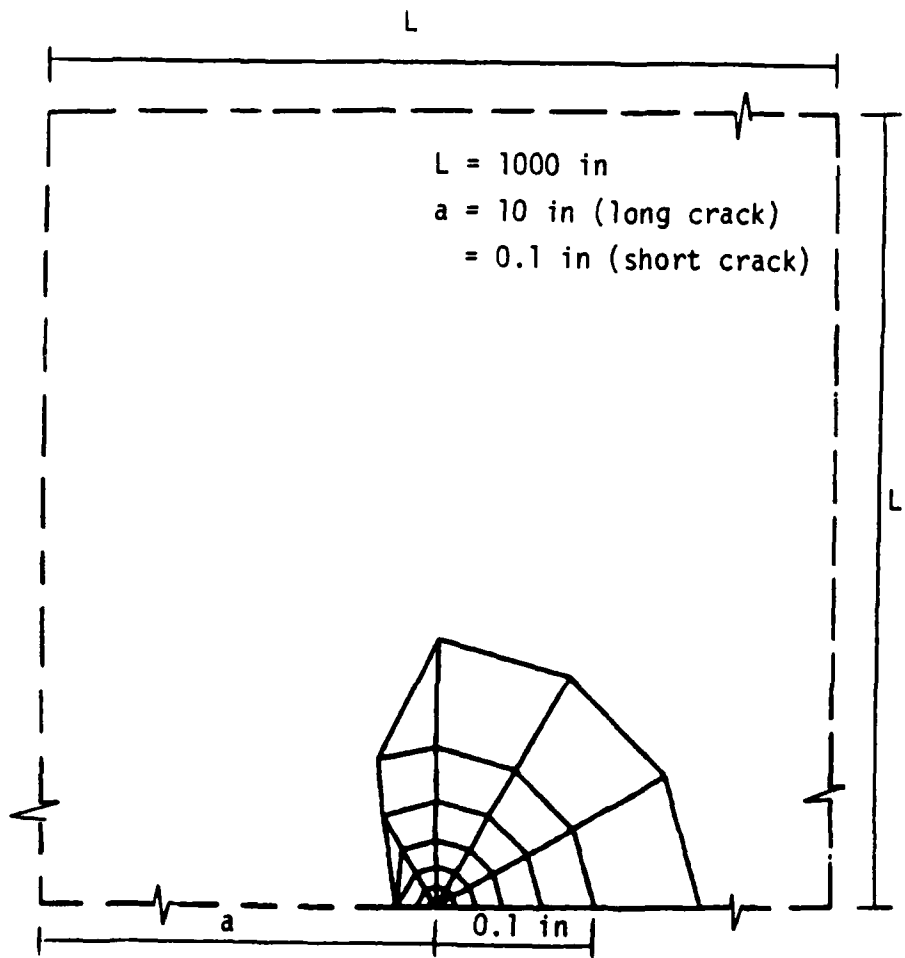
Figure 2. Domain Discretization for
Long and Short Cracks--Stationary Crack

differentiated at the singular point boundary which is excluded from the integral in a principal value sense. As a result of the differentiation at the boundary of the exclusion region surrounding the singularity, one obtains E_{iklj}, an elastic constant tensor which differs for plane strain and plane stress. The boundary data is given as the increment in boundary traction $\dot{t}_k$ and boundary displacement $\dot{u}_j$; the increment in plastic strains (inside plastic domain A) is given by $\dot{\epsilon}_{kl}{}^P$.

Equation (1) should be seen as the complete statement regarding the elastoplastic field problem. That is, the total strain field is mathematically complete. The stresses obtained from (1) can be shown to fully satisfy equilibrium at all interior points. The requirement on the plastic strain increments is only that they be no more singular than a 1/R singularity, where R is the distance from the crack tip, (true for perfect plasticity at crack tips), as discussed in [13]. The plastic strains are allowed to be discontinuous and permit a slip line interpretation for fully developed plasticity problems.

2.2.2 Strain Intensity Factor

The total strain field in Eq. (1) contains both explicit and implicit singular behavior near the crack tip. The details of the singular behavior are discussed in detail in [13] and are now briefly outlined. The boundary terms in Eq. (1) explicitly depend on the inverse of the square-root of the crack tip distance near the crack tip. The influence of plastic strain is discussed in [11,12] for both singular and non-singular plastic strains.

When the plastic strains are non-singular, then the total strain contribution from the integral in Eq. (1) is also inversely proportional to the square-root of the crack tip distance. For such problems the total strain

contains the same singular behavior as for the LEFM problem. A stress
intensity factor result, based on the strain singularity is given from [10]
as:

$$K_{I,II} = \int_S R_i u_i dS + \int_S L_i t_i dS + \int_A M_{ij} \epsilon_{ij}^P dA \qquad (2)$$

In Eq. (2) the mixed mode (Mode I and Mode II) stress intensity factors are
given as simple vector products of the boundary data with the boundary vector
potentials, R_i and L_i, and the inner product of the total plastic strains with
the volume potential tensor M_{ij}, taken over the domain of plastic strains.

For the case of singular plastic strains, Eq. (1) reduces to a
homogeneous integral equation containing only the plastic singularity. The
order of the singularity is shown in [10] to be implicitly determined, based
on the numerical results for the strain hardening characteristic of the
material. The limit on the order of the singularity for convergence of the
volume integral in Eq. (1) has been shown to correspond to the plastic strain
singularity for perfect plasticity (1/R).

Equation (2) provides a unique means for investigating the plastic
zone of a stationary or propagating fatigue crack. At any state of plastic
strains, Eq. (2) may be used to compute a strain intensity factor at the crack
tip. The plastic strain distribution for a given crack size affects the
residual stresses ahead of the crack. This residual stress effect may be
calculated from Eq. (2) by increasing the crack length parameter "a" to $a + \Delta a$,
and then by allowing an elastic iteration of the numerical solution; the
elastic iteration is required to satisfy the traction-free boundary conditions
on the new crack surface. The procedure is entirely equivalent to calculating
the residual stress effect for any elastic crack propagating through a plastic
strain distribution due to prior load history (see [15]). In the case of the
plastic strains due to the crack itself, Eq. (2) has been analytically shown
[13] to be nonconvergent at $\Delta a = 0$; numerical data in [15] confirmed this. The

interpretation at $\Delta a > 0$, Eq. (2) provides a direct means for calculating the effect of all prior plastic strains on the crack tip stress intensity factor. It should be noted that while Eq. (2) is reported in terms of stresses, it is directly computed from the strain field limit approaching the crack tip times the material stiffness matrix. Thus, the result is in reality a strain intensity factor. The stresses have no singular interpretation for elastoplastic fracture mechanics analysis.

The direct application of this mathematical condition is to calculate retardation effects and crack closure effects for fatigue crack overload conditions. The details of the overload retardation and closure calculations, as well as an exploration of the implications for fatigue crack growth are reviewed in the following sections of this text.

2.2.3 Crack Opening Displacement

The Somigliana identity for the interior displacements in elastoplastic fracture mechanics problem is given as:

$$\dot{u}_i = - \int_S T_{ij}\dot{u}_j dS + \int_S U_{ij}\dot{t}_j dS + \int_{<A>} \Sigma_{ijk}\dot{\epsilon}_{jk}^p dA \qquad (3)$$

where T_{ij} and U_{ij} are the boundary tractions and displacements on the uncracked surface S for point loads applied in each of the x_j directions. The tensor Σ_{ijk} is generally the interior stress state for the elastic cracked body due to the point loads. The displacement in Eq. (3) may be evaluated on the boundary of the crack, without major algorithmic problems. It is easily shown, following the same procedures as in [13], that the crack opening field near the crack tip contains a square-root-R behavior due to the boundary data, and a term due to the (singular) plastic strains.

The crack opening displacement result exactly parallels the one above for the total strains. Thus, the effect of the plastic strains on crack opening displacement is directly linked to the effect of plastic strains on the strains ahead of the crack tip. Thus, if the plastic strains are bounded,

or the elastic crack tip is extended to a+Δa, the total crack opening field near the crack tip is dependent on the square-root of the crack tip distance, R. For the elastoplastic fracture mechanics solution, the near crack tip behavior will depend on the implicit crack tip singularity of plastic strains. The numerical results will expand on this more fully.

2.2.4 Plastic Slip Line Solutions

The last area of potential exploitation of the elastoplastic BIE formulation for the fracture mechanics problem is its use in modeling fully developed plastic fields. As discussed in [16], the elastoplastic field is theoretically hyperbolic, such that the plastic strains may be discontinuous along characteristic lines whose directions depend on the solution geometry.

The BIE formulation in Eq. (1) admits such discontinuous plastic strains without difficulty. The derivation of Eq. (1) requires only that the plastic strains be integrable in the volumetric sense; no derivatives of the plastic strains are required. The boundary terms in Eq. (1) are the result of an integration of the displacement gradients through the divergence theorem. The application of the divergence theorem only requires that the displacements be continuous and differentiable, a condition satisfied by compatibility.

An example of the application of Eq. (1) and, more specifically, Eq. (2) to a problem of a discontinuous plastic field was given in [12] for the problem of a modeled weld bead with a narrow zone of high residual plastic strain. The application was to the computation of crack tip stress intensity factors for cracks within the plastic field, and for crack tips extending beyond the plastic field. The solution was essentially exact.

The implications of this result are not yet fully explored. However, it is clear that the BIE formulation for this class of problems admits the possibility of modeling slip line plastic strain solutions without the need for special domain elements or special element refinement near the

zone of discontinuity. This contrasts with the finite element method which requires the use of many small elements along such lines of discontinuity for any degree of accuracy.

2.3 Model Problems for Short and Long Cracks

2.3.1 Stationary Crack Modeling

The material is assumed to be elastic-perfectly plastic. The modulus is taken to be $30*10^6$ psi while the yield stress is taken to be 50 ksi. These are arbitrary constants and none of the conclusions specifically depends on these values. The stationary load case refers to a load/unload cycle at the original crack length. Cyclic crack modeling refers to a load/unload cycle, a crack extension by some increment, and then another load/unload sequence, etc. A validation model for the load application phase using the elastoplastic BIE code is reported in [14], and is repeated in Figure 3. The results were compared in Figure 3 to numerical FEM results from ADINA to establish the validity of the results.

Two crack lengths are used in the current study, based on a desire to have small-scale and large-scale yielding. The crack lengths are taken to be 10.0" and 0.1" with applied stress intensity factors (elastic) of 20 ksi. √in. The plate is taken to be 1000" wide and long to minimize the effects of finite geometry. Based on a Dugdale model, the plastic zone size for plane stress is 0.062" for both crack sizes. The plane strain value might be estimated to be one-third of that size, or 0.021".

Thus, in the case of the large crack, the normalized size of the plastic zone (r_p/a) is 0.0063, while for the short crack case the value is 0.63. Clearly, the two problems do not possess similitude of the plastic strain fields and may serve as good comparisons for large crack and short crack results.
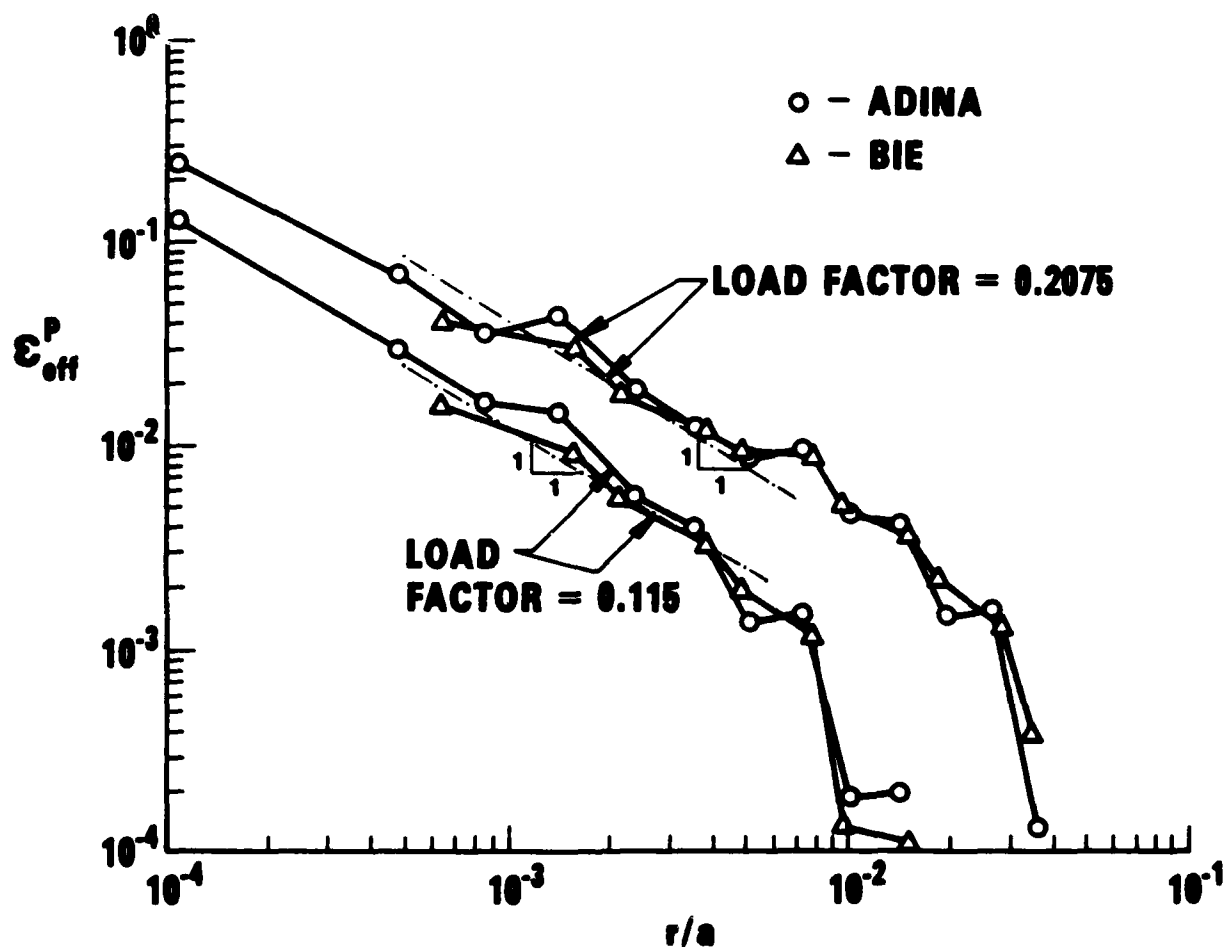
Figure 3. Distribution of Effective Plastic Strain for a
Model Problem to 21% Net Section Yield (c.f. [11])

Figure 2 shows the domain discretization currently used for analysis of the stationary (non-propagating) crack. The mesh is much cruder than used in the study reported previously [13] but produces essentially the same plastic strain results. The loading was applied incrementally to an equivalent elastic stress intensity factor of 20 ksi./in and thereby removed incrementally. The plastic strains at the crack tip are thereby reversed, but no recycling of the loading is performed.

In order to define the size of the plastic zone in an unambiguous manner, use is made of the concept of elastic crack extension through the plastic strains for the stationary crack analysis. For this analysis, the stress (strain) intensity factor is computed using Eq. (2) for various crack extensions; the plastic zone taken from that for the the original crack size and the above loading conditions and material properties.

Figures 4 and 5 show the resulting values of elastic stress intensity factors. As discussed in [14], the computation for (2) treats the prior load plasticity as a residual strain distribution and provides the effect of the residual strains on the stress intensity factor for various crack lengths. The elastoplastic solution is first obtained so that a plastic strain distribution is known. Then the BIE code is exercised in a strictly elastic sense. The crack size is incremented by " Δa " into and through the plastic zone of the previously analyzed elastoplastic condition. Each elastic calculation from Eq. (2) is then a computation of any elastic stress intensity factor, including the effect of the prior elastoplastic zone. The resulting stress intensity factor, while not strictly physical, directly computes the effect of the previous plasticity on the crack tip strain field for the larger size crack. Thus, this is an unambiguous estimate of the residual plastic zone effect for propagating fatigue cracks. The closest parallel to previous crack modeling strategies is the estimate of overload plasticity effects on the elastic stress intensity factor for the fatigue load condition [8].
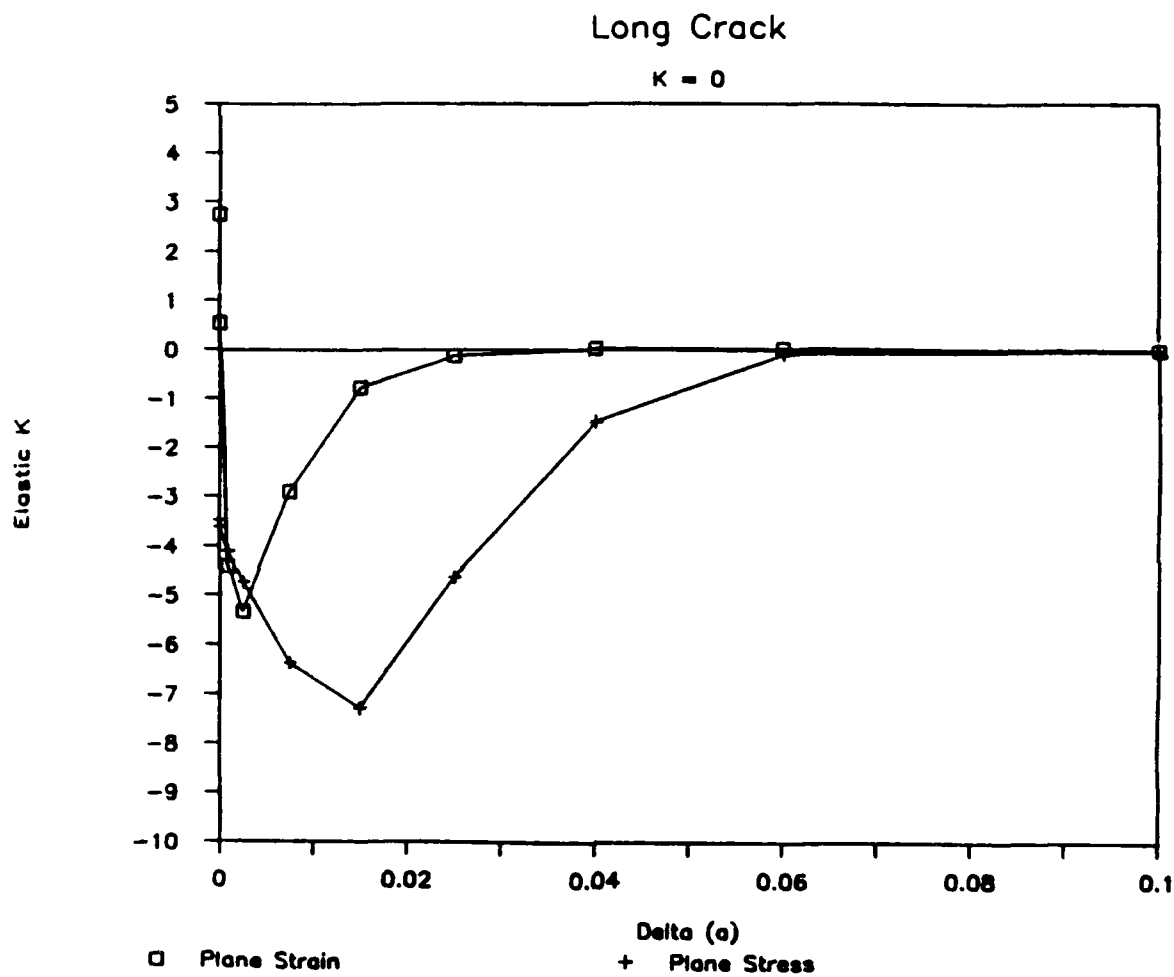
Figure 4. Residua. Strain Effect on Crack Tip Stress Intensity Factor
for Various Crack Extensions--Long Crack at No Load
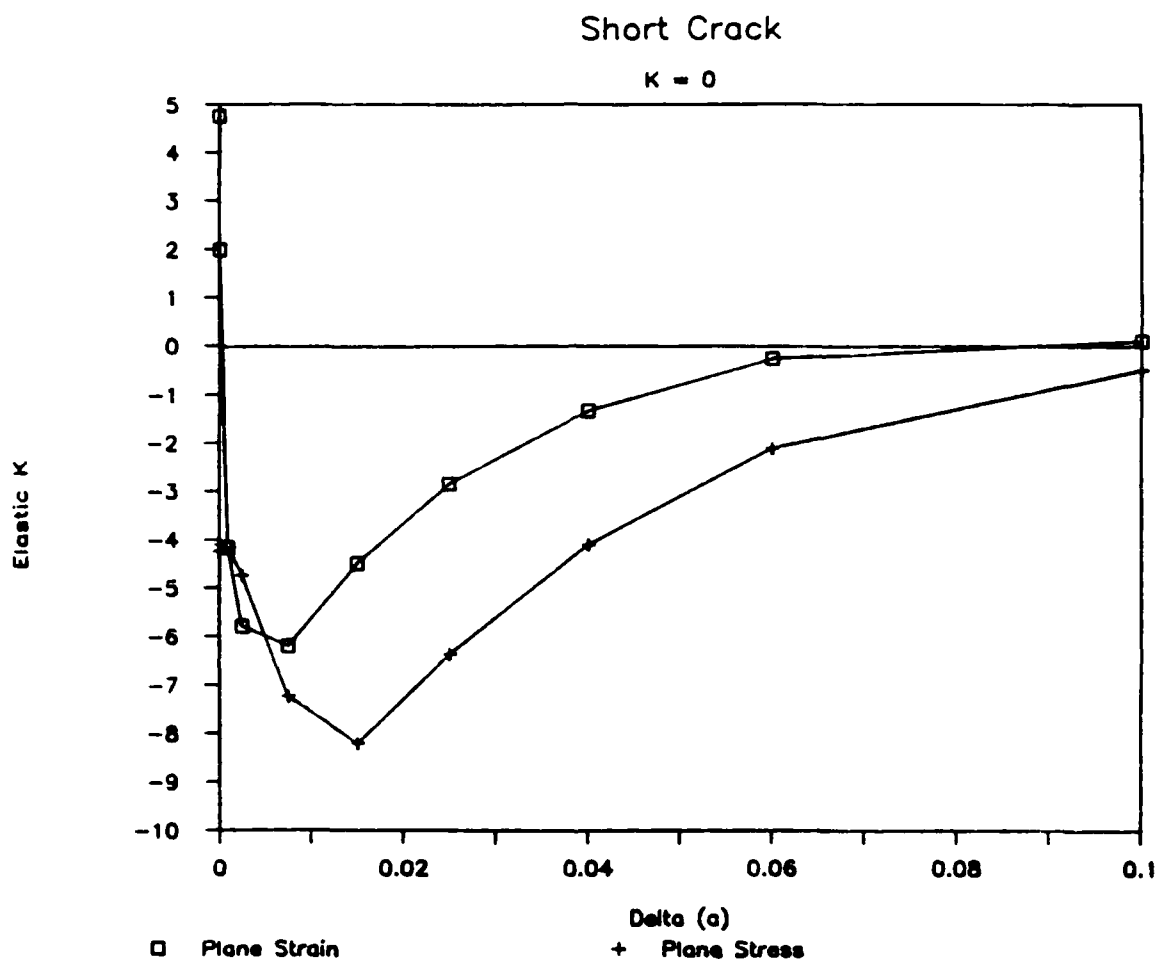
Figure 5. Residual Strain Effect on Crack Tip Stress Intensity Factor
for Various Crack Extensions--Short Crack at No Load

Table 1 compares the estimated plastic zone size from these
results to the Dugdale (plane stress) and plane strain plastic zone sizes.

Table 1

Comparison of Plastic Zone Sizes

Long Crack	r_p(est.)	r_p(cal.)
Plane Stress	0.063	0.060
Plane Strain	0.021	0.025
Short Crack		
Plane Stress	0.063	0.110
Plane Strain	0.021	0.080

As can be seen, the BIE results compare quite favorably to the estimates for
the long crack case but not for the short crack case. The effect of the
plastic strains for the short crack case is substantially greater than for the
long crack case; the difference between the plane strain and plane stress
plastic zones is quite diminished. These results seem quite consistent with
the expectation.

2.3.2 Crack Extension Modeling

Figure 6 shows the domain discretization for the plastic strains
used for a study of the crack propagating as in fatigue. That is, the crack
is incrementally loaded to 20 ksi./in and unloaded at each crack size. The
yield stress in compression is taken to be the same as in tension (no
Bauschinger effect). The original crack tip is as shown for the length "a".
In the current study, crack tip plastic strains are allowed to reverse before
the crack is extended. This strain reversal accounts for what others model as
the interference of the plastic wake for a propagating crack [4,6].

The surfaces of the crack are not constrained against
inter-penetration upon further unloading to zero load. By reversing the

1000 in.

a = 10 in. (Long Crack)

a = 0.1 in. (Short Crack)

1000 in.

a   0.1 in.
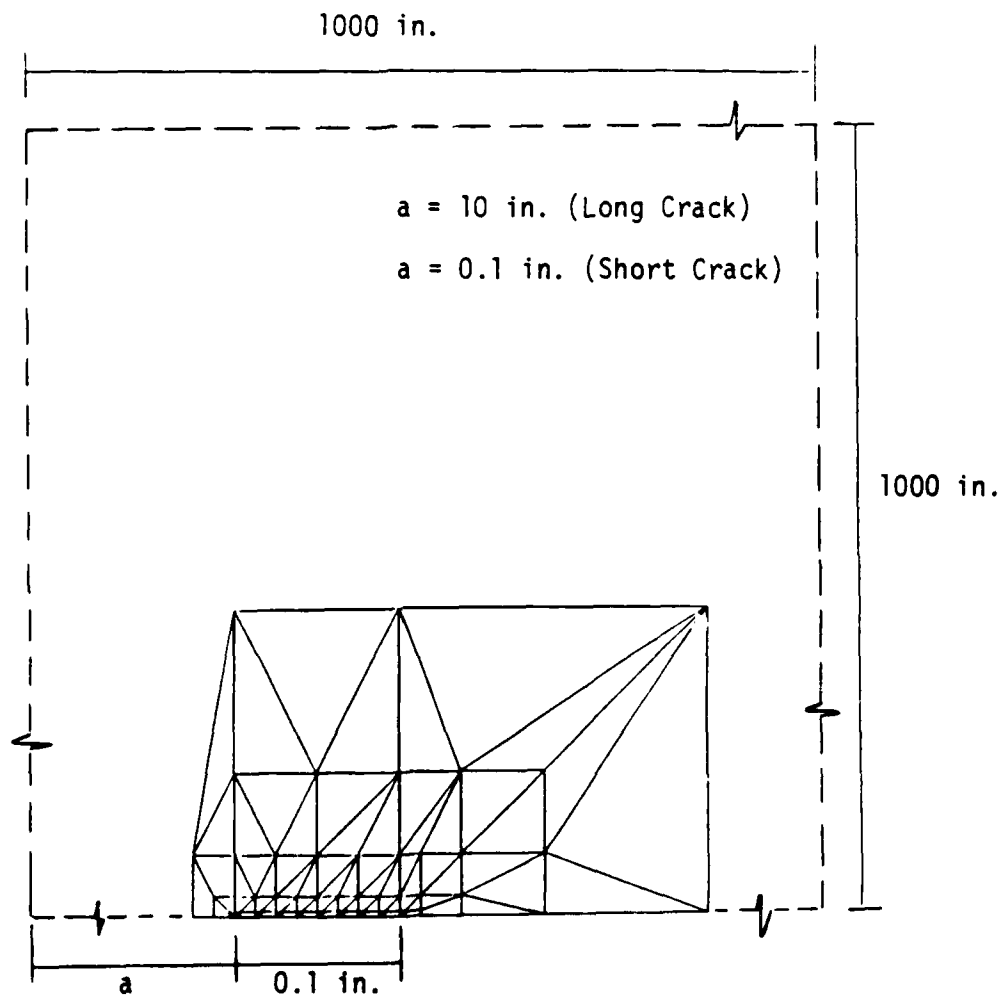
Figure 6.   Domain Discretization for Propagating Crack

plastic strains near the crack tip during unloading and before the crack has been extended, the primary effect of crack surface interaction on the plastic strains in the wake is computed. Somewhat higher cyclic plastic strains are predicted very near the crack tip, due to the additional plastic strain occurring at loads lower than the load at which closure occurs. The bulk of the closure effect beyond reversing the plastic strains for the material just ahead of the crack tip prior to extension is the elastic problem of loads on the crack surface to maintain zero closure. This nonlinear contact stress problem is fully reversible upon load application and does not affect the plastic results.

The crack length is increased after unloading so the crack tip will be at the next domain element boundary (0.0125 units long in the domain mesh used). Extension of the crack is achieved in the elastoplastic BIE code by assigning a new length to "a" and then by a single iterative cycle to achieve elastic load redistribution. Thus, the traction free condition on the crack surface is exactly satisfied without any mesh changes. The load/unload cycle is repeated, followed by crack extension, etc. until the crack plasticity results stabilize. The stabilization of the cyclic plastic zone took about 2 to 3 crack extensions. Stability of the numerical results was greater for the plane strain than for the plane stress condition.

Figures 7 and 8 plot the results obtained by calculation of the stress intensity factor from Eq. (2) for various elastic crack tip locations displaced from the tip of the analyzed crack size ("a + Δ a"). As in the case of the stationary crack reported above, the computation of stress intensity factor is a direct calculation of the effect of prior plasticity on a propagating fatigue crack.

In all problems only three extensions of the crack showed that the plastic strains had converged acceptable to a steady-state condition, particularly for the long crack solution. In fact, the cyclic results did not differ much from the monotonic results. The plane stress results for the
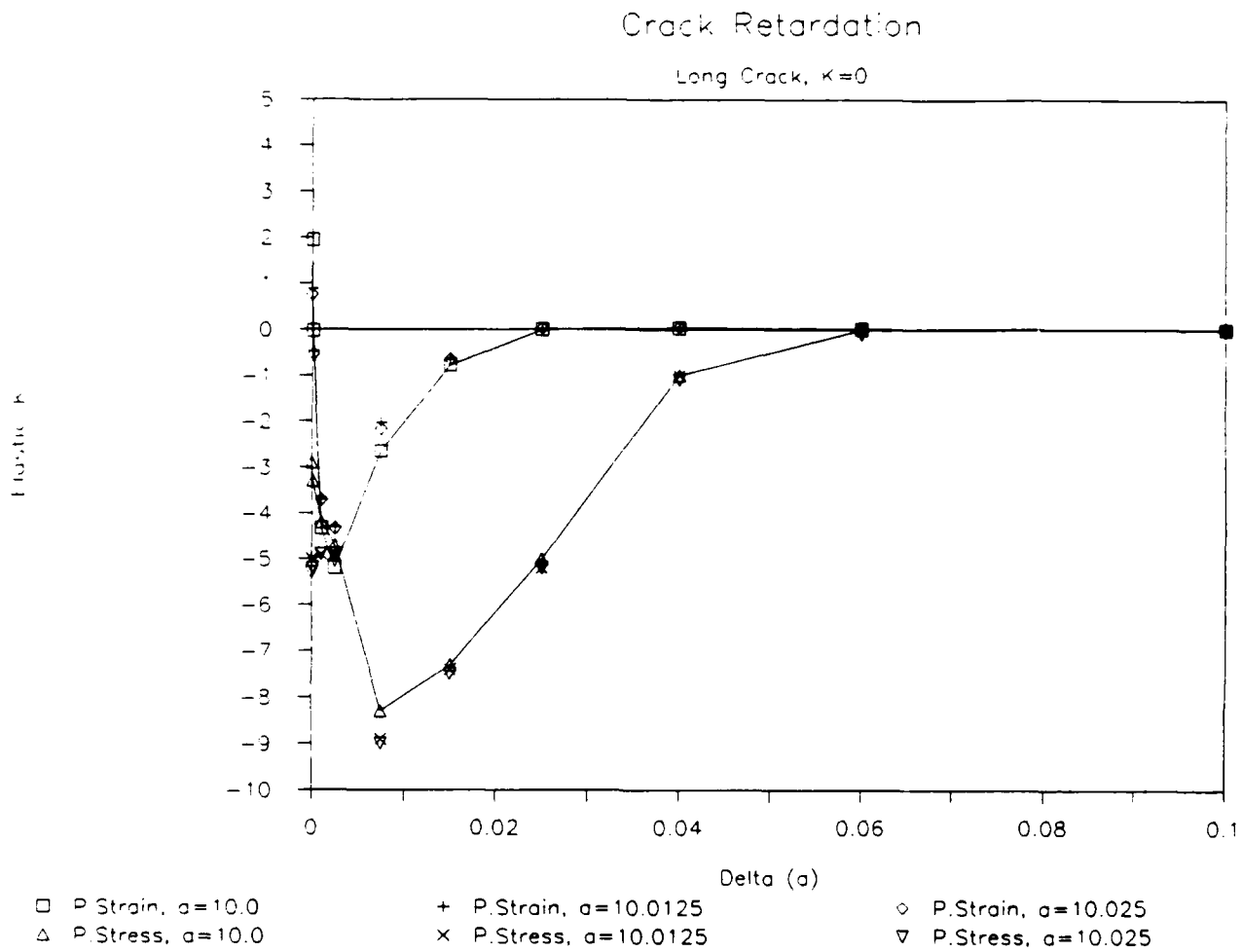
Figure 7. Residual Strain Effect on Crack Tip Stress Intensity Factor
for Propagating Cracks at No Load--Long Crack

Crack Retardation
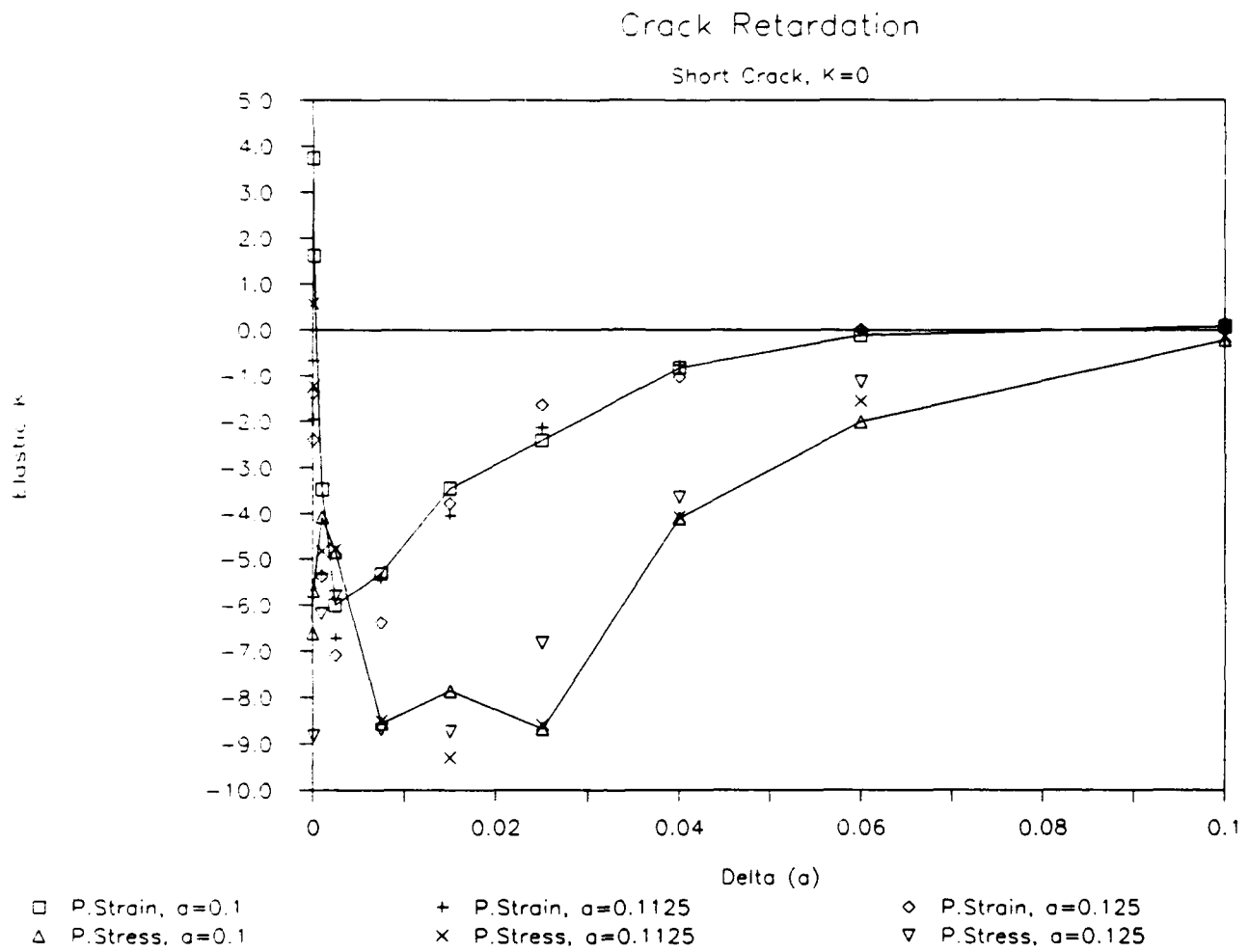
Short Crack, K=0

**Figure 8.   Residual Strain Effect on Crack Tip Stress Intensity Factor
for Propagating Cracks at No Load--Short Crack**

short crack showed the weakest convergence, both in terms of the crack extension comparisons but also in terms of the numerical algorithm. The short crack, plane stress case has the weakest constraint on the plastic strains, and this would seem a reasonable source of the difficulty.

It can be seen that the computed plastic stress intensity factors are somewhat oscillatory for short crack extensions. The oscillations occur when the crack extension is inside the smallest crack-tip domain element. However, by ignoring the plastic strain (Eq. (2)) within the smallest domain element, the elastic stress intensity factor is made regular as seen in Figure 9. The Figure shows increasingly negative values of strain intensity factor from Eq. (2) as the smallest domain element is reduced in size. This divergence in K occurs as expected due to the higher order plastic singularity in crack tip strain. What was not expected was the apparently small (perhaps indefinitely small) zone over which the divergence affects the calculated K in Eq. (2). This zone was seen to reduce as the domain element as the crack tip was reduced. This implies a discontinuity in the behavior of Eq. (2) for small Δa. At $\Delta a=0$, the result is divergent. For $\Delta a>0$, the result seems to converge to finite values of K for small Δa.

The cross-data points in Figure 9 correspond to values from Eq. (2) obtained by setting the plastic strain in the smallest element to zero. It is seen in Figure 9 that the effect of the plastic strain in the first and smallest domain element zone at the crack tip is limited to Δa values only within that element.

2.3.3 Closure vs. Retardation Results

The crack tip opening was calculated from Eq. (3) for both stationary (monotonic loading) and propagating cracks. The algorithm is based on monitoring the displacement at a pre-defined point on the crack surfaces at a distance of .00001" behind the crack tip. This is an arbitrary location but
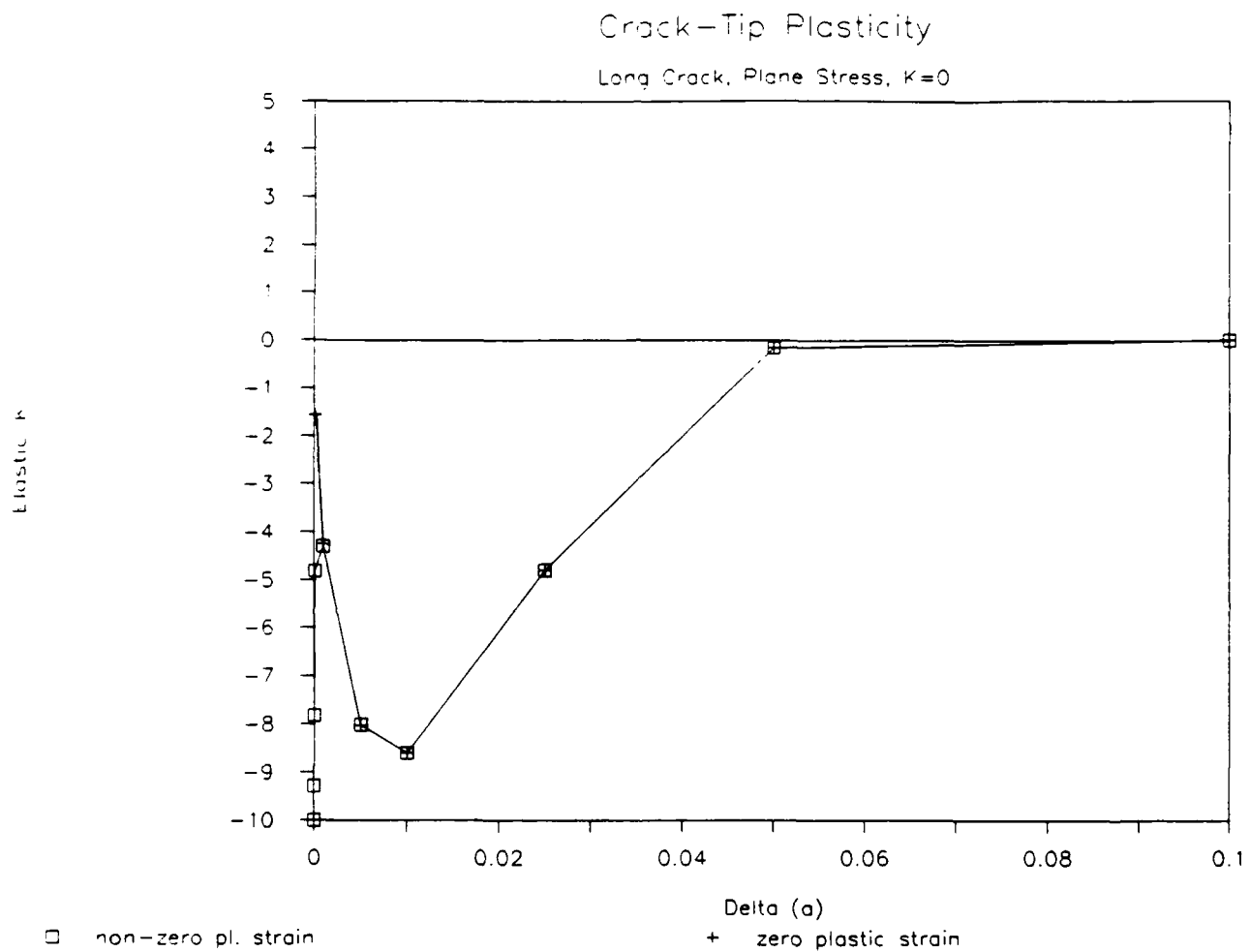
Figure 9. Effect of Plastic Strain in Crack Tip Element on Crack Tip Stress Intensity Factor

reflects the experimental capability [11]. Similitude is not maintained as 0.0001/a equals 10^{-6} for the long crack case and equals 10^{-4} for the short crack case.

Loading for crack closure monitoring is applied elastically, as the plastic effect cannot resume until after the crack tip is open. The load at which the displacement at this monitoring location goes from negative (overleaving of the crack) to positive is defined as the crack tip opening load. Interpolation of the numerical results was used to select this point. The load for opening is then converted into an equivalent elastic stress intensity factor corresponding to crack opening.

The results for the propagating crack are shown in Figures 10 and 11. The methodology used for the residual solution is obtained for a given crack size, then the BIE code elastically computes the effect of the plastic strains on the crack opening load for various elastic extensions of the crack. This corresponds then to calculating the effect of the plastic wake on crack closure. It should be recalled that the elastoplastic loading and unloading are done for a given size crack so that the effects of interference of the plastic wake from both sides of the crack is taken fully into account (see [7]).

The numerical data in Figures 7-8 and 10-11 show a very important piece of insight into the fatigue crack growth problem. Namely, the effect of the plastic wake on the apparent stress intensity factor for crack opening is identical (with a sign change) to the effect of the residual stress ahead of the crack on retardation of the stress intensity factor. Apparently, Kanninen and his coworkers reported the same finding for the super-dislocation plasticity model discussed in Chapter 8 of his book [6]. The theoretical reason for this is clearly seen from Eqs. (1) and (3), which relate to crack tip strain field and crack opening displacements. The strain field Eq. (1) is computed by differentiation of the displacement field Eq. (3) resulting in a mathematical equivalence for any elastoplastic field.
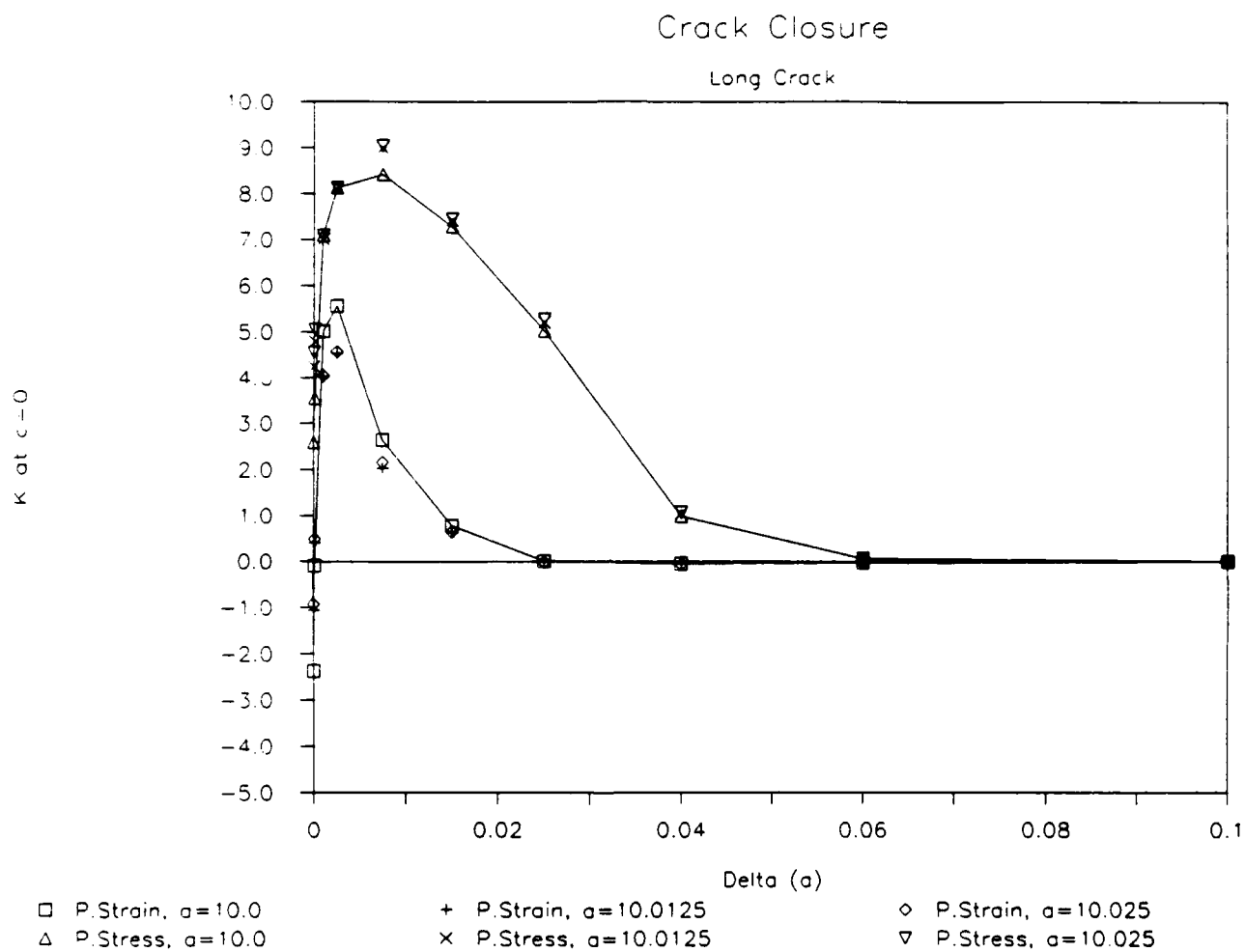
Figure 10. Residual Strain Effect on Crack Tip Opening Load--Long Crack
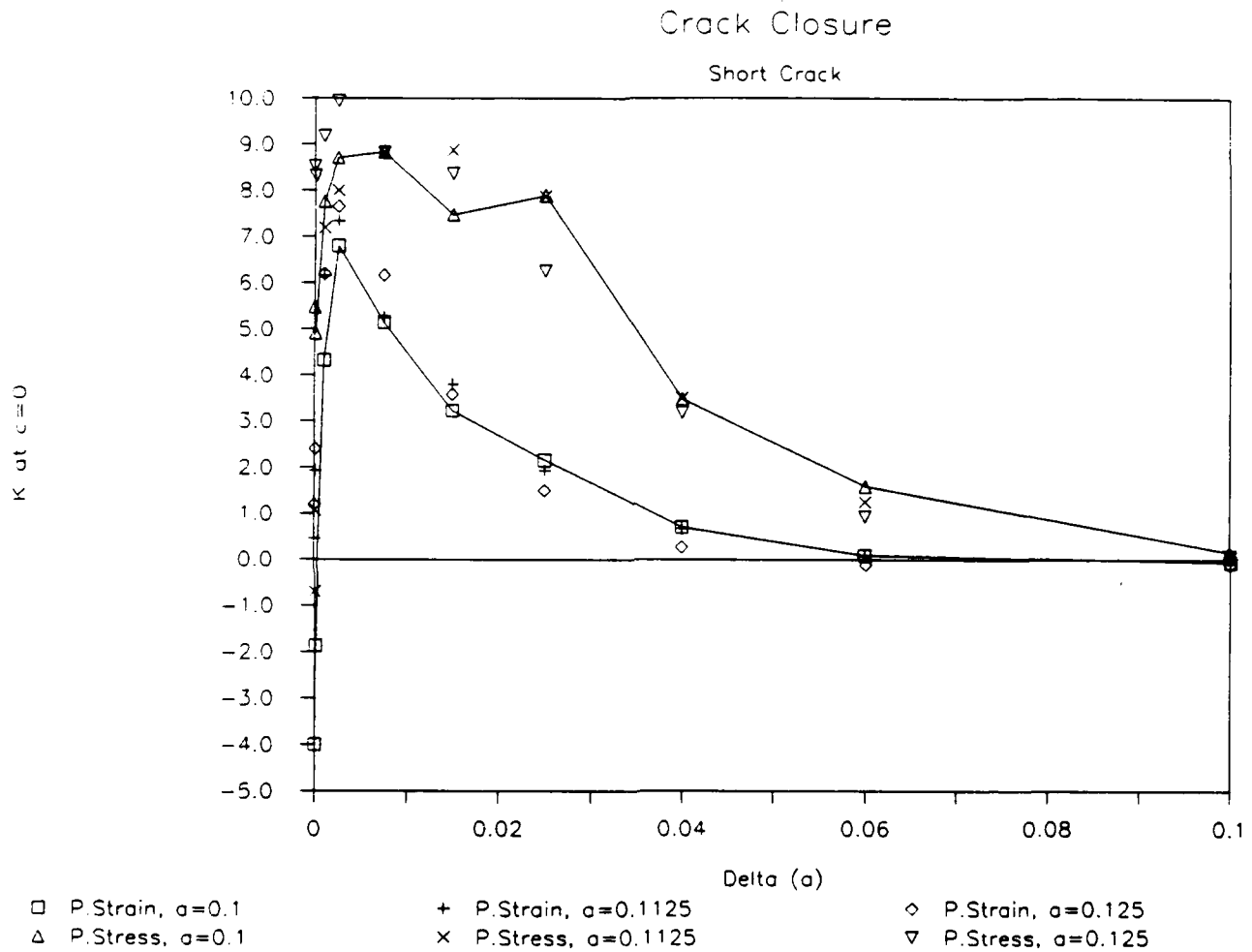
Figure 11. Residual Strain Effect on Crack Tip Opening Load--Short Crack

The duality of residual stress and crack closure effects was also found for the case of the stationary crack subjected to an elastoplastic load/unload solution. The application of this result would be for overload modeling, with the conclusion that accurate modeling of retardation and closure effects of the overload would produce identical effects on the crack tip cyclic response. This is true during fatigue crack propagation with plastic wake effects, as crack tip opening occurs as the last event after the rest of the crack has been opened during loading [6,7].

2.3.4 Crack Opening Displacement

Figure 12 plots normalized crack opening displacements for the long crack under plane strain conditions at the crack length of a=10.0. The displacements are normalized by the elastic crack opening displacement function:

$$u = \frac{2K}{H\sqrt{\pi a}} (2ar-r^2)^{1/2} \qquad (4)$$

where r is the crack tip distance and $H = E$, $E/(1 - v^2)$ for plane stress and plane strain. The solutions are plotted during loading unloading and show the crack opening during loading at $K = 5$ ksi./in, which is elastic due to the finite size of the smallest domain element for plastic strain modeling, at $K = 10$ ksi./in and at 20 ksi./in. The exact solution is seen to fit the elastic behavior of the crack tip solution out to a value of $r/a = 0.01$. At higher stress intensity factors, the crack opening displacement is seen to be increasingly compliant, resulting in higher displacements over a length from the crack tip somewhat larger than the plastic zone size of the problem. During unloading, only a portion of the plastic stretch is reversed, thus, the ratio of computed to elastic crack opening displacement becomes progressively higher. The same behavior was observed for both plane strain short crack and plane stress long and short crack cases.
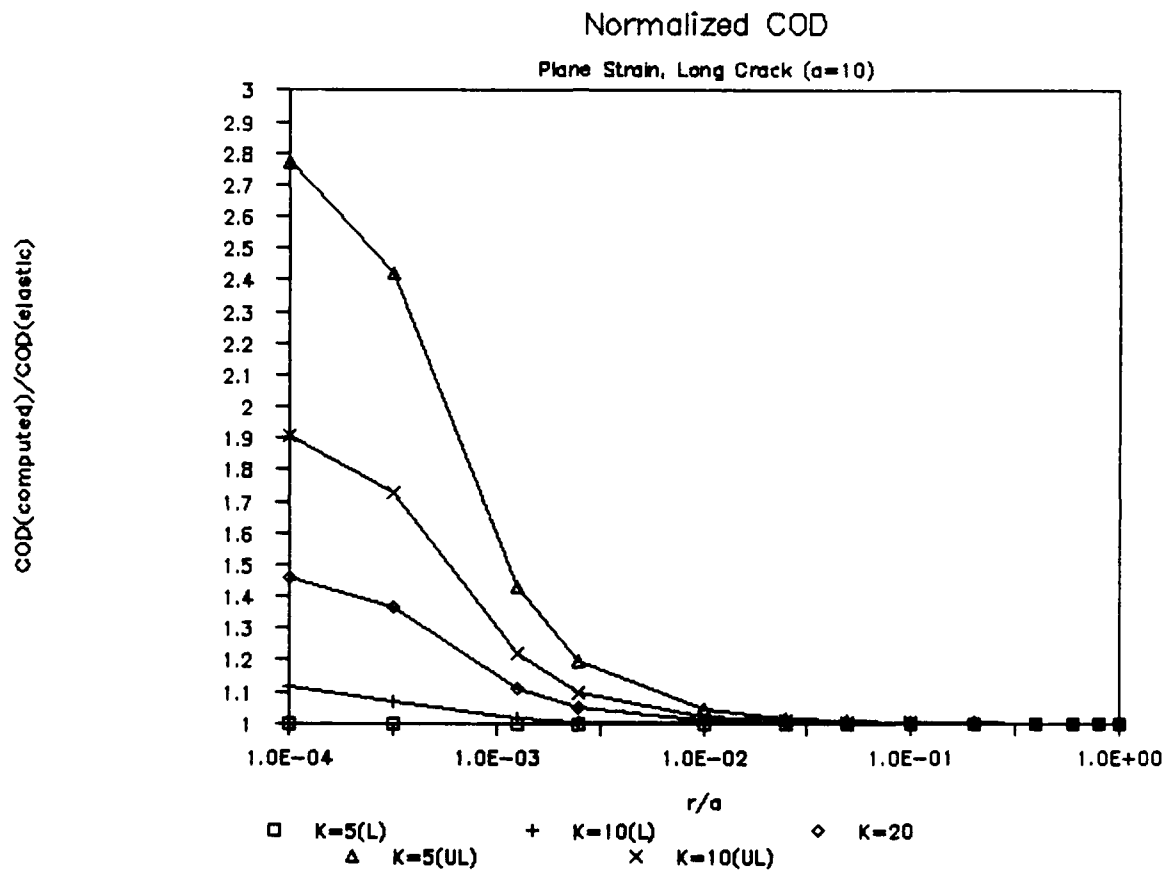
Figure 12. Stationary Crack: Normalized Crack Opening Displacement--
Plane Strain, Long Crack (a=10)

Figure 13 plots the same results for the case of the crack which has been extended by 0.0025a. The plastic wake effect has the result of reducing the crack opening displacements to the elastic values down to r/a < 0.001. Given a reasonable hypothesis that cyclic crack extension is associated with crack tip cyclic deformation, then the cyclic crack opening displacement values for the long crack plane strain results indicate that the LEFM model should be applicable. Of course, this is just as expected. The role of the elastic strain field for the small-scale yielding problem is to force the plastic zone to conform to the deformation of the elastic singularity, near the crack tip. The conformance is clearly achieved during the unloading when reversed plasticity is incurred.

Figure 14 plots the same type of COD data for the short crack problem where the crack is extended by 0.25a. The effect of plasticity on crack opening compliance is now seen by the reduction of the COD below the elastic value, thus, achieving closure at positive loading. Therefore, the crack opening displacement values for short crack results indicate that the LEFM model is not applicable. The data also shows large relative crack opening near the crack tip, indicative of blunting.

The plane stress COD solution for both long and short cracks are plotted in Figures 15 and 16, respectively. The plane stress results show an enduring plastic wake for both long and short cracks; the difference between the plane strain and plane stress results is decreased. The increased plastic wake size for plane stress is due to diminished constraint. It should be noted that, realistically, the plane stress condition occurs only at very thin plates or at a very small layer at the boundary. Similitude for long crack fracture mechanics, therefore, implies that plane strain elastoplastic behavior must be occurring for real, three-dimensional cracks.
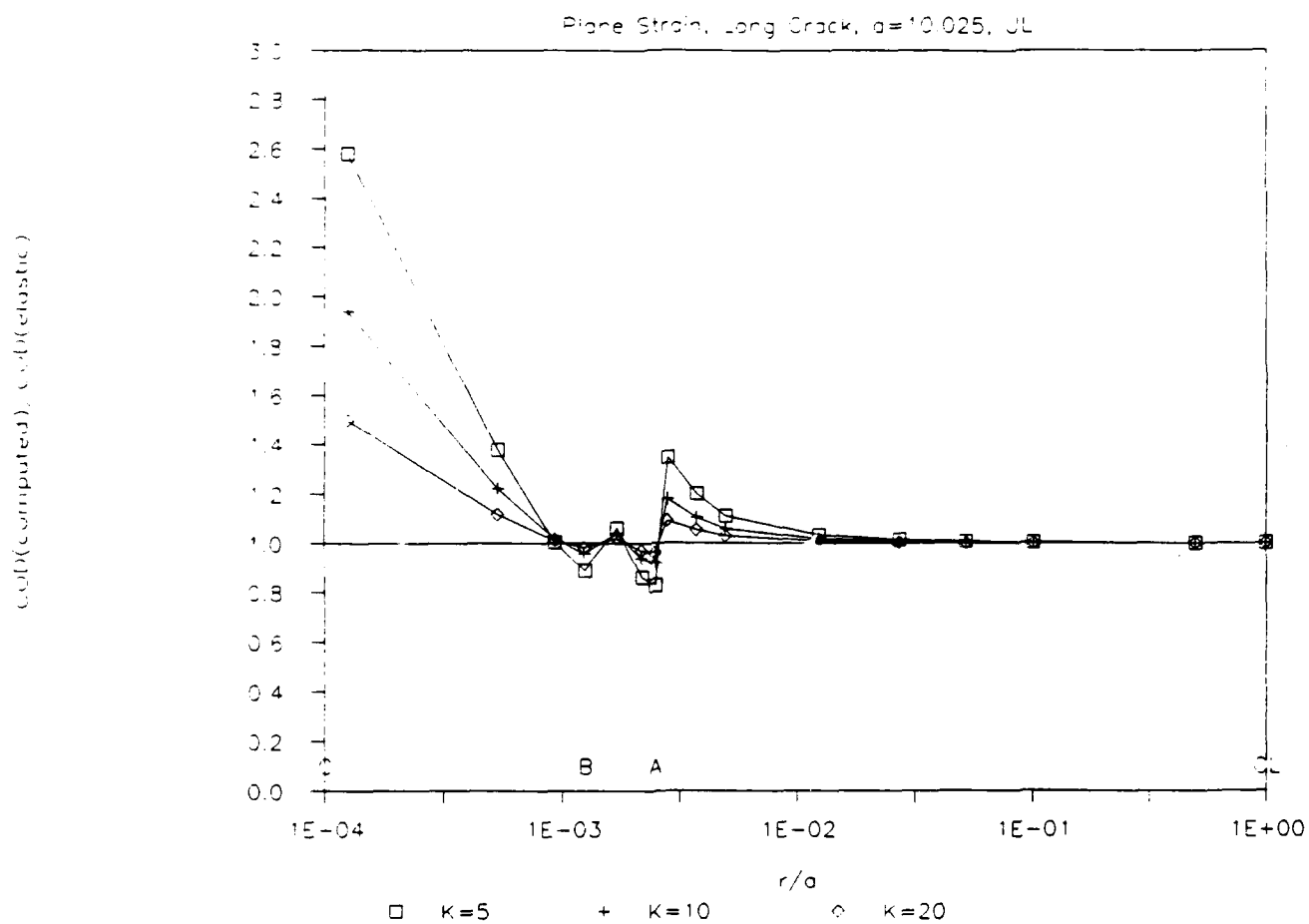
**Figure 13. Normalized Crack Opening Displacement--
Plane Strain, Long Crack (a=10.025)**
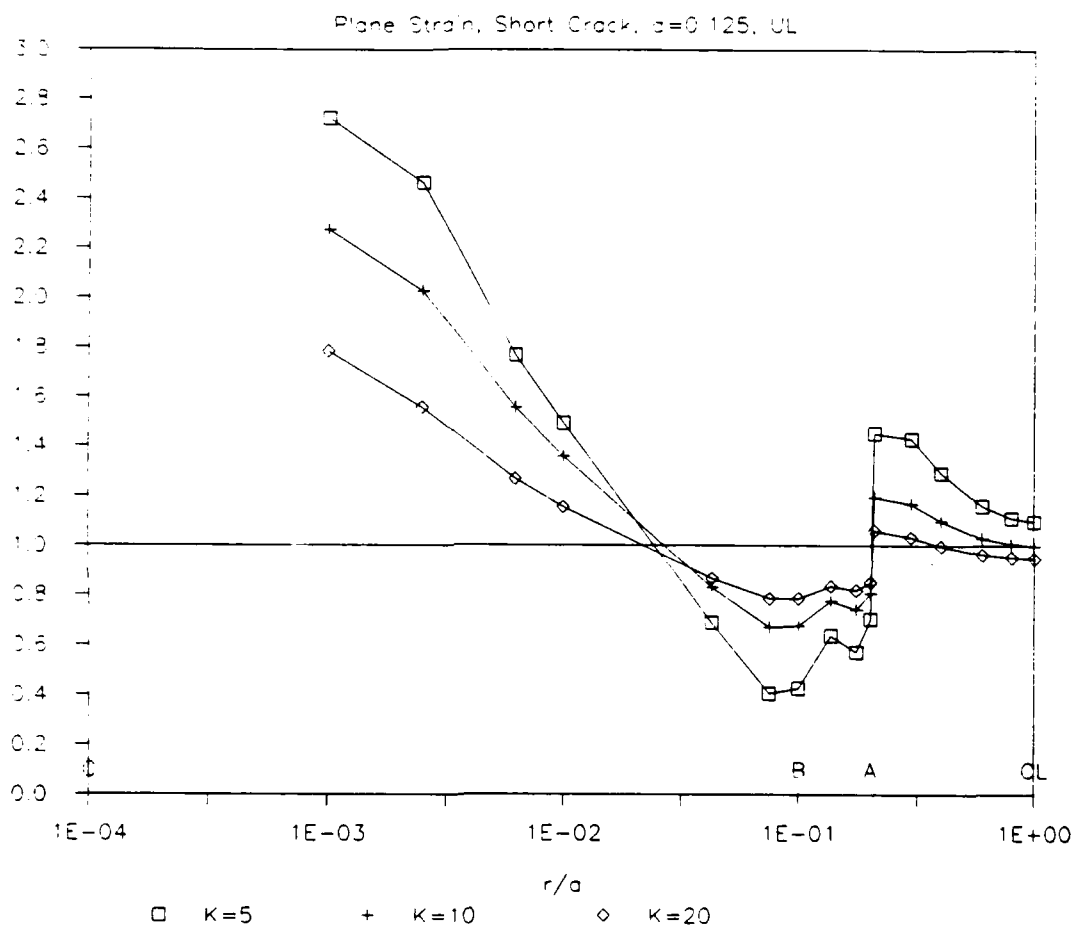
Figure 14. Normalized Crack Opening Displacement--
Plane Strain, Short Crack (a=0.125)
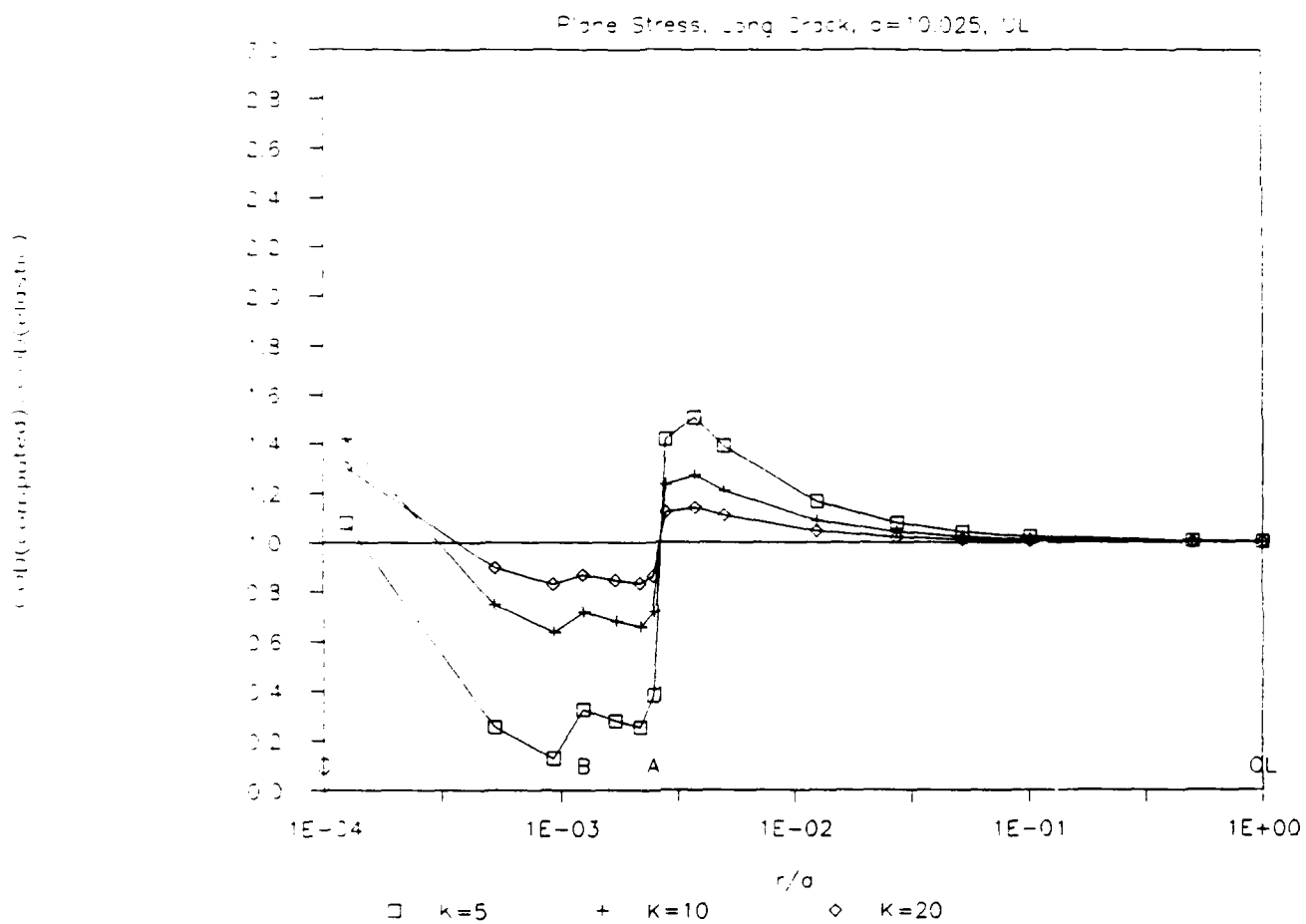
Figure 15. Normalized Crack Opening Displacement--
Plane Stress, Long Crack (a=10.025)
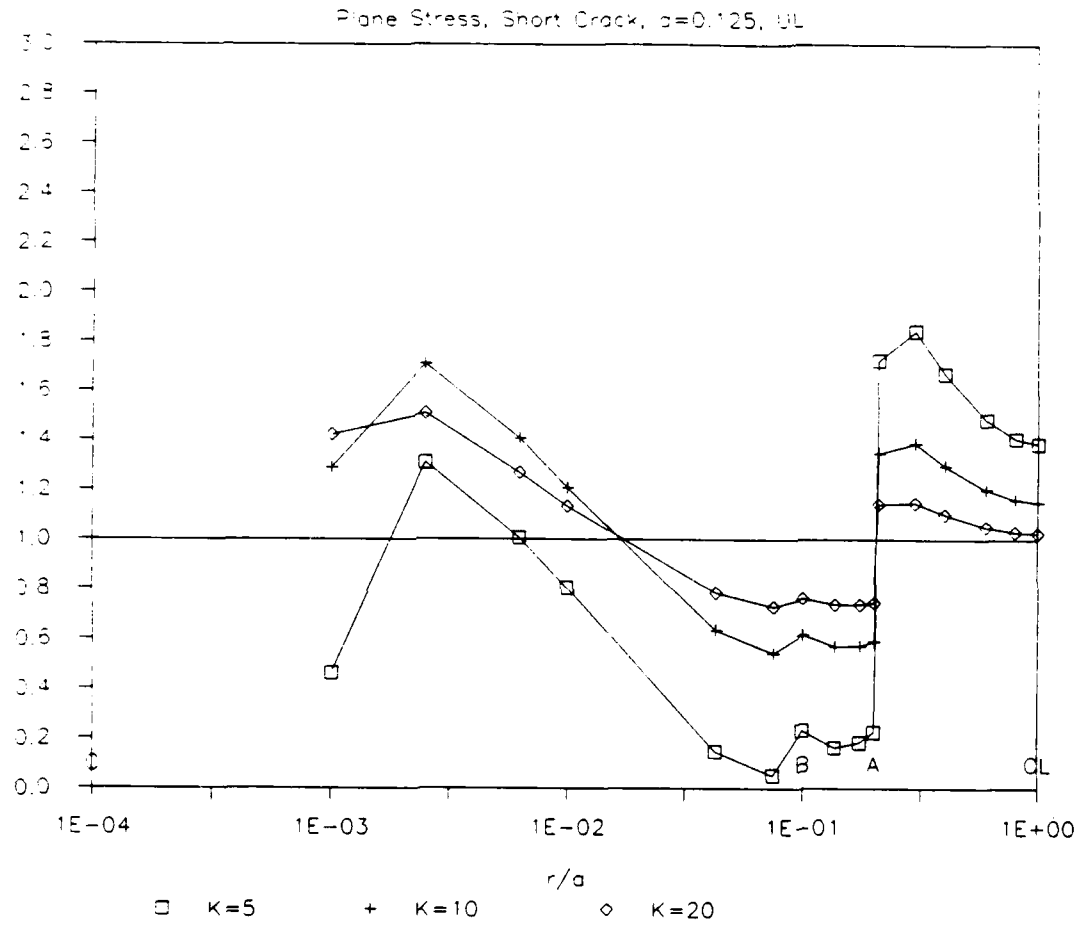
Figure 16. Normalized Crack Opening Displacement--
Plane Stress, Short Crack (a=0.125)

2.3.5 Long and Short Crack Results

The two model problems considered in this study are for equally applied elastic stress intensity factors. In the short crack case, this results in a ratio of applied stress to yield stress of slightly more than 71%. At this load level, the elastoplastic plane strain, long crack results predict that the crack responds in accordance with LEFM.

The short crack results show that the effect of plastic wake on COD at a region near the crack tip is predicted to be significant for the plane strain and plane stress cases. The plastic wake for short cracks is seen to be the result of high, unreversed crack tip stretch plasticity. The fact that the crack tip stretch within the scale of the cyclic crack tip zone is greater than the LEFM prediction may provide the mechanics for increased short crack fatigue crack growth. The increased crack tip stretch shows up physically as a plastic wake.

2.4 Closure and Growth of Cracks

One of the important aspects of the fatigue crack analysis is to correlate and predict the rate of growth of cracks for given combinations of geometry, material properties, and load history. Many theories have been proposed to predict the crack growth rate of cracks that fall under the small scale yield categories. Most of the current models are based on the concept that average growth per loading cycle can be related as a power low function of the stress intensity factor, K [17,18]. However, under large scale yielding conditions, accurate prediction of crack growth is not possible even with the use of modified forms of stress intensity factors. Many alternative parameters such as strain based stress intensity factors (e.g., [19,20]), crack opening displacements (e.g., [21-24]), equivalent stress intensity factors (e.g., [25-27]), and J-Integrals (e.g., [28,29]) have been suggested for the investigation of fatigue crack growth where LEFM is not applicable. However, since first noted by Elber, crack closure concept is considered as a very important criterion in explaining the propagation of the crack. He used

an effective stress intensity factor, corresponding to the portion of loading over which the crack remains open, as a correlating parameter. In this section, we further study the effect of crack closure on crack growth. A detailed study of crack closure under plane stress conditions using finite element method has been reported recently by McClung [30].

McClung's investigation focussed on crack closure and factors that control its magnitude for constant amplitude of stress level. He noted the pronounced decrease in normalized opening stress with increasing maximum stress that is largely ignored in many experimental research. Also, he confirmed an earlier finding by Iyyer and Dowling [31,32] that the ratio, U, of the effective stress over which the crack remains open to the total applied stress depends on the maximum stress amplitude.

Five crack lengths ranging from 0.07 in. to 10 in. were selected to examine the dependence of U on the maximum stress amplitude in the current study. In addition to the constant stress amplitude case, S(max), investigated by McClung, crack closure due to constant stress intensity factor amplitude case, K(max), under plane stress as well as plane strain conditions were studied. For K(max) case, the value of maximum stress was reduced progressively with crack advance. The values of the ratio of maximum stress amplitude to the yield stress at the initial crack length for various cases considered are given below.

Crack Length, a	S(max)/S(yield)
0.07	0.8
0.10	0.71
0.20	0.50
0.50	0.32
10.00	0.07

2.4.1 Constant Stress Intensity Factor Amplitude Loading

As explained in Section 2.3, the crack was extended by arbitrary increments of 0.0125 in. at zero load and incrementally loaded to the maximum value and unloaded, subsequently. In the first study, the value of K(max) was kept constant. As noted previously in Figures 14-16, the crack remained closed during a portion of the loading cycle. The crack closing stresses were computed by monitoring the maximum load at which the crack surfaces initiate contact during the unloading cycle. It was generally observed that the initial contact occurred at or near the location of last crack tip before the current extension. The crack closing stress normalized with respect to the maximum stress amplitude is plotted during crack extension in Figure 17 for the plane stress case and in Figure 18 for the plane strain case. The results indicate that after an initial increase, the crack closing loads stabilize, generally after about 5 increments.

To see the dependence of the crack opening stress on the maximum stress amplitude, the stable crack closing stresses normalized with respect to the maximum stress for different maximum stress amplitudes are plotted in Figure 19 for the plane stress case and in Figure 20 for the plane strain case. The results indicate that the normalized crack closing stress increases with increase in maximum stress amplitude. In other words, the normalized crack closing stress increases with decreasing crack length, going from long crack to short crack. These findings are inconsistent with the finite element method crack opening stress results reported for the plane stress case using constant amplitude loading [30,33].

To examine the difference in the crack opening and closing stresses, the crack was reloaded at the final crack length without crack extension. A comparison of the normalized crack opening and closing stresses shown in Figure 21 indicates that whereas the crack opening stresses are higher than the closing stresses for the plane stress case, the values are essentially identical for the plane strain case. However, the crack opening stresses still show increase with increase in applied maximum load.
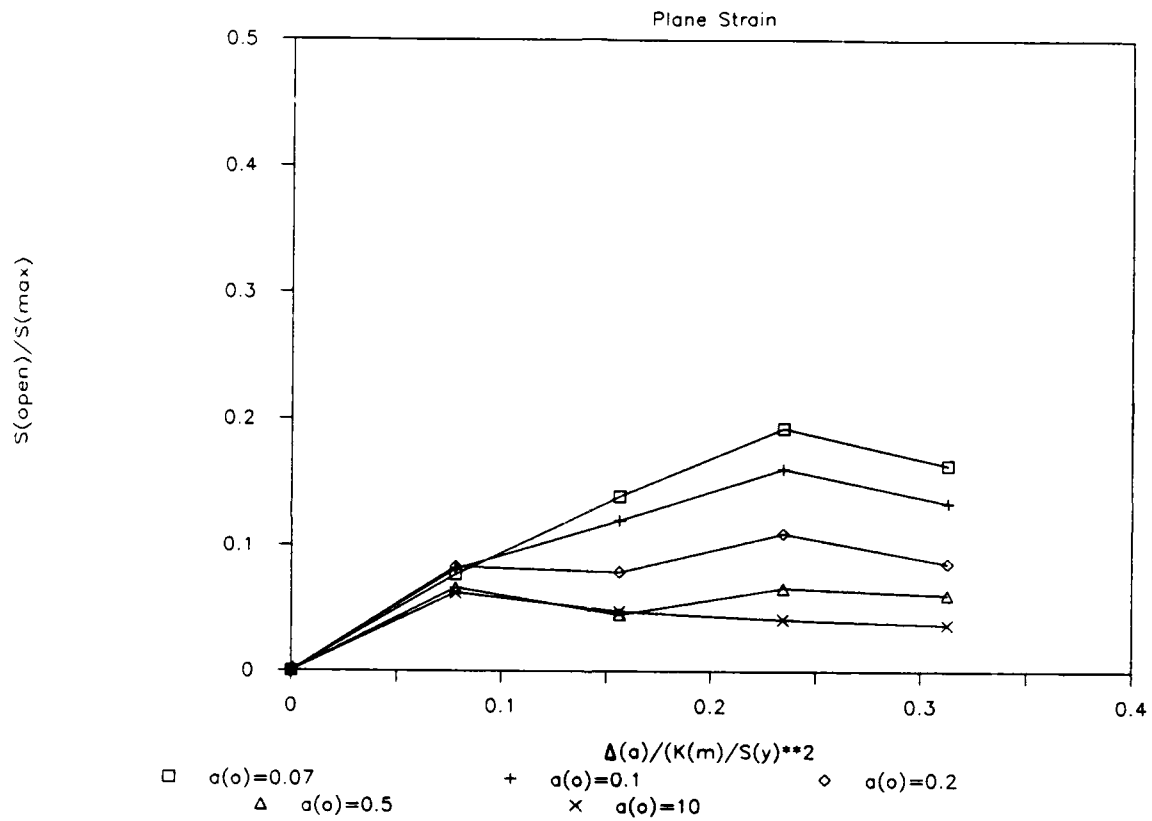
Figure 17. Crack Closing Stresses Through Extension--
Plane Strain, Constant K (max)
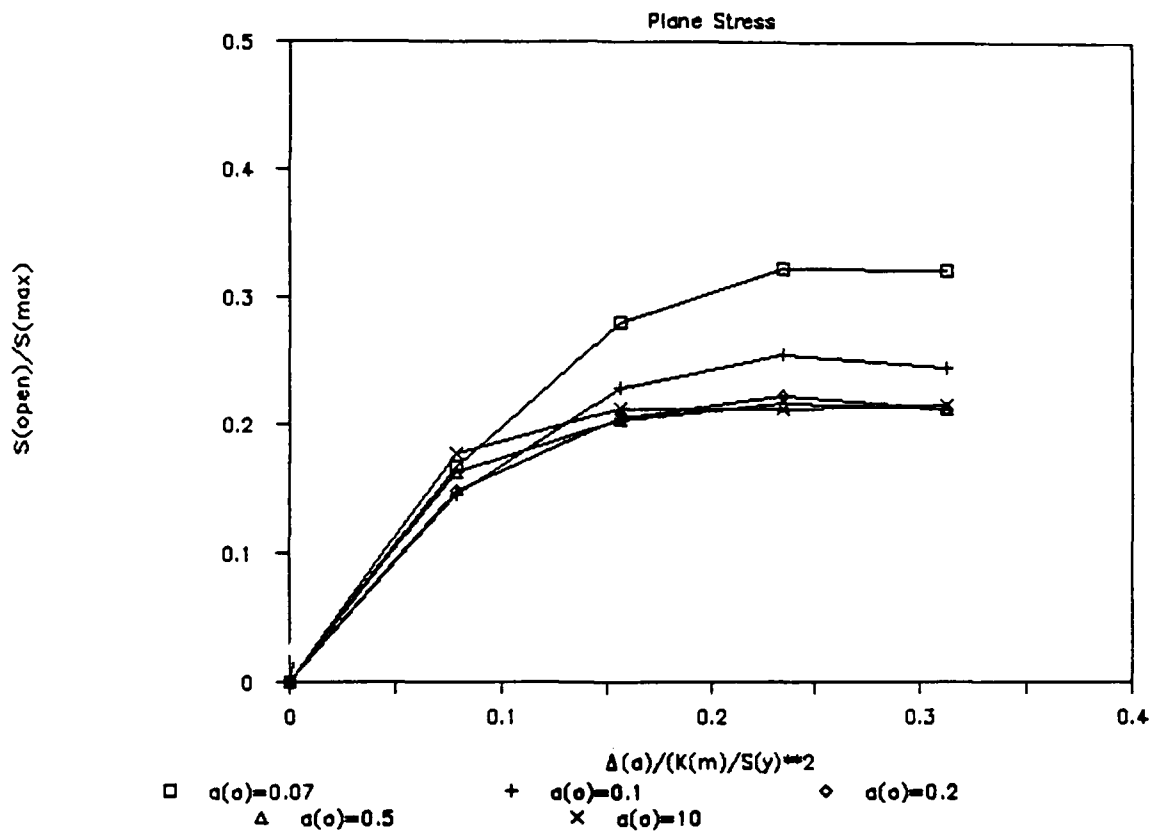
Figure 18. Crack Closing Stresses Through Crack Extension--
Plane Stress, Constant K (max)

Normalized Crack Opening/Closing Stress
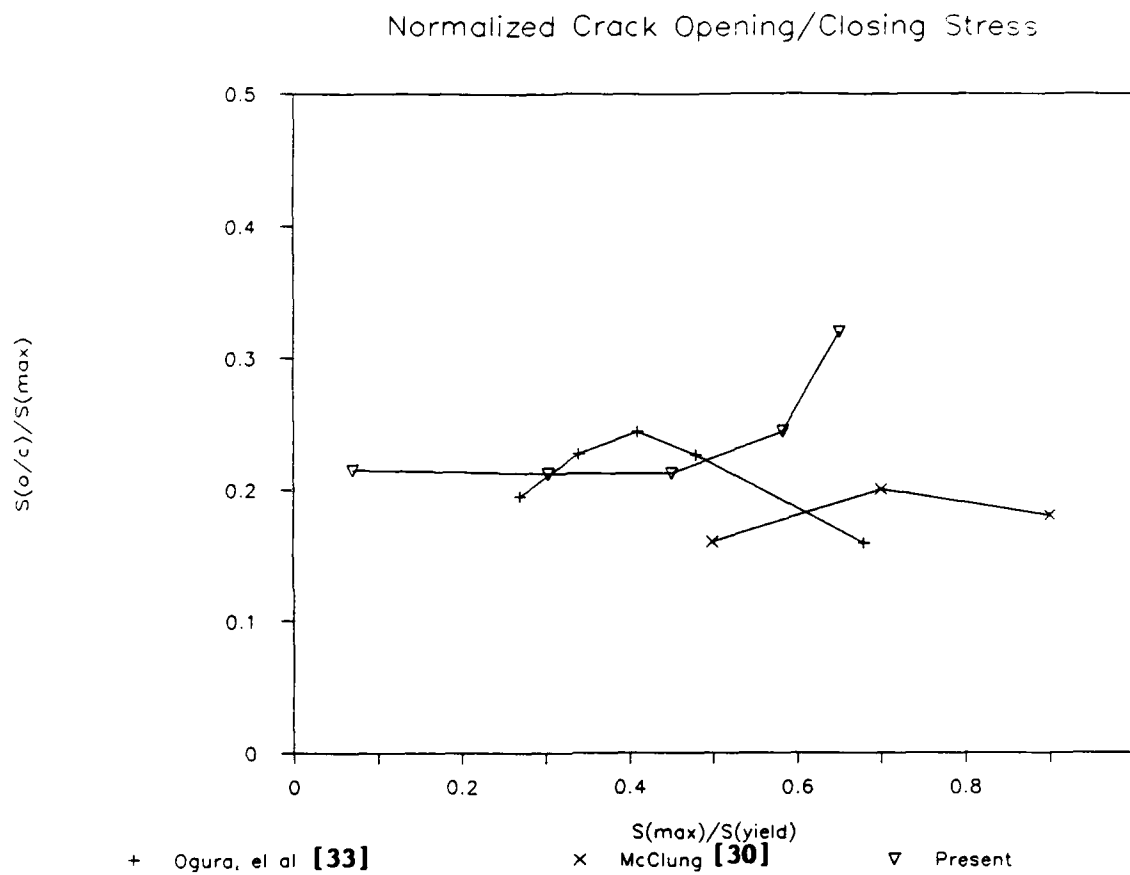
Figure 19. Crack Closing Stresses at Stable State--
Plane Stress, Constant K (max)

Normalized Crack Closing Stress
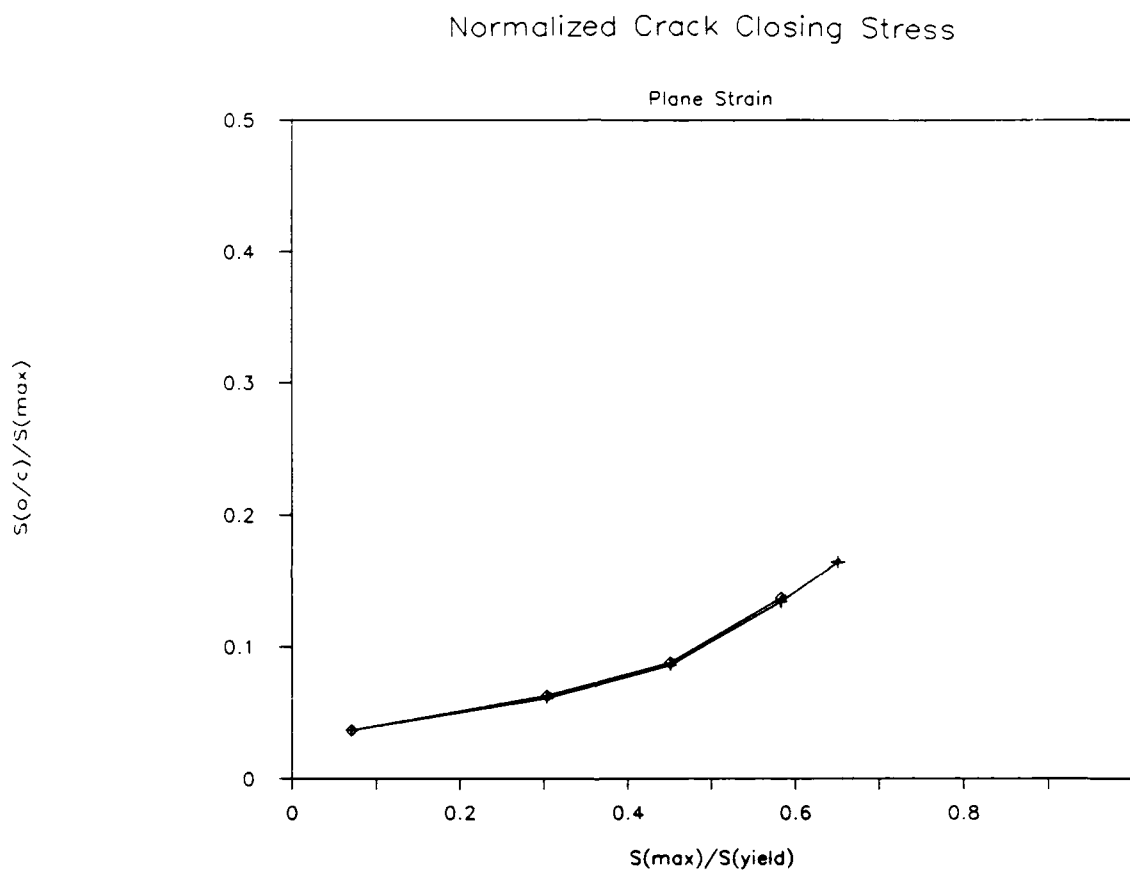
Figure 20.   Crack Closing Stresses at Stable State--
Plane Strain, Constant K (max)
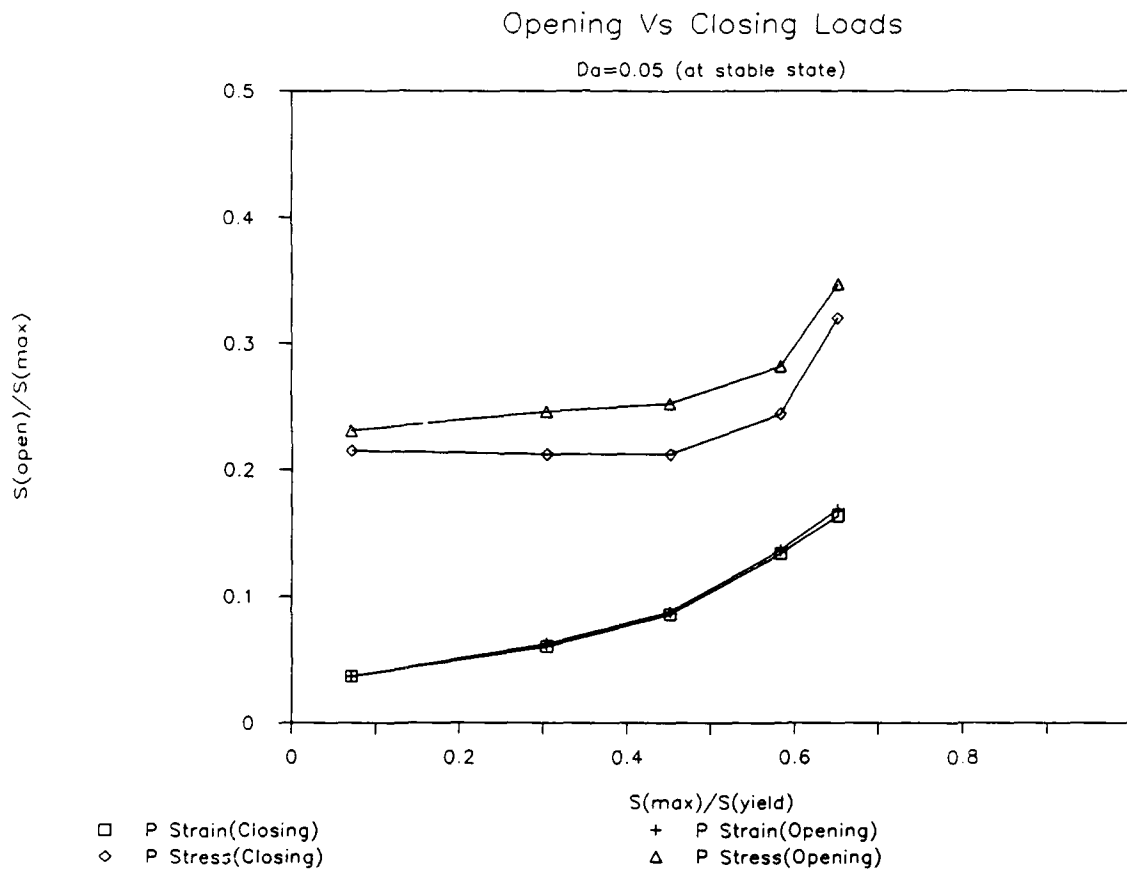
Figure 21. A Comparison of Crack Closing and Opening Stresses at Stable State

2.4.2 Constant Stress Amplitude Loading

The same investigation was conducted at constant stress loading. The normalized crack closing stresses for various crack extensions are plotted in Figure 22 for the plane stress case and in Figure 23 for the plane strain case. The results seem to stabilize after about 10 crack increments, however, the stabilization is weaker for this loading than the constant K loading reported earlier, especially for short crack cases. The normalized crack closing stresses for various stress amplitudes for the plane stress case shown in Figure 24 indicate that the closing stresses decrease with increasing applied maximum loads, which is consistent with the results reported by McClung [30] and Ogura, et al., [33] for high stress amplitudes. The plane strain results in Figure 25 also indicate decrease in closing stresses at high stress amplitudes.

It should be noted that there are discrepancies in the modeling approaches used by the finite element method [30,33] and the current BEM approach. In the finite element method the crack extension was simulated by a node release scheme at the maximum load level and the crack opening stresses were computed during the subsequent loading cycle. In the current approach the crack was extended to zero load and the closing levels were monitored during the unloading cycle. Also, in the finite element scheme, the crack surface at contact was fixed against further displacement in the plane normal to the crack surface, whereas the cracks were allowed to interpenetrate in the BEM modeling. While the first modeling inconsistency is not expected to have substantial influence on the results, the second modeling difference may be the cause of the discrepancies in the results, since the premature closing of crack changes the crack tip locations. The crack tip singularity which drives the reversed plastic strain effectively vanishes at the initial crack tip, as a consequence, the development of reversed plastic strain is greatly restrained. Nevertheless, the fact that different crack opening/closing

CRACK CLOSING STRESSES
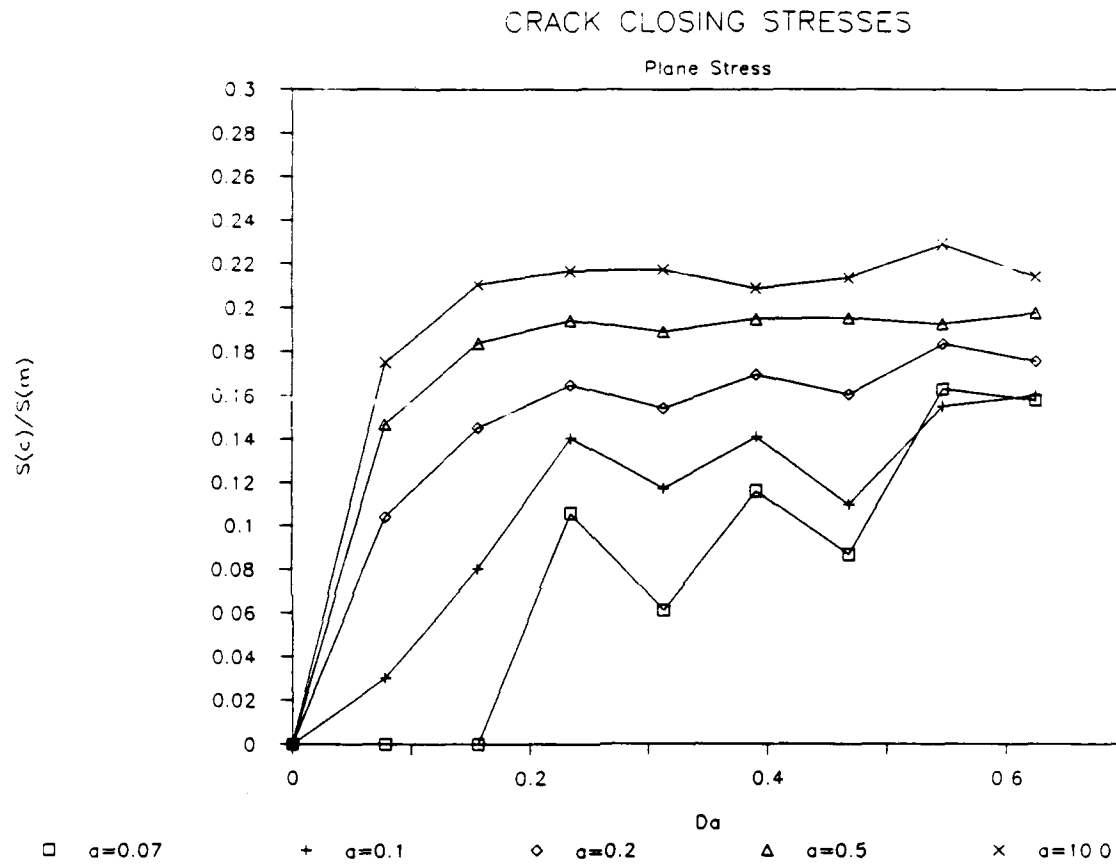
Plane Stress

Figure 22. Crack Closing Stresses--
Plane Stress, Constant S (max)

CRACK CLOSING STRESSES
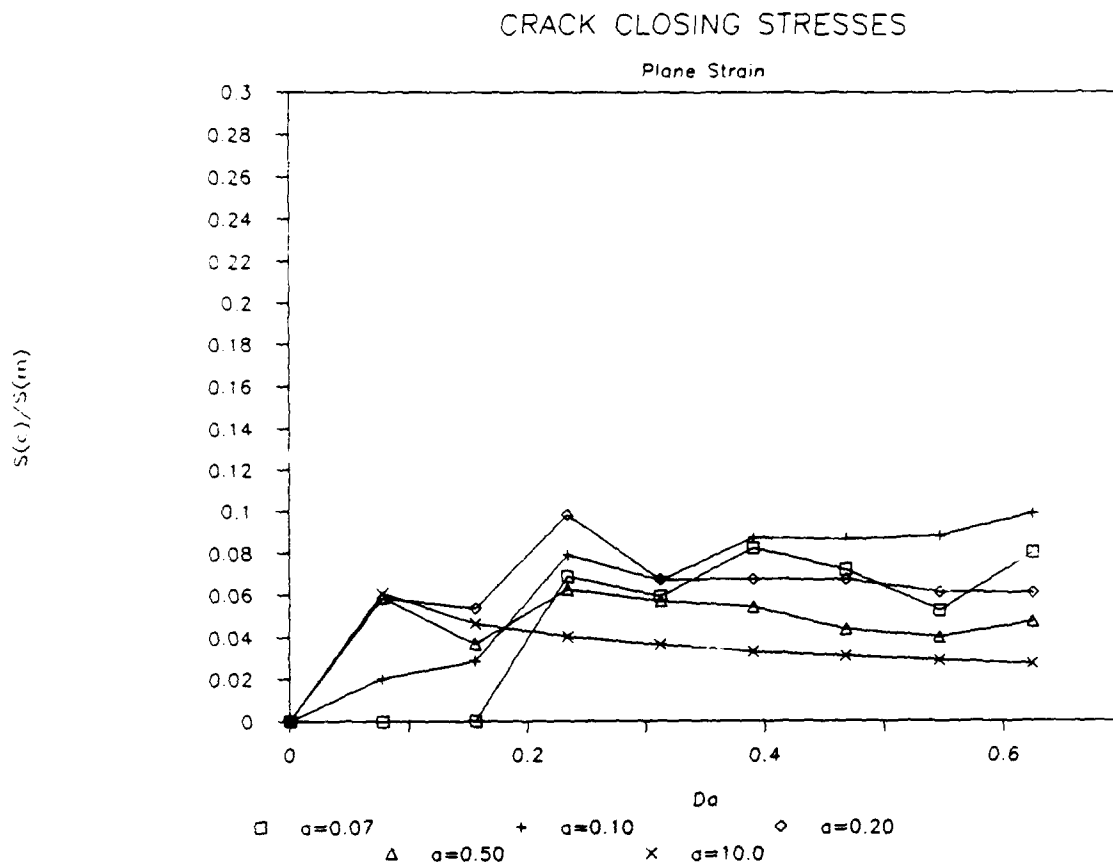
Figure 23.   Crack Closing Stresses--
Plane Strain, Constant S (max)
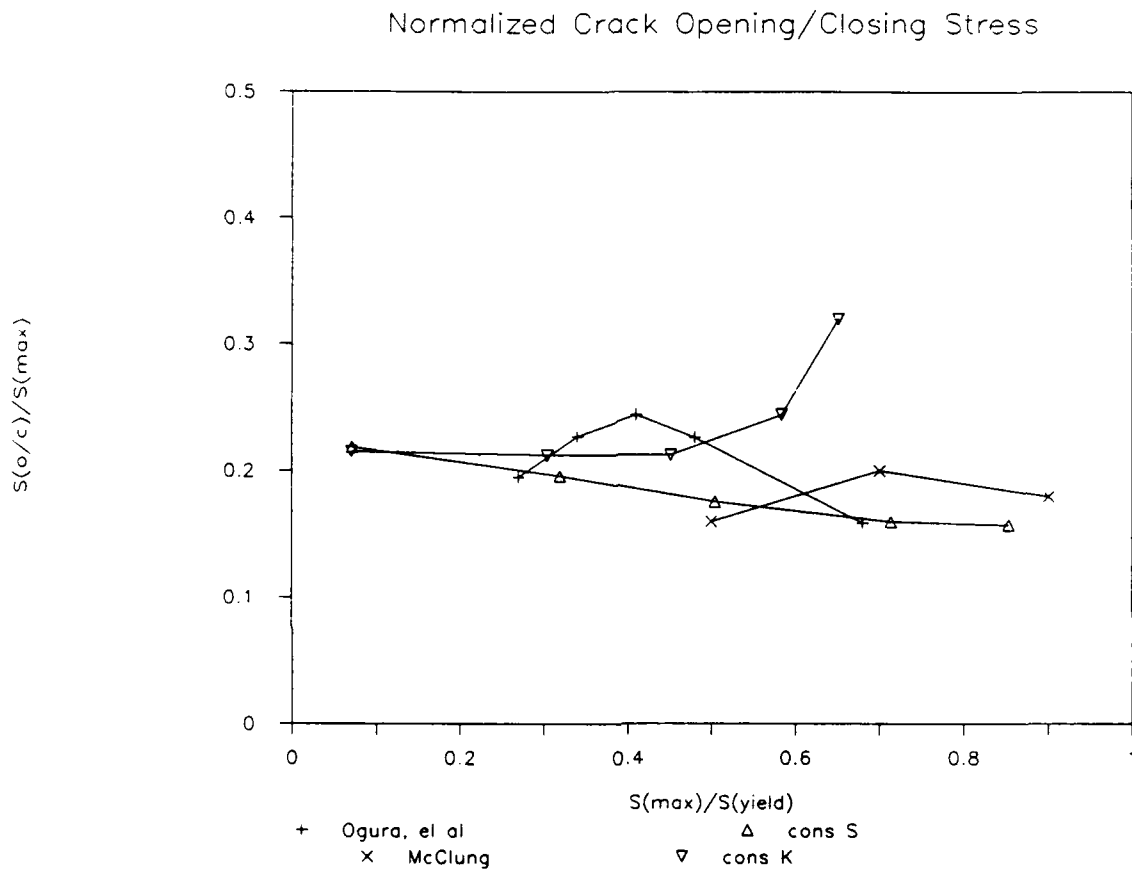
Figure 24. Comparison of Crack Opening/Closing Stresses for
Constant K and Constant S Cases--Plane Stress

Normalized Crack Closing Stress
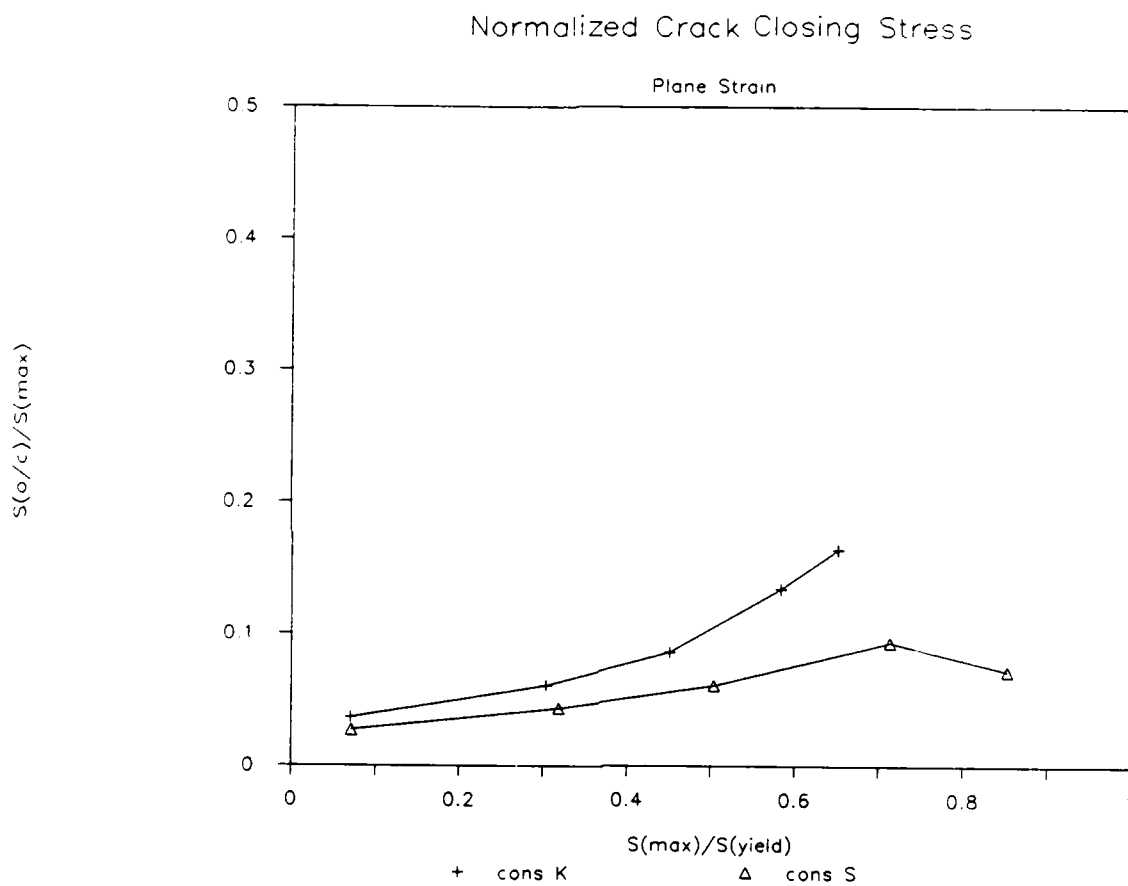
Figure 25. Comparison of Crack Opening/Closing Stresses for Constant K and Constant S Cases--Plane Strain

behavior for different loading situation (i.e., constant S(max) vs. constant K(max)) using the same approach suggests different correlation between crack opening/closing stress and maximum stress amplitude.

2.4.3 Long vs. Short Crack Results

Of the crack cases considered, two situations corresponding to crack lengths of 10 in. and 0.1 in. were studied in detail. The long crack case corresponds to a ratio of applied maximum stress to yield stress of about 0.71 and the short case corresponds to a ratio of 0.07. Given a reasonable assumption that cyclic crack extension is associated with crack tip deformation, thereby, with the crack opening displacements, the results reported earlier for the long crack plane strain constant K case (Figure 13) predict that the crack responds in accordance with LEFM. The same conclusion can be drawn from the normalized crack opening displacement for the constant stress case plotted in Figure 26.

The short crack results in Figure 14 and 16 for the constant K case and in Figures 27 and 28 for the constant stress case show the effect of plastic wake on COD at the region near the crack tip as a result of high, unreversed crack tip stretch plasticity. The plane stress results for both long (Figures 15 for constant K, and Figure 29 for constant S) and short (Figure 16 for constant K, and Figure 28 for constant S) cracks show enduring plastic wake for both cases. The higher stretch within the scale of the cyclic crack tip zone than the LEFM prediction may provide the mechanics for increased short crack fatigue crack growth.

On the other hand, the measure of the closure, evaluated in terms of crack opening/closing stress levels, does not seem to provide the explanation for fatigue crack growth. The amount of plastic wake affects crack closure, but the closure seems not to be the cause of increased fatigue crack damage. Yet, the amount of closure is an indication of the excess crack tip damage and
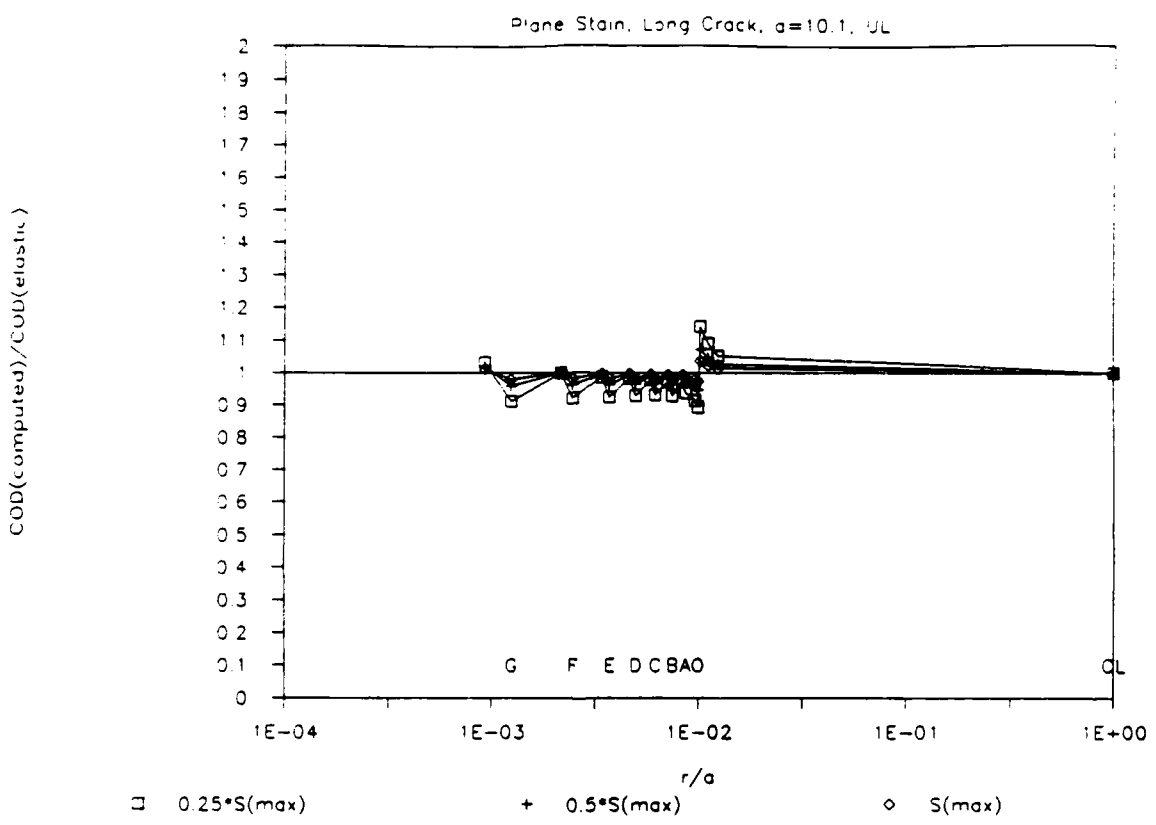
Figure 26. Normalized COD--Plane Strain, Long Crack, Constant S (max)
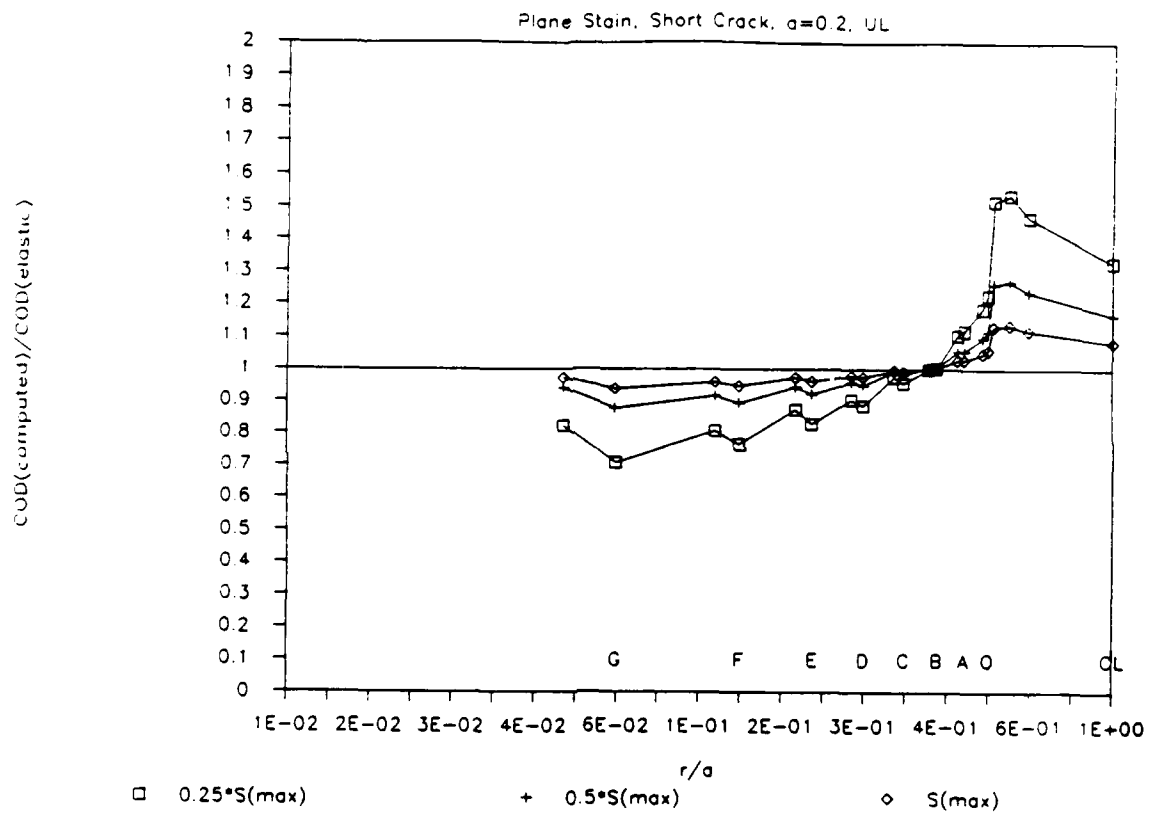
Figure 27. Normalized COD--Plane Strain,
Short Crack, Constant S (max)
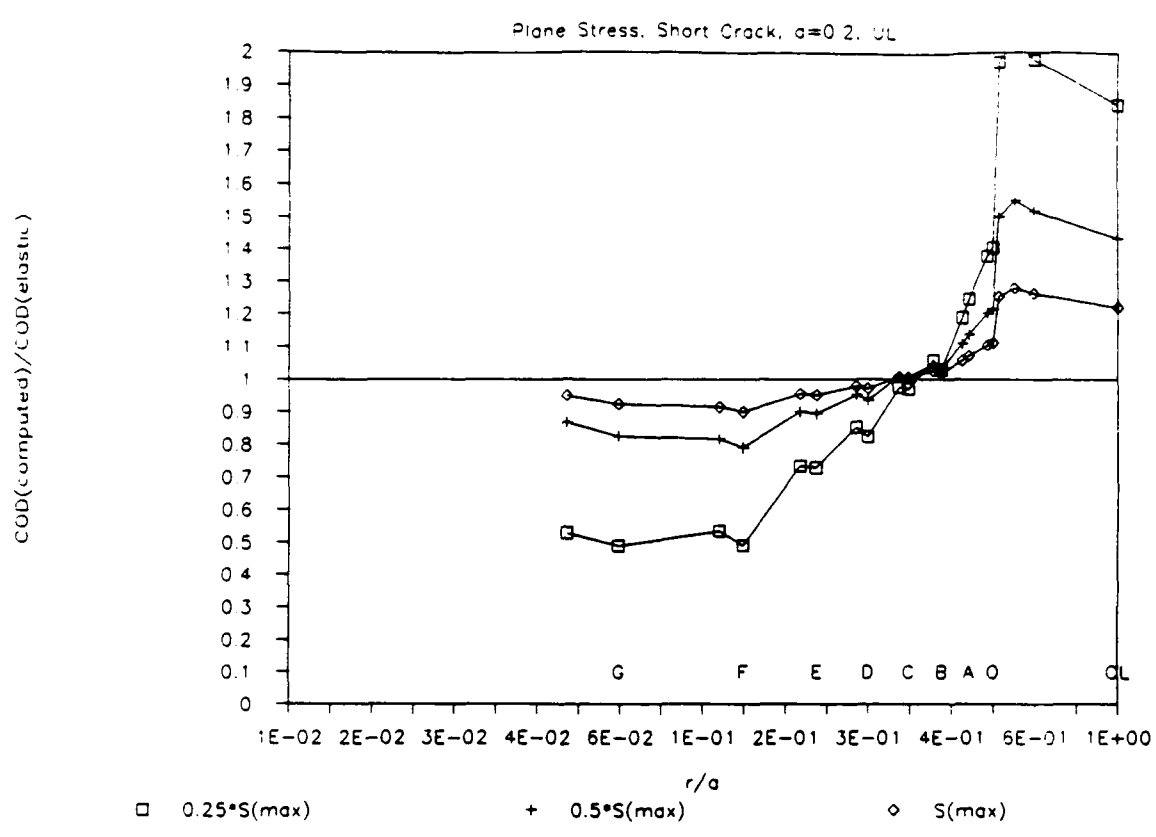
Figure 28. Normalized COD--Plane Stress,
Short Crack, Constant S (max)
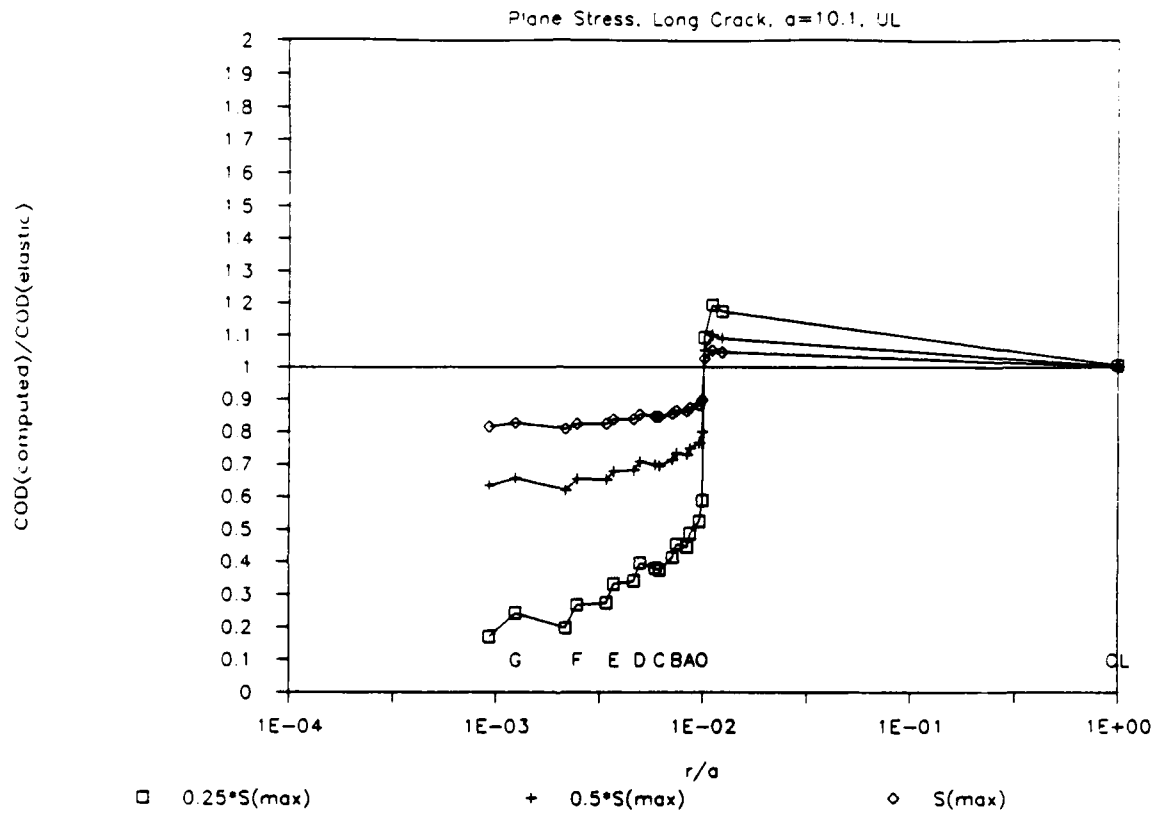
Figure 29. Normalized COD--Plane Stress,
Long Crack, Constant S (max)

thus serve, in a secondary manner, as a correlating parameter for short crack growth rate data. It is hypothesized that stretch, rather than closure is the concern in predicting the short crack growth rates observed in testing.

3.0 THREE-DIMENSIONAL FRACTURE MECHANICS MODELING

3.1 Overview of LEFM and BEM Analysis

Material deficiencies in the form of pre-existing flaws initiate cracks and fractures in structures. The presence of a crack in structural element generally induces high stress concentration at the crack tip and thereby reduces the strength of the structure. Fracture mechanics provide satisfactory means for the characterization of this local crack tip stress fields as well as the elastic deformations of the material in the neighborhood of the crack. In LEFM, the inelastic deformation in the vicinity of the crack tip due to stress concentrations is deemed to be small compared to the size of the crack and other characteristic lengths.

Elastic modeling of crack tip behavior makes use of deformation due to three primary modes of loading as illustrated in Figure 30. The three modes are: the opening mode (Mode I) due to normal stress, sliding mode (Mode II) due to in-plane shear stress, and tearing mode (Mode III), due to out-of-plane shear.

Consider the crack problem of Figure 31, representing an infinite plate under triaxial stress. The stresses and displacements for traction free cracks may be given as an infinite series in r, where r is the distance from the crack tip. For the antiplane problem (see [6]), the near crack tip field is given by:

$$\begin{Bmatrix} \sigma_{31} \\ \sigma_{32} \end{Bmatrix} = \frac{K_{III}}{(2\pi r)^{1/2}} \begin{Bmatrix} \sin(\theta/2) \\ \cos(\theta/2) \end{Bmatrix} \tag{5}$$

and

$$u_3 = \frac{2K_{III}}{\mu}(\frac{r}{2\pi})^{1/2} \sin(\theta/2) \tag{6}$$

Mode I   **Mode II**   **Mode III**
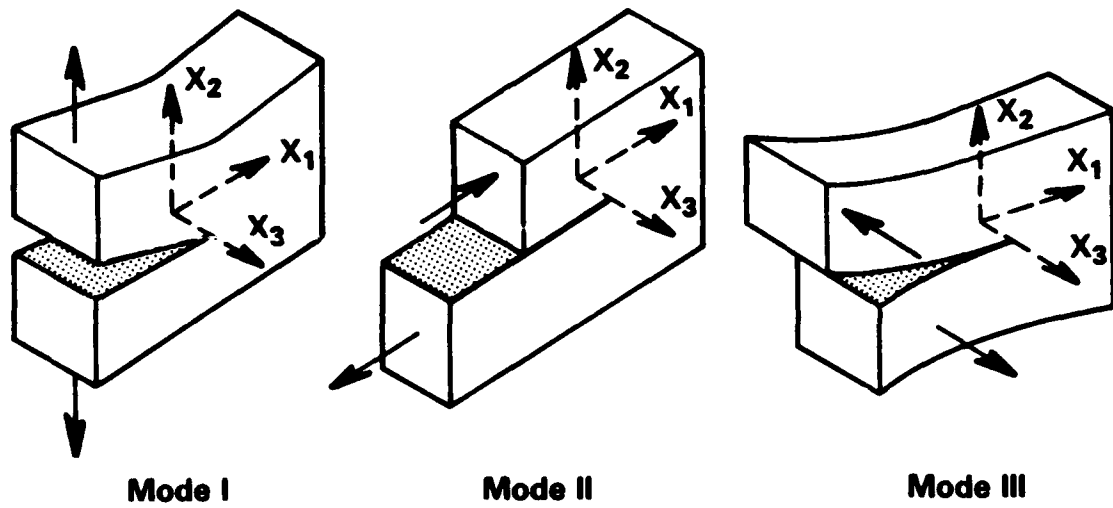
Figure 30.   Three Primary Loading Modes of a Cracked Body
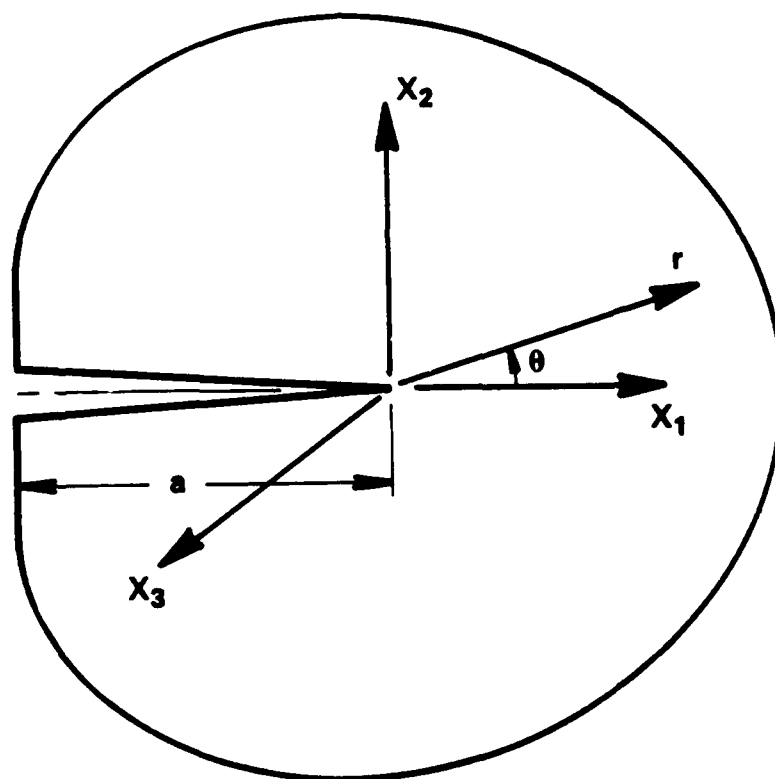
Figure 31. Infinite Plate Under Triaxial Load

where u_i is the displacement, σ_{ij} is the stress and μ is the shear modulus. The Mode III stress intensity factor, K_{III}, is established by the far field boundary conditions and is a function of applied loading and the geometry of the cracked body. The Mode III stress intensity factor is defined by:

$$K_{III} = \lim_{r \to 0} \left\{ (2\pi r)^{1/2} \sigma_{32} \Big|_{\theta = 0} \right\} \tag{7}$$

For the plane problem, assuming plane strain conditions,

$$\begin{Bmatrix} \sigma_{11} \\ \sigma_{12} \\ \sigma_{22} \end{Bmatrix} = \frac{K_I}{(2\pi r)^{1/2}} \cos(\theta/2) \begin{Bmatrix} 1 - \sin(\theta/2)\sin(3\theta/2) \\ \sin(\theta/2)\cos(3\theta/2) \\ 1 + \sin(\theta/2)\sin(3\theta/2) \end{Bmatrix} \tag{8}$$

and

$$\begin{Bmatrix} u_1 \\ u_2 \end{Bmatrix} = \frac{K_I}{2\mu} \left(\frac{r}{2\pi}\right)^{1/2} \begin{Bmatrix} \cos(\theta/2) [k - 1 + 2\sin^2(\theta/2)] \\ \sin(\theta/2) [k + 1 - 2\cos^2(\theta/2)] \end{Bmatrix} \tag{9}$$

where K_I is the Mode I stress intensity factor, defined by:

$$K_I = \lim_{r \to 0} \left\{ (2\pi r)^{1/2} \sigma_{22} \Big|_{\theta = 0} \right\} \tag{10}$$

and

$$k = 3 - 4\nu$$

The corresponding relationships for Mode II field are:

$$\begin{Bmatrix} \sigma_{11} \\ \sigma_{12} \\ \sigma_{22} \end{Bmatrix} = \frac{K_{II}}{(2\pi r)^{1/2}} \begin{Bmatrix} -\sin(\theta/2)[2+\cos(\theta/2)\cos(3\theta/2)] \\ \cos(\theta/2)[1-\sin(\theta/2)\sin(3\theta/2)] \\ \sin(\theta/2)\cos(\theta/2)\cos(3\theta/2) \end{Bmatrix} \quad (11)$$

$$\begin{Bmatrix} u_1 \\ u_2 \end{Bmatrix} = \frac{K_{II}}{2\mu}\left(\frac{r}{2\pi}\right)^{1/2} \begin{Bmatrix} \sin(\theta/2)[k+1+2\cos^2(\theta/2)] \\ -\cos(\theta/2)[k-1-2\sin^2(\theta/2)] \end{Bmatrix} \quad (12)$$

where Mode II stress intensity factor K_{II}, is defined by:

$$K_{II} = \lim_{r \to 0} \{(2\pi r)^{1/2}\sigma_{12}\big|_{\theta=0}\} \quad (13)$$

3.1.1 Boundary Element Method for Fracture Mechanics Analysis

The analytical basis of the method is the transformation of the governing equilibrium equation of an isotropic, homogeneous, elastic element by an integral identity, using Betti's reciprocal work theorem. The identity for the displacement at a point $P(x)$ is given by (e.g., [34]):

$$C_{ij}(P)u_j(P) = -\int_S T_{ij}(P,Q)u_j(Q)ds(Q) + \int_S U_{ij}(P,Q)t_j(Q)ds(Q) \quad (14)$$

where $t_i(Q)$ and $u_i(Q)$ are the boundary values of traction and displacement, $T_{ij}(P,Q)$ and $U_{ij}(P,Q)$ are tractions and displacements, respectively, in x_i directions at $Q(x)$ due to orthogonal unit loads in the x_j directions at $P(x)$. The discontinuity term C_{ij} is equal to 1/2 for smooth boundary points and can be evaluated indirectly using rigid body translation as described by Cruse [42], for non-smooth boundary points.

The utility of the method as a general practical solution tool is facilitated by two approximations; one is the description of the boundary S by

a finite number of surface elements, the second is the representation of the field variables (u_i, t_i) and geometry by known interpolation functions within individual elements. In the present analysis, triangular and quadrilateral elements are used for surface representation. The field variables, as well as geometry, are represented by isoparametric quadratic interpolation functions. Numerical evaluation of discretized integrals, as well as the use of special crack tip elements employed in the current analysis, are described in a later section.

3.1.2 BEM Modeling of Cracked Bodies

The numerical solution of Eq. (14) is straight-forward for a general three-dimensional stress analysis. However, the presence of two coplanar surfaces preclude the use of the method for general solution of cracked bodies. Therefore, several different modeling strategies have been employed for three-dimensional cracked bodies, as illustrated in Figure 32. The first approach is to model the crack as an open notch as reported by Cruse (41). The major deficiency of this modeling approach is that the results become inaccurate when the surfaces are modeled too far apart, however, the system equation becomes badly conditioned when the surfaces are modeled too close together. One form of avoiding this difficulty is the dislocation or traction BIE modeling approach as developed in different forms by Cruse [42], Guidera and Lardner [45], Bui [38] and Weaver [49]. The singular nature of the integrals is this method poses difficulty in the numerical implementation as reported by these authors. Significant improvements have been reported recently by Polch, et al. [48] and others. However, further research is required before the full potential of this utility can be realized.

Modeling of symmetric cracks is rather straight-forward since only a symmetric part of the body that contains one crack surface needs to be modeled. Earlier application of this modeling has been reported by Cruse and VanBuren [40], Cruse [42], and Cruse and Meyers [44]. These results have been subsequently improved by using isoparametric interpolation functions by Cruse
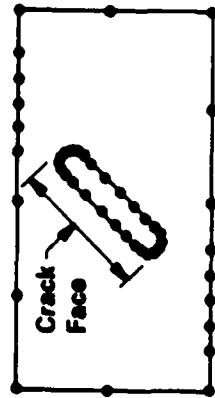
(a) Open Notch Modeling
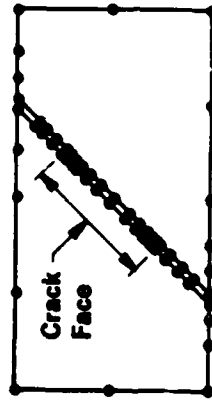
(b) Multi-region Modeling
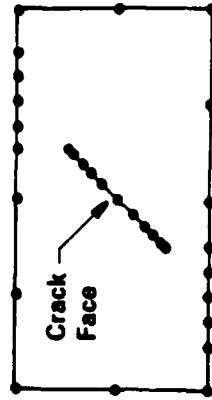
(c) Dislocation or Traction BIE Modeling

Figure 32. BEM Modeling Strategies for Three-Dimensional Cracks

and Wilson [43]. The accuracy of the results has been further improved by the use of special crack tip elements that accurately model the crack tip field. Improved results using higher order interpolation functions for geometry and field variables and special crack tip elements are also reported by Cruse and Wilson [43]. A detailed description of special crack tip elements is given in the following section.

A modeling strategy applicable for a general three-dimensional non-symmetric crack is the sub-region model. In this approach, the body is substructured into separate regions through the crack plane such that each crack surface is in a different region. The overall solution is obtained by satisfying compatibility and continuity conditions at the interface of the regions except along the crack surface. Numerical results using this strategy for two-dimensional structures have been reported by Blandford, et al. [37]. Results for three-dimensional bodies are reported in Section 3.2.

3.1.3 Use of Singular Elements

The accuracy of the numerical computations is enhanced by proper representation of the field variables in the vicinity of the crack tip. It is well-known that the crack tip opening displacement varies with square of the distance (r) from the crack tip, whereas, the stresses produce $1/\sqrt{r}$ singularity. The crack tip elements are modified such that they capture these variations.

It has been observed by Barsoum [36] that the placement of midpoint nodes of the element sides emanating from the crack tip at quarter points leads to the required displacement and stress variation in the finite element method. By using quarter point (QP) elements (Figure 33) on both sides of the crack in BEM, the displacements and tractions are made to vary in physical space as:

$$\left\{ \begin{array}{c} u(r) \\ t(r) \end{array} \right\} = A_1 + A_2 \sqrt{(r/\ell)} + A_3 (r/\ell) \tag{15}$$
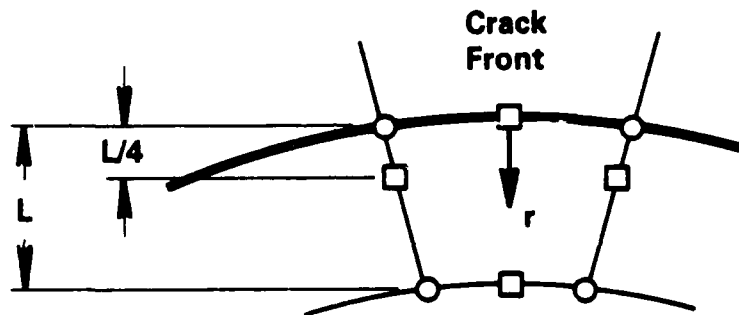
Figure 33. Crack-Tip Elements

where r is the normal distance from the crack tip, l is the element length in that direction, and A_1, A_2, A_3 are functions of nodal displacements or tractions. However, unlike the finite element method in which the tractions (or stresses) are derived from the spatial derivative of displacements, the displacements and tractions are independently approximated in BEM. The use of quarter point elements on both sides of the crack front, thus, will give the same variation for both displacements and tractions and, therefore, Eq. (15) does not give the required singularity for crack tip tractions. The simplest way to obtain this singularity appears through the use of singular shape functions. However, the numerical integration scheme employed in the current analysis requires subsegmentation of elements, as described in the following section, which makes the implementation difficult. Instead, the traction singularity is contrived by the multiplication of shape function by a non-dimensional parameter $\sqrt{(l/r)}$ as:

$$t(r) = \sqrt{(l/r)} \cdot \hat{t} \tag{16}$$

where $\hat{t}$ is the normal traction defined by equation (15). The variation of traction in these traction singular (TS) elements is then given by:

$$t(r) = \frac{A_1}{\sqrt{(r/l)}} + A_2 + A_3 (r/l)^{1/2} \tag{17}$$

The use of these special elements improve the accuracy substantially as seen by the numerical results reported herein.

3.1.4 Stress Intensity Factor Evaluations

The stress intensity factors may be computed using displacements or traction BEM solution from Eqs. 5-14. Mode I and Mode II stress intensity factors are computed from:

$$K_{I \text{ or } II} = \frac{\mu}{4(1-\nu)} \sqrt{(\frac{2\pi}{r})} u_{I \text{ or } II}(r) \qquad (18)$$

where u_I and u_{II} are decoupled displacements along Mode I and Mode II directions at the quarter point, and r is the distance of the quarter point from the crack front. Mode III stress intensity factors may be computed similarly from:

$$K_{III} = \frac{\mu}{4} \sqrt{(\frac{2\pi}{r})} u_{III}(r) \qquad (19)$$

Alternatively, the stress intensity factors can be computed from decoupled tractions at the crack front. As an example, the Mode III stress intensity factor may be evaluated from:

$$K_{III} = \sqrt{(2\pi\ell)} \hat{t}_{III} \qquad (20)$$

where t_{III} is the decoupled nominal traction defined by Eq. (16). However, in the present analysis, the stress intensity factors are computed using quarter point displacements (Eqs. (18) and (19)), since the values using crack front tractions (Eq. (20)) generally over-estimated the stress intensity factors by about 10%. It is believed that one of the reasons for the discrepancy may be that higher accuracy is needed for the integration of traction singular element than the one used in the present analysis. Another reason may be that, though the first term in Eq. (17) provides the required singularity, the higher order terms of standard quadratic element expression (15), through traction singular modification, are the suitable ones for the representation

of traction variation. However, the use of traction singular modification with quarter point elements improved the accuracy of the displacement based stress intensity factors and are, therefore, used in the current analysis.

3.1.5 Evaluation of Discretized Boundary Integrals

In the present analysis, the geometry as well as field variables are represented by isoparametric quadratic shape functions. The use of higher order interpolation functions, in general, preclude the use of analytical integration and, therefore, numerical quadrature is used in the current development. Non-singular Kernel function-shape function products, in principle, can be directly approximated by the application of Gauss-Legendre quadrature formula. However, to maintain a certain level of accuracy, element subdivision may be required. Following Lachat and Watson [46], the minimum element side length for a given error tolerance and quadrature order is determined from error analysis. The element is then subdivided to satisfy this requirement.

The non-singular integration is performed through a polar coordinate transformation which eliminates the singularity. To accomplish this, the element is subdivided through the singular point and the polar coordinate system is constructed through the singular apex as described by Banerjee and Raveendra [35].

To achieve the required crack tip field variation, considerable mesh refinement at crack tip is necessary. Because of this non-gradual mesh refinement, the subdivision scheme employed for non-singular integration does not always work efficiently. In order to avoid a large number of subdivisions, a modified singular integration scheme is used for these non-singular integrations.

3.2 Numerical Modeling of Elastic Crack

The solution procedure outlined in the previous section has been applied for the solution of many symmetric and non-symmetric cracked specimens. The numerical solutions obtained by using the current computer code CRX3D are validated against known analytical solutions, in some cases, and are compared to finite element solutions in other cases.

3.2.1 Circular Crack

Figure 34 shows the BEM map used for the analysis of a buried circular crack problem. Due to symmetry, only one-eighth of the body was modeled. In addition, the symmetric planes of the body were not modeled. The crack opening displacements using standard quadratic element and modified crack tip elements are compared to analytical results in Figure 35 which indicate that the results are improved by the use of modified crack tip elements. The analytical solution plotted in the figure is for an infinite body. To further assess the accuracy, the Mode I stress intensity factors were evaluated for standard and modified crack-tip element models. A comparison with the empirical value that takes the finite dimension of body into account demonstrated that the stress intensity factors using quarter point element (QP) is approximately 5% in error, compared to standard element results which is approximately 10% in error. Further enhancement was obtained by using traction singular (TS) modification to the quarter point element, which improved the stress intensity factor value to within 1% of the predicted value.

3.2.2 Elliptical Surface Crack

Figure 36 shows the BEM map for one-fourth of a finite cracked plate. Whereas the symmetric Y-Z plane was not modeled, the X-Z plane was modeled to allow the solution of elliptic buried and semi-elliptic surface cracks to be modeled by a change in boundary condition. Figure 37 shows the normalized Mode I stress intensity factor for buried crack using modified
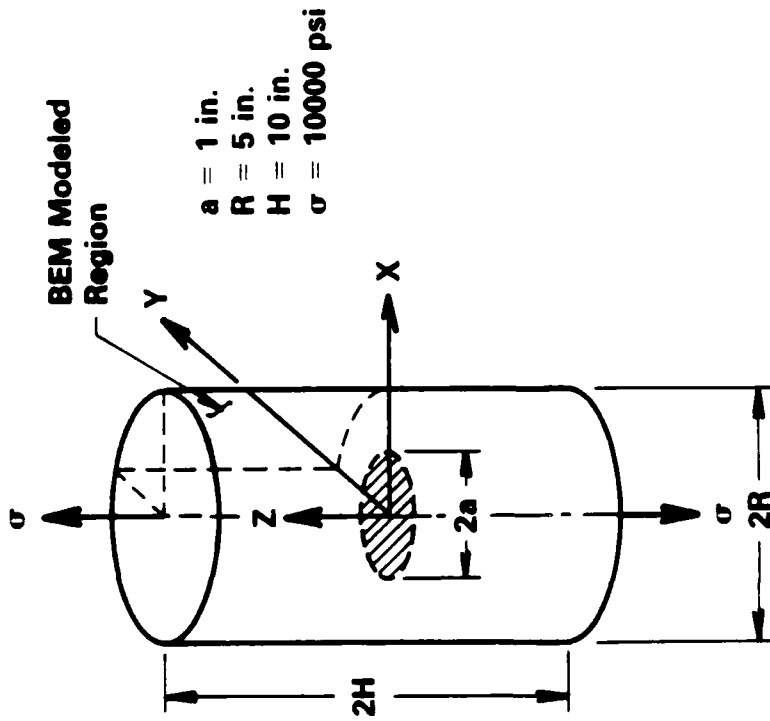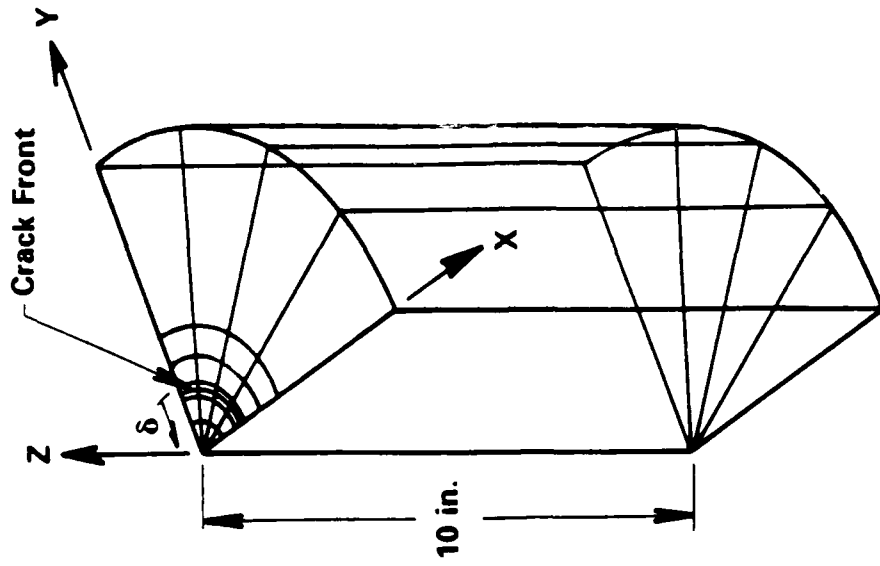
Figure 34. Cricular Crack--BEM Map
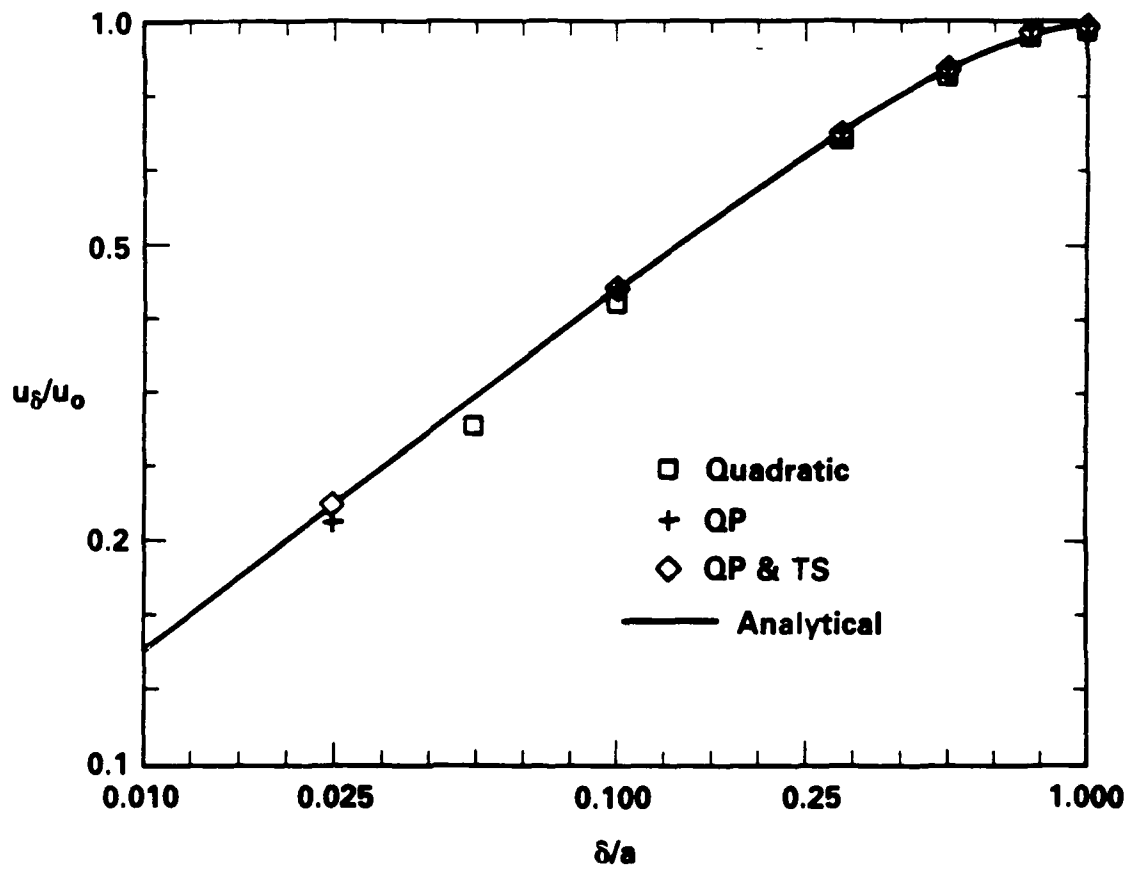
Figure 35. Crack Opening Displacement for Circular Crack

BEM Modeled Region

c = 2 in.
a = 1 in.
W = 20 in.
H = 20 in.
t = 4 in.
σ = 1000 psi
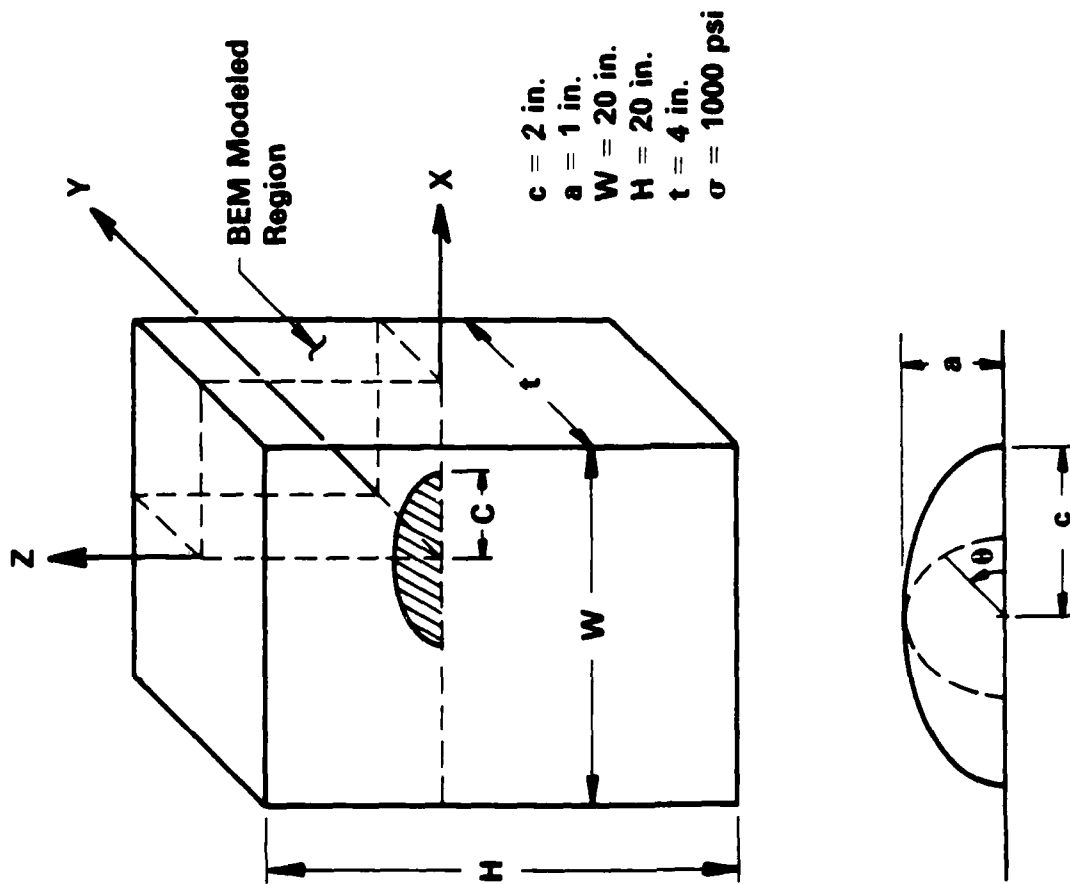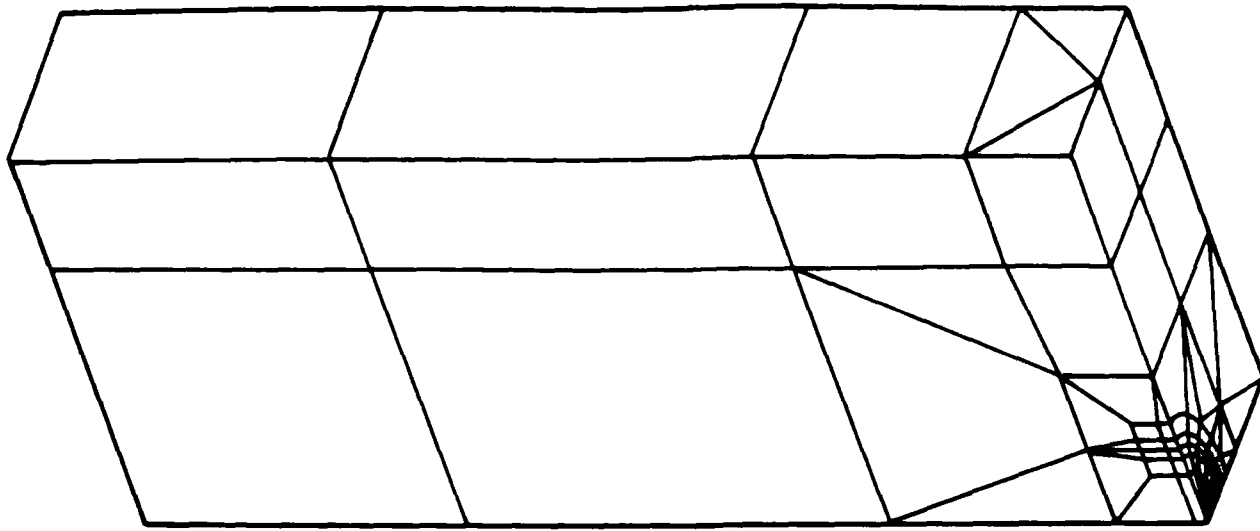
Figure 36. Elliptical Crack--BEM Map
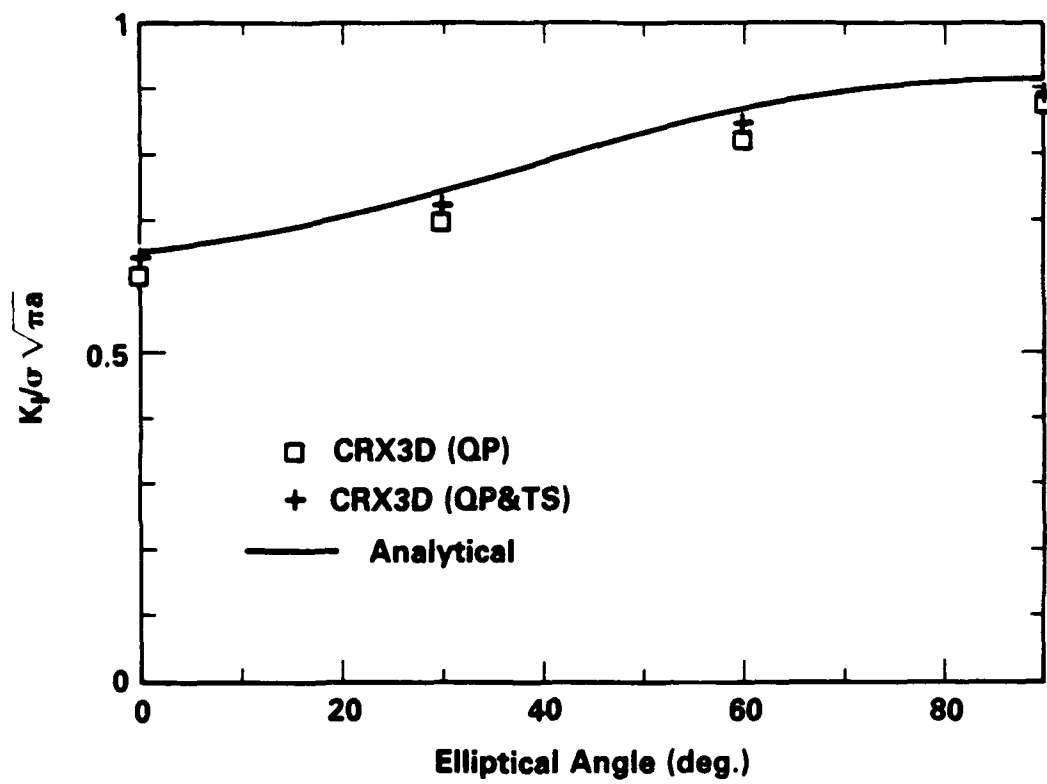
Figure 37. Mode I Stress Intensity Factor for Buried Elliptical Crack

crack tip elements compared to the finite body solution. The figure indicates that the accuracy of the solution was again improved by the use of the traction singular model.

The semi-elliptic surface crack model was subjected to both tensile and bending loads. Figures 38 and 39 show good agreement between CRX3D results and the empirical Mode I stress intensity factors provided by Newman and Raju [47] for both loading cases.

3.2.3 Inclined Circular Crack

Due to the symmetry, only one surface of the crack was modeled in the previous examples. However, as explained in the previous section, the non-symmetric cracks were modeled using subregion modeling strategy. CRX3D code was validated for non-symmetric crack cases by analyzing a circular crack which is inclined 45% to the loading direction. Figure 40 shows the BEM model of one-half of the cracked body. Stress intensity factors for all three modes compared well to the infinite body analytical solution, as shown in Figure 41.

3.2.4 T-Joint with Elliptical Surface Flaw

The final example solved is a T-Joint section (Figure 42(a)) that comprises a part elliptic surface flaw. A BEM model of one-half of the body is shown in Figure 42(b)). Again, a substructure modeling strategy was used. The body was modeled into four subregions to further improve the accuracy. Figure 44 shows the Mode I stress intensity factor normalized with respect to a two-dimensional plane strain model result (Figure 43). The behavior indicates that while the stress intensity factor is higher at the free-surface of the body, the solution at the mid-surface is comparable to the two-dimensional solution as expected. Mode II and Mode III stress intensity factors are also computed for the model and are shown in Figure 45.
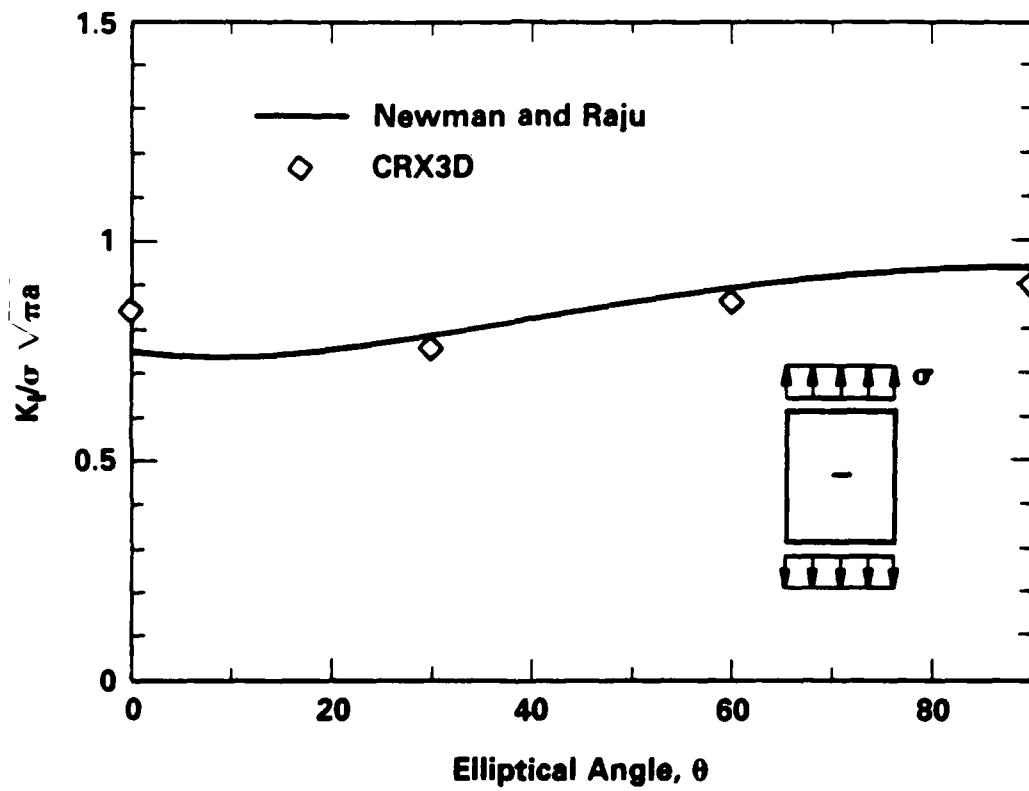
Figure 38. Mode I Stress Intensity Factor for
Semi-Elliptic Surface Crack--Tensile Load
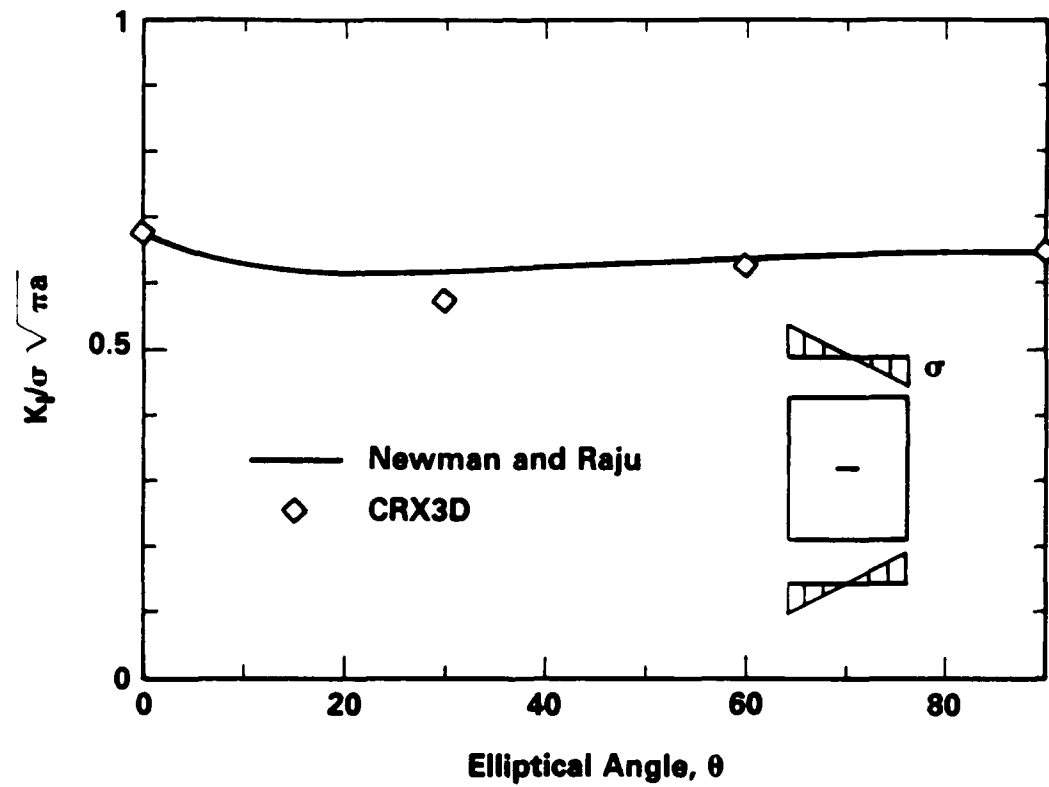
Figure 39. Mode I Stress Intensity Factor for
Semi-Elliptic Surface Crack—Bending Load
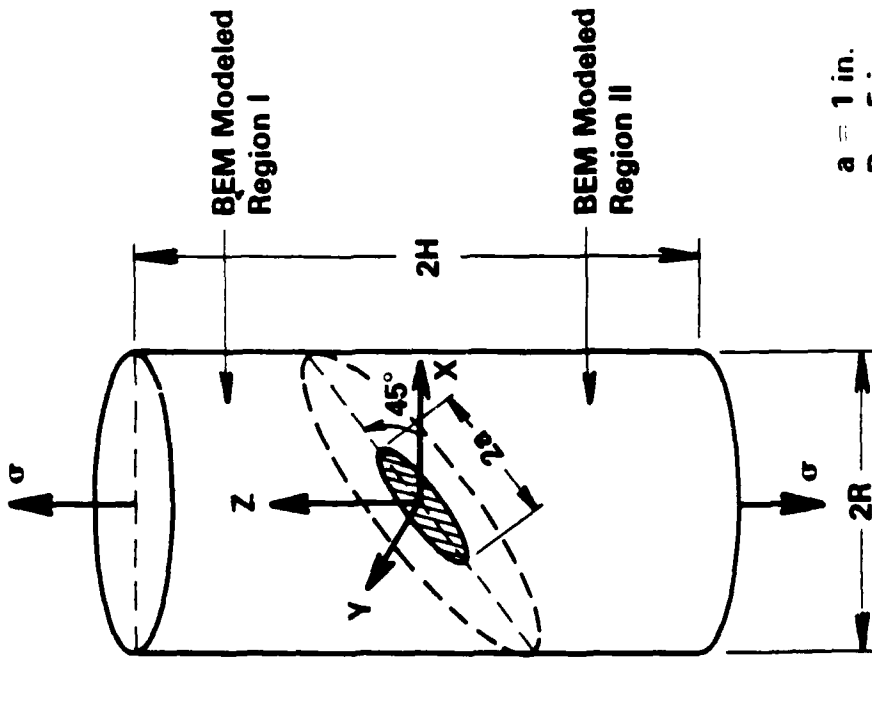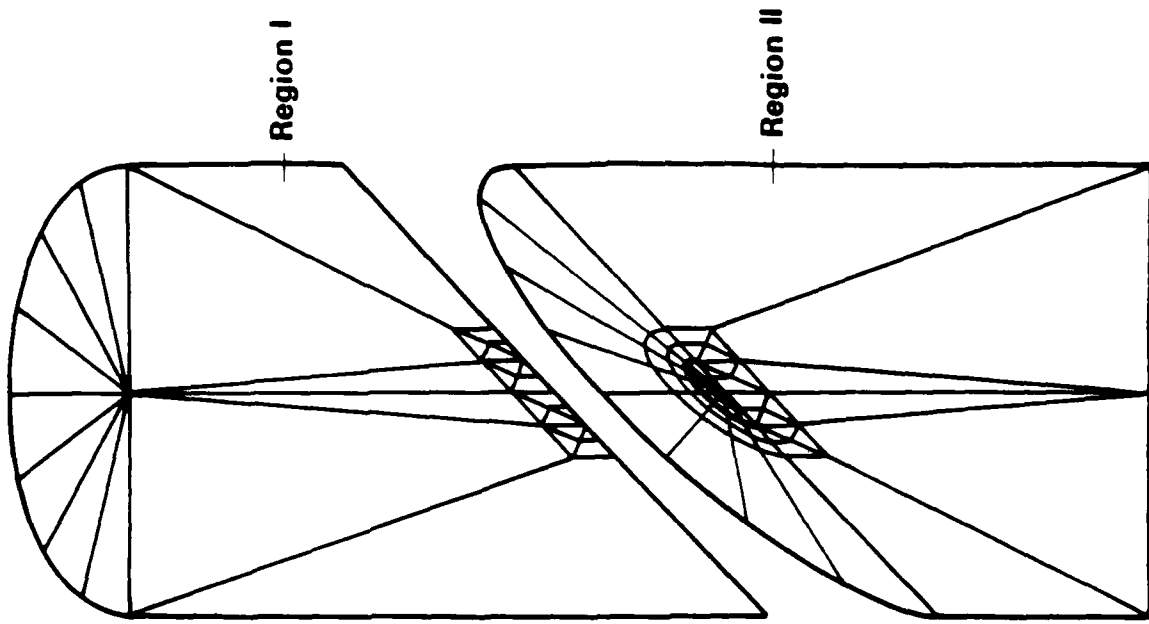
Figure 40. Inclined Circular Crack--BEM Map

BEM Modeled
Region I

2H

BEM Modeled
Region II

Region I

Region II

a = 1 in.
R = 5 in.
H = 10 in.
σ = 10000 psi

$$K_o = 2\sigma \sqrt{a/\pi}$$

+ K_I
△ K_{II}
▽ K_{III}
—— Analytical (Cherepanov, 1979)
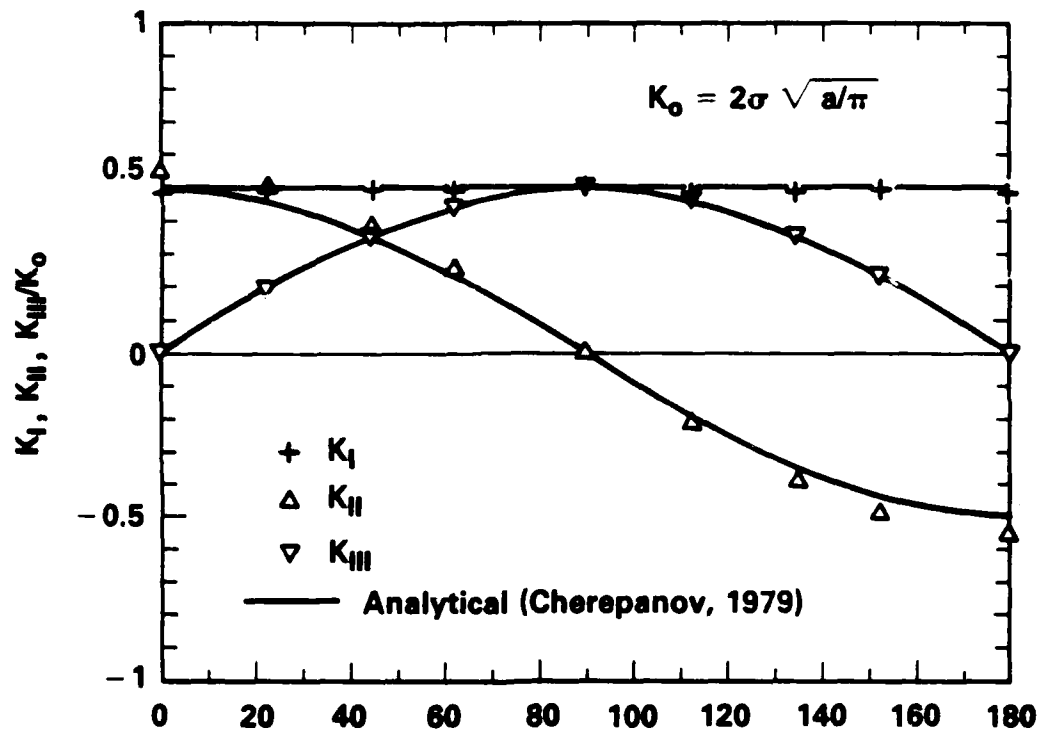
Figure 41. Stress Intensity Factors for Inclined Circular Crack
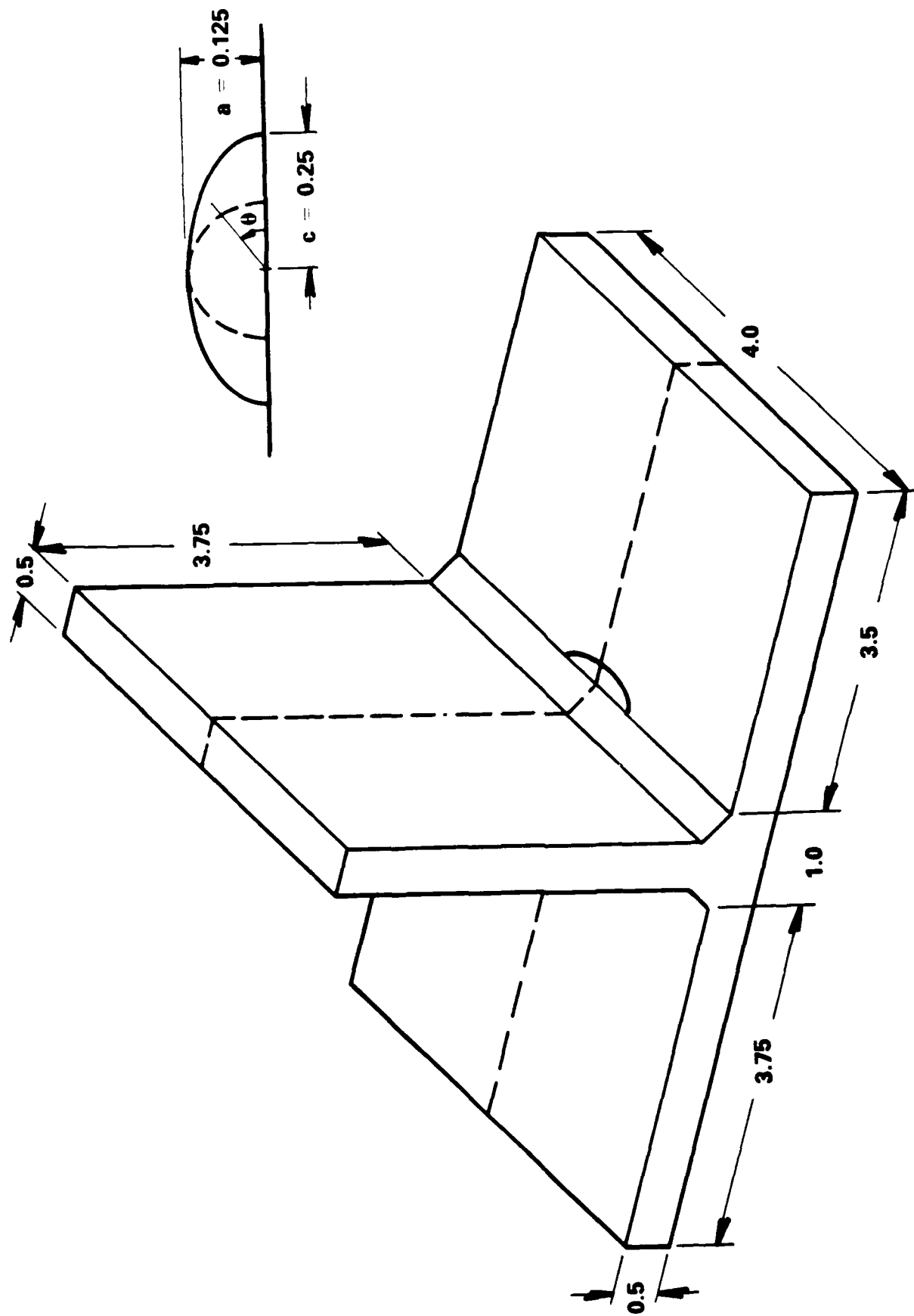
Figure 42(a). T-Joint Section with Elliptical Flaw

Region III

Region IV

Region II

Region I

Crack Front
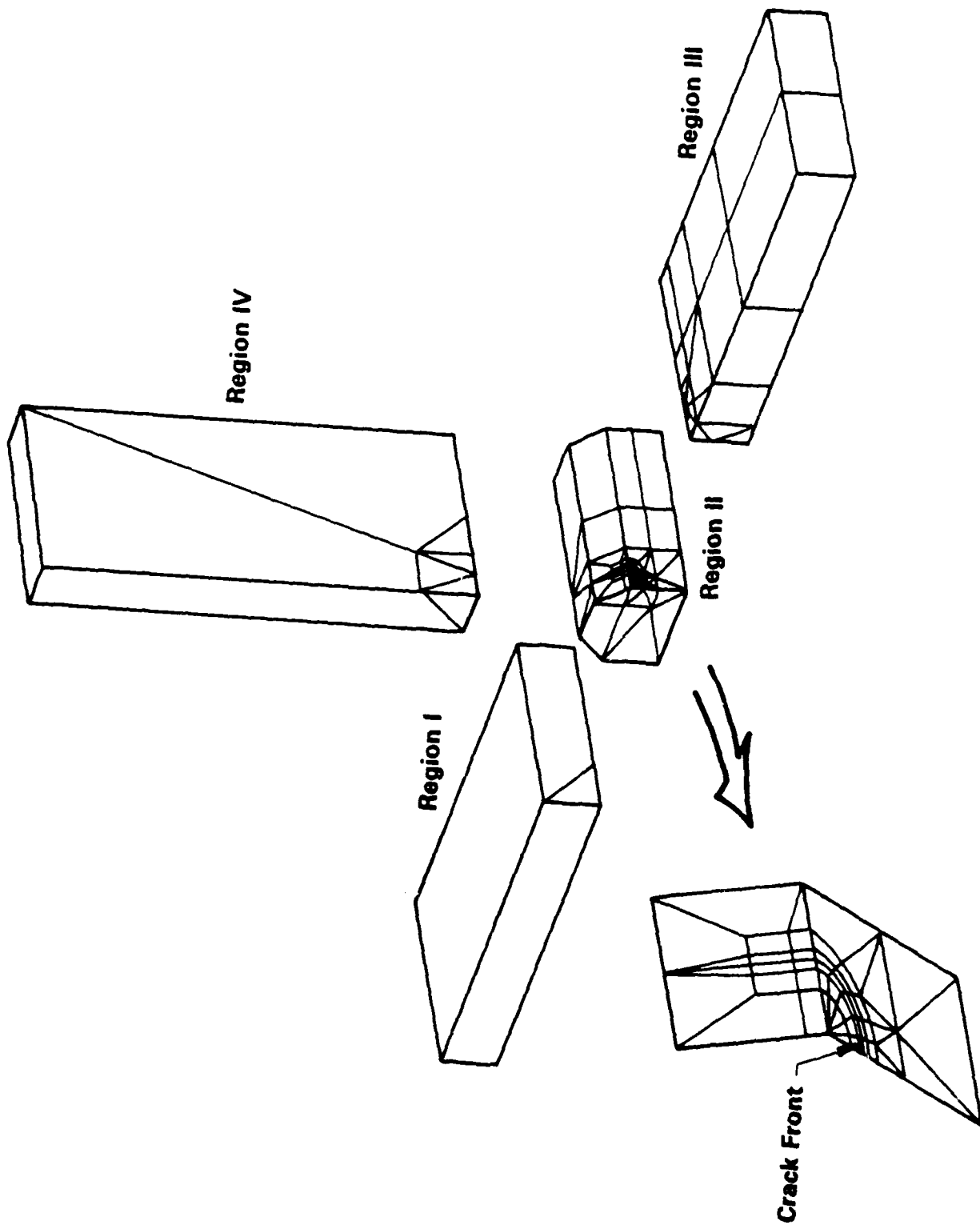
Figure 42(b). BEM Map for T-Joint Model
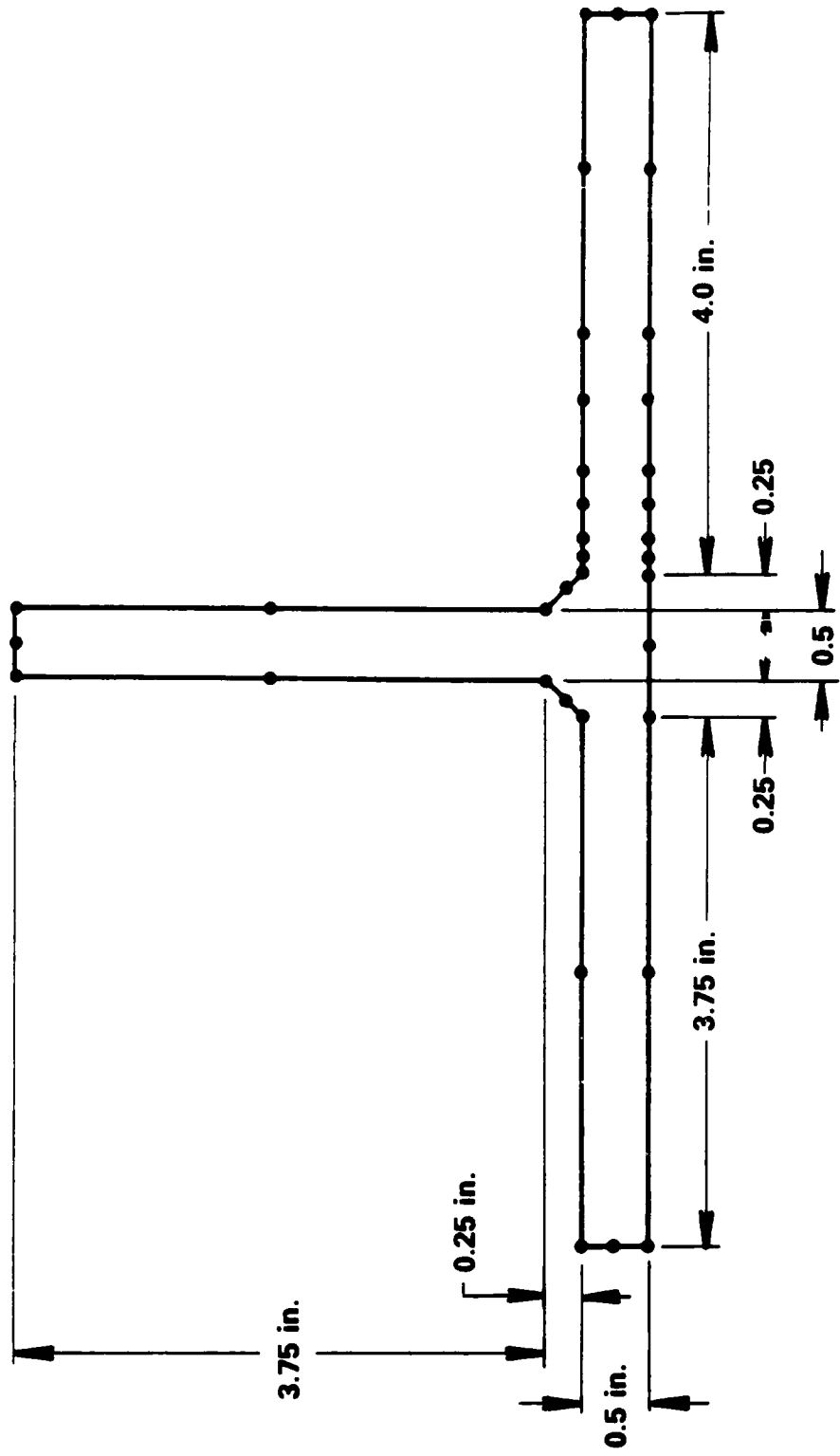
Figure 43. BEM Map for Plane Strain T-Joint Model
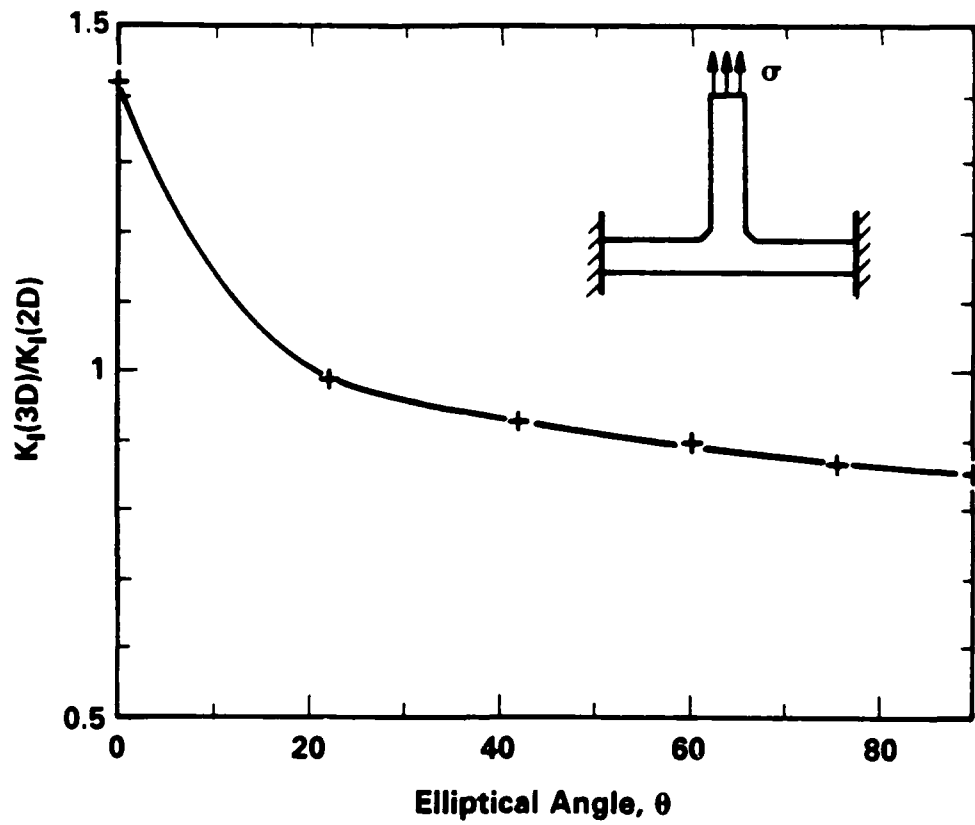
Figure 44. Mode I Stress Intensity Factor for T-Joint Model
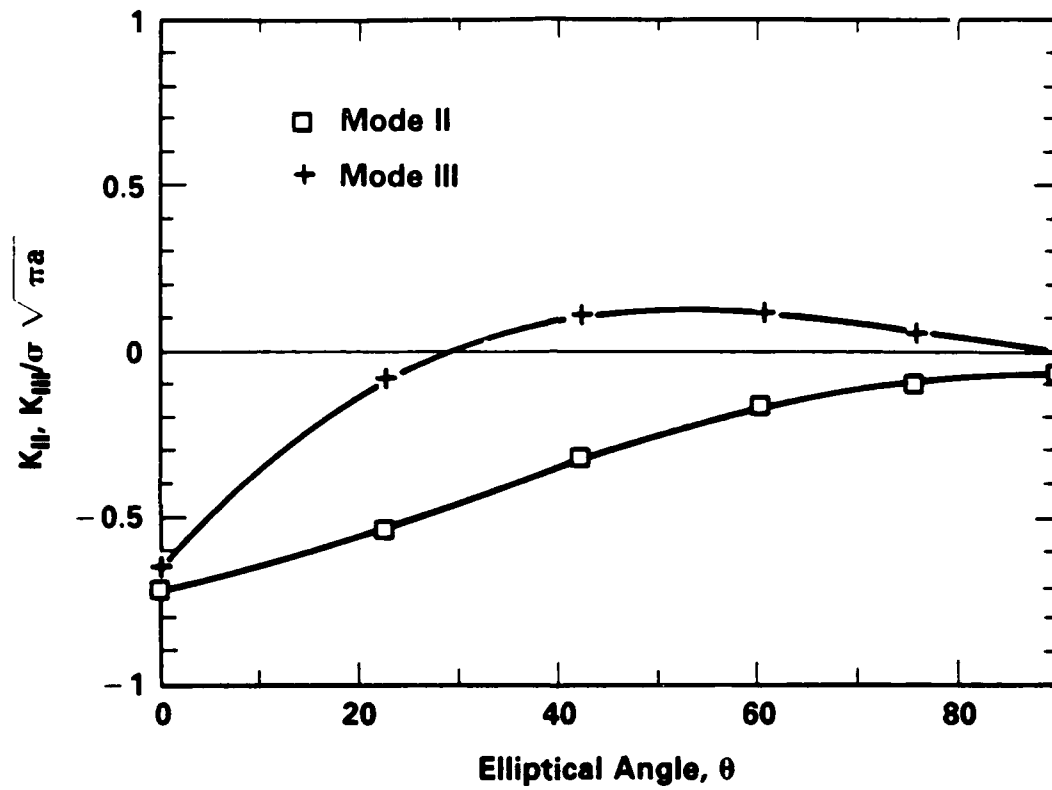
Figure 45. Mode II and Mode III Stress Intensity Factors for T-Joint Model

3.3 Elastoplastic Fracture Mechanics Modeling

As seen in the previous section, unlike the two-dimensional approach in which the use of special fundamental solution that satisfies the stress free condition at the crack surface eliminates the crack surface modeling, crack surfaces are modeled in the three-dimensional approach. In modeling the three-dimensional crack problem, the surface of the body is discretized into quadrilateral and triangular elements over which the variables are approximated by quadratic interpolation functions. The interior plastic strains are modeled using rectilinear cells over which the plastic strains are assumed constant. Due to the use of higher order interpolation functions, the surface integrals in BIE, which cannot be evaluated analytically, are evaluated numerically. The volume integrals, however, are evaluated analytically. The elastoplastic boundary element solution approach involves iterative solution of the displacement as well as the displacement gradient forms of the boundary integral equation, as described in detail in the first annual report. The boundary integral equation (BIE) corresponds to the displacement gradient is deduced from the derivative of the displacement equation, thus, the singularity of the integrands are increased. Generally, the evaluation of these hyper-singular integrals are numerically challenging for both singular and near singular cases. Especially for crack problems, one must have small domain elements for proper plastic strain modeling. The need to compute the near singular displacement gradient integrals at the centroid of the domain cells which are close to the crack surface imposes a heavy burden on the analyst. While adaptive transformation techniques are used to ease the numerical burden and improve the accuracy of these integrals to some extent, the magnitude of the problems is still substantial. Due to the constraint imposed by the need to accurately evaluate the hyper-singular integrals and to limit the overall computing size a somewhat coarse mesh was used in the current analysis.

The model investigated in the current study is that of a center, through crack of length 0.2 in. in a square plate of length 20 in, and thickness 2 in. Due to symmetry, only one quadrant of the cracked body is modeled. This model corresponds to the two-dimensional short crack case investigated in Section 2.0.

Adequate modeling of crack tip requires small elements near the crack tip region of a crack that is small compared to the overall geometry of the body. Since a single region boundary element modeling approach will affect the numerical stability of the solution adversely, the crack was modeled into two regions, an inner region around the crack as shown in Figure 46, and an outer region as shown in Figure 47. The interior plastic strains were modeled using the cells shown in Figure 48. The material properties used are the same values used for the two-dimensional case. Only the constant amplitude stress loading is considered. Loading consisted of incremental loading up to a maximum value corresponding to 20 ksi./in and subsequent unloading to zero value. Crack is simulated by imposing zero boundary condition normal to the crack plane along the plane that contains the crack except at the crack surface. Crack extension is simulated by changing the boundary condition to the appropriate new crack locations.

3.4 Numerical Results for Elastoplastic Cracks

During the first loading cycle, the crack opening displacements were monitored along the crack surface. The crack opening displacement normalized with respect to the elastic value at the center of the crack is plotted in Figure 49. The crack opening displacement at K = 5 ksi./in during the loading cycle is essentially elastic due to the finite size of the smallest domain element used for the plastic strain modeling. At the maximum load of K = 20 ksi./in, the plasticity causes the displacement to be higher than the elastic value and this is seen for all crack points. The ratio of the crack opening displacement computed during the unloading cycle is higher since only a portion of the plastic stretch is reversed during unloading. The same plot at
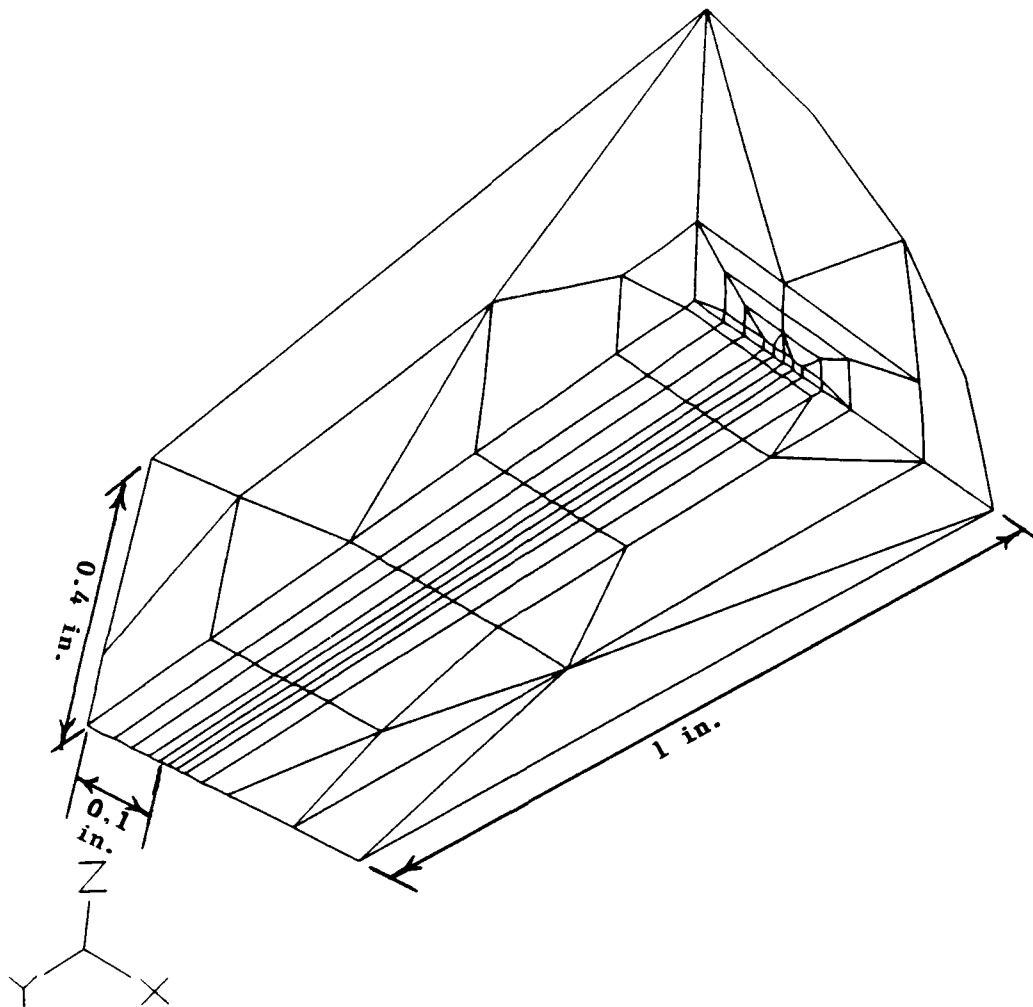
**Figure 46. Boundary Discretization of Crack Tip Region**
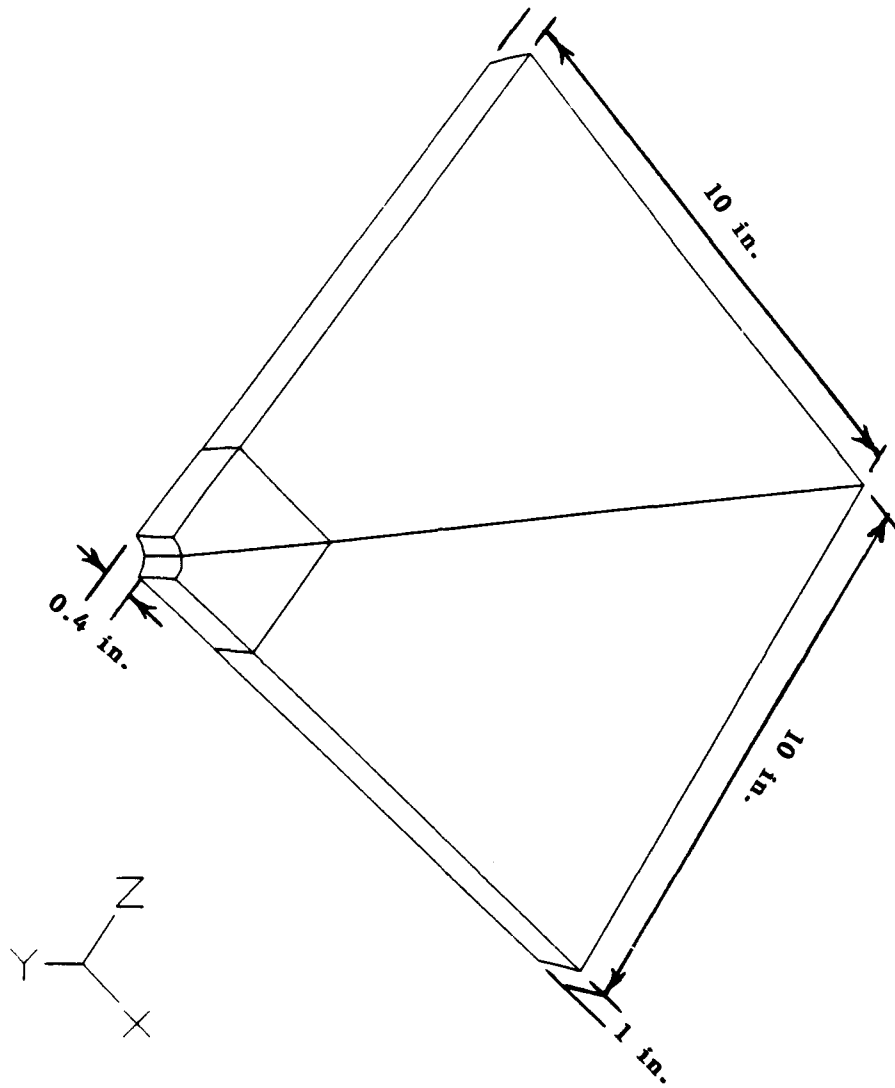
Figure 47.   Boundary Discretization of Outer Region
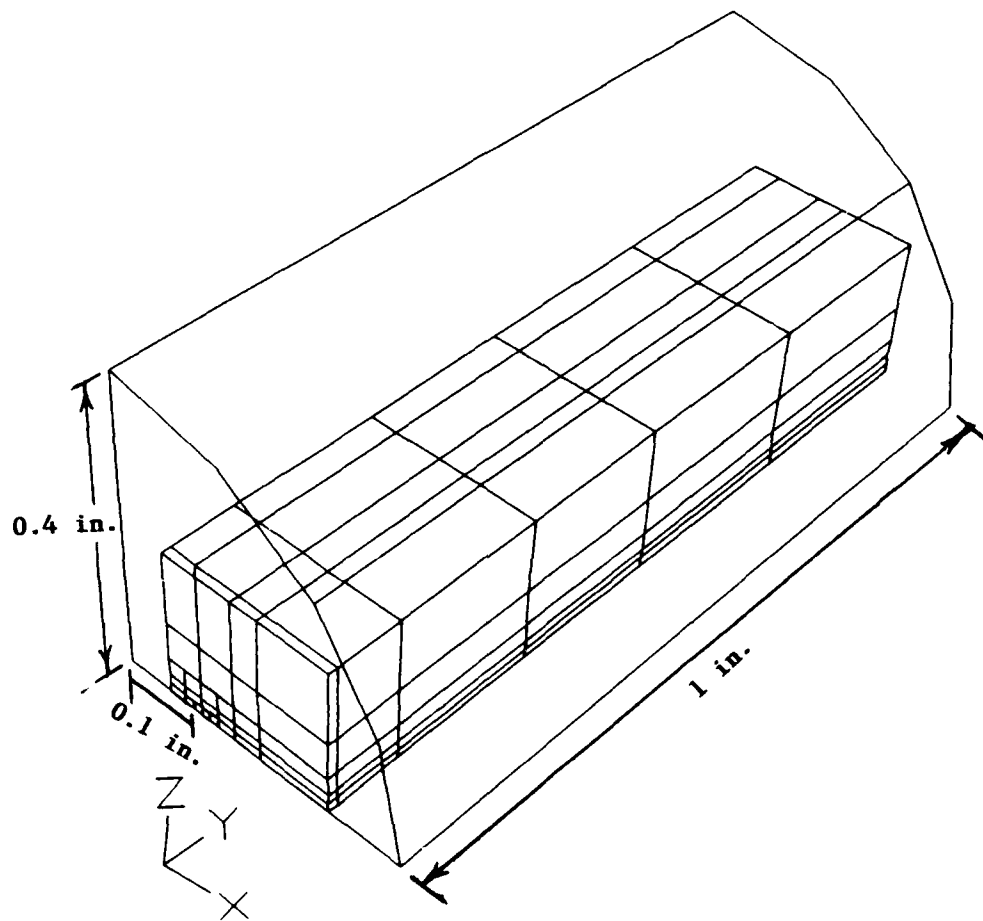
Figure 48. Domain Discretization

Crack Opening Stretch, y/a=10 (center)
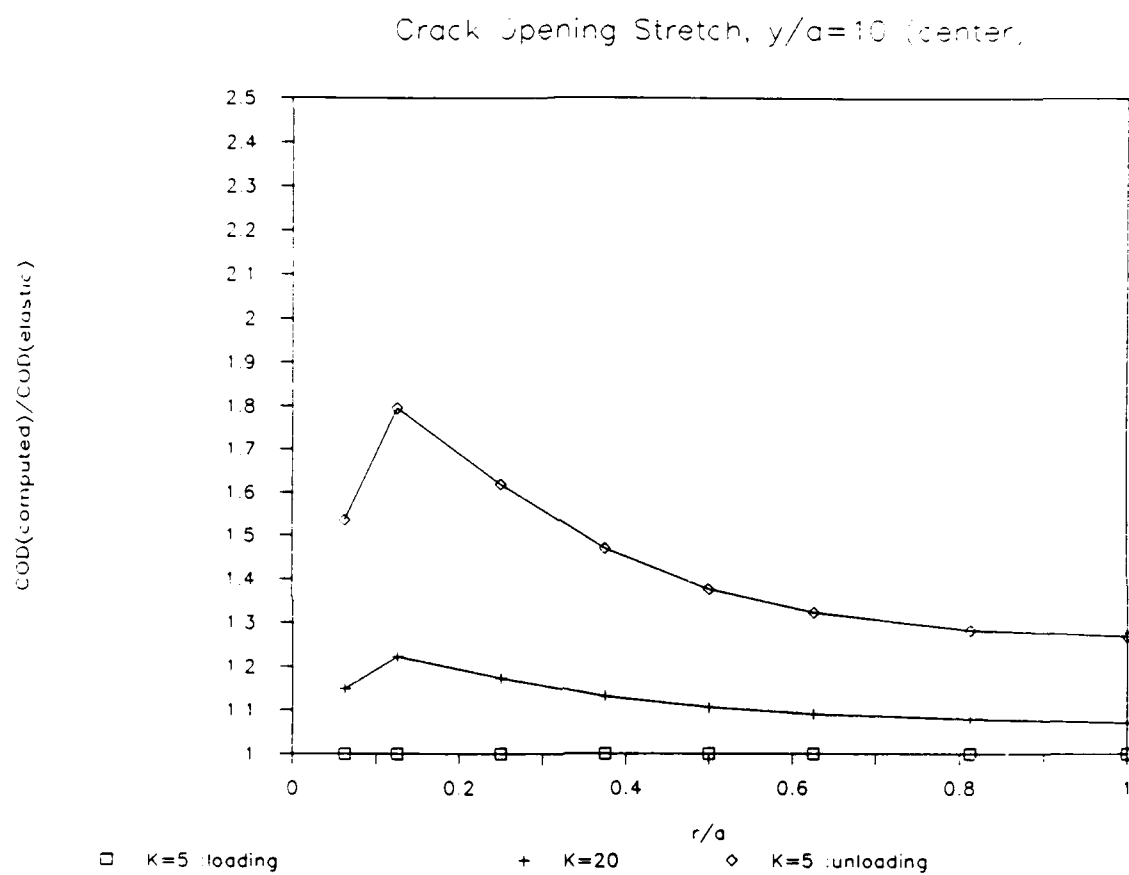
Figure 49. Normalized COD at Initial Crack Location--y/a=10

the free surface shown in Figure 50 indicates similar behavior. However, as seen in Figure 51, the crack opening displacements increase progressively from the center of the crack (y/a-10) to the free surface (y/a-0).

The crack was extended by finite amounts of 0.125a and the loading cycle was repeated at each of the new crack length. Equilibrium at the new crack length was achieved by solving an elastic problem with previous plastic strain, by a single iterative cycle. Figure 52 plots the crack opening displacement normalized to the elastic values at the center crack during the unloading cycle after extending the crack by 0.25a. The situation at the center of the crack approaches plane strain conditions, however, unlike the plane strain results reported earlier, these results indicate no closure. The same plot at the free surface, Figure 53, where the condition corresponds to plane stress situation, also indicates no closure. These results are inconsistent with the expectations. The cells yielded at the maximum and minimum loads are plotted in Figure 54. The stresses at no load during unloading is compressive, therefore, it is reasonable to expect closure.

The crack opening displacement nearest to the crack tip during the initial and final loading cycles are plotted in Figure 55 at the center of the crack. The displacements are normalized to the elastic value at the maximum load. The results show that when extended at zero load the crack barely closes even though compressive stresses are present. During the subsequent loading, the combination of reduced stiffness and small size of reversed plasticity compared to the large amount of forward plasticity seems to cause the crack to remain open at no load. Similar results are obtained for the crack tip node at the free surface (see Figure 56). Since the size of the plastic cells used in the three dimensional model case is much larger than the two-dimensional model, a comparable two-dimensional model was created to analyze the influence of mesh. However, the two-dimensional results for the plane stress and plane strain cases, shown respectively in Figure 57 and 58, indicate closure.

Crack Opening Stretch, y/a=0 (surface)
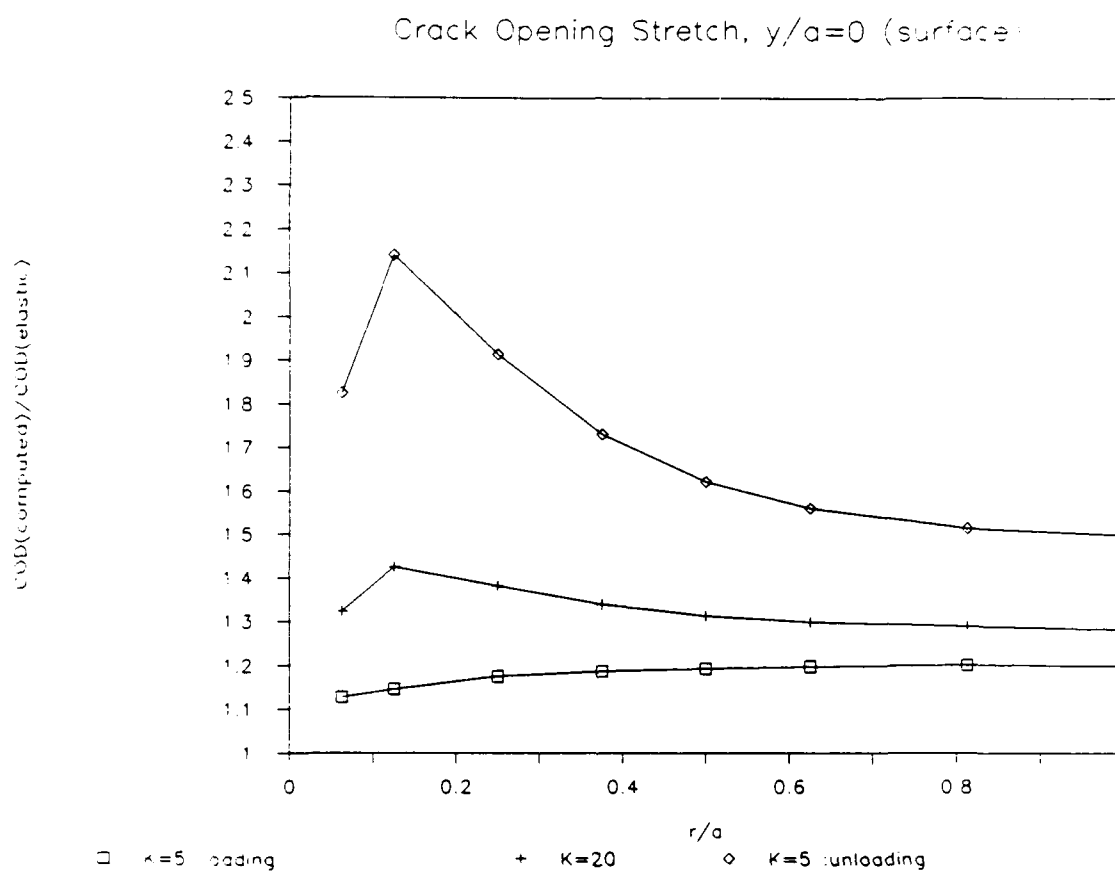
Figure 50. **Normalized COD at Initial Crack Location--y/a=0**
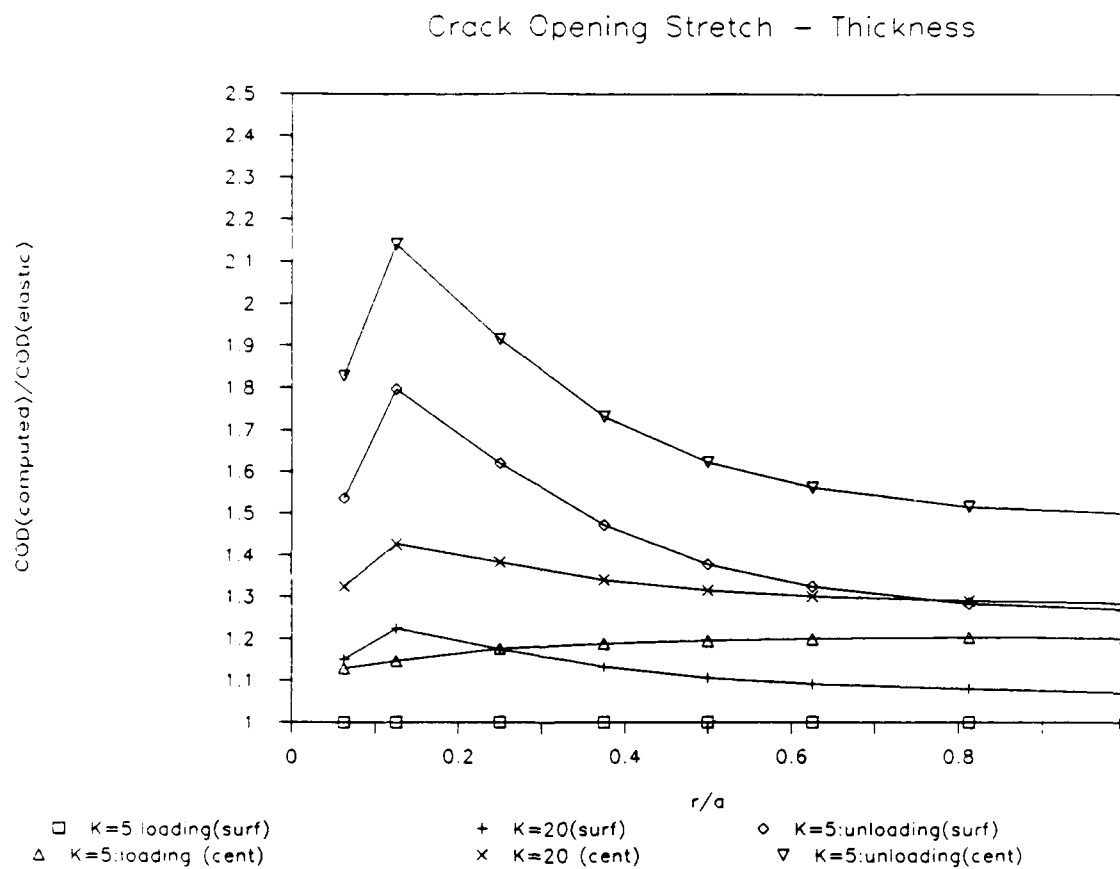
Figure 51. Variation of COD Through Thickness

Crack Opening Displacement

At mid-surface, da/a=0 25

$\square$ S/S(y)=0.71   +   S/S(y)=0.20
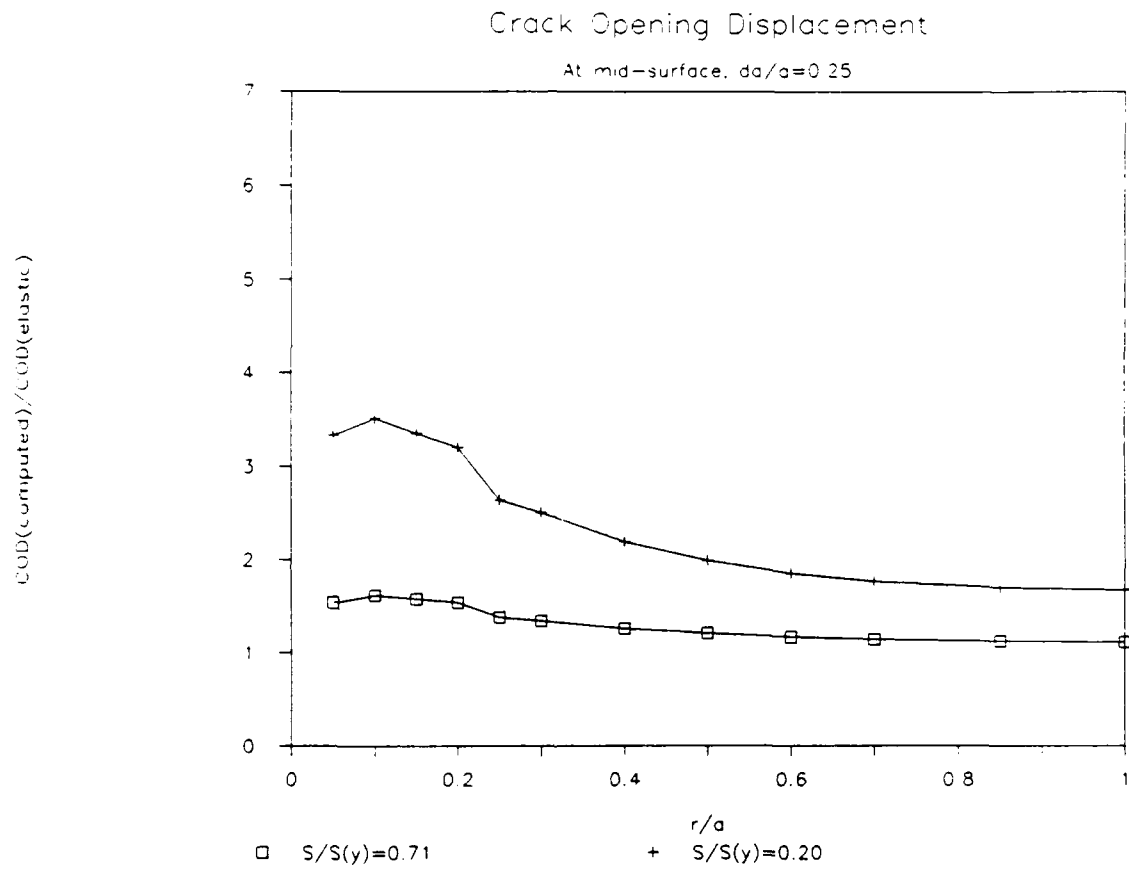
Figure 52.   Normalized COD After Crack Extension--y/a=10
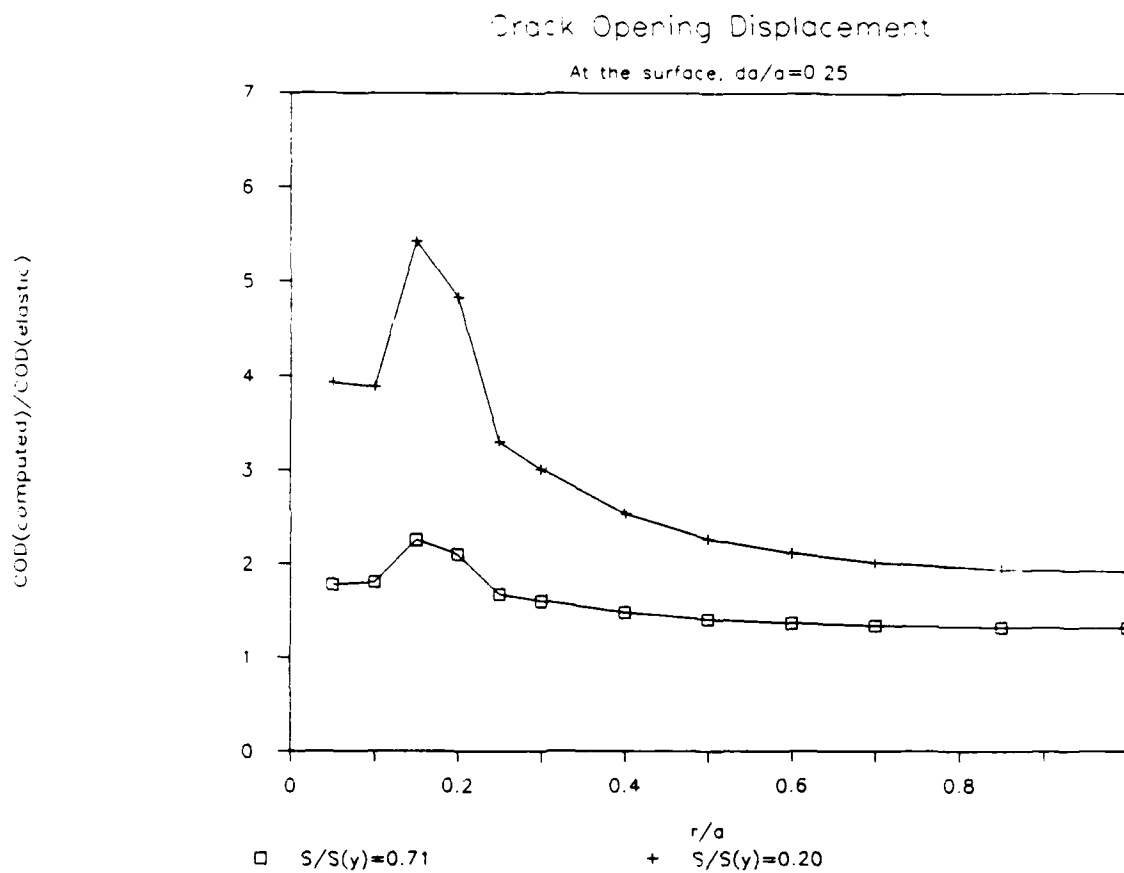
Figure 53. Normalized COD After Crack Extension--y/a=0
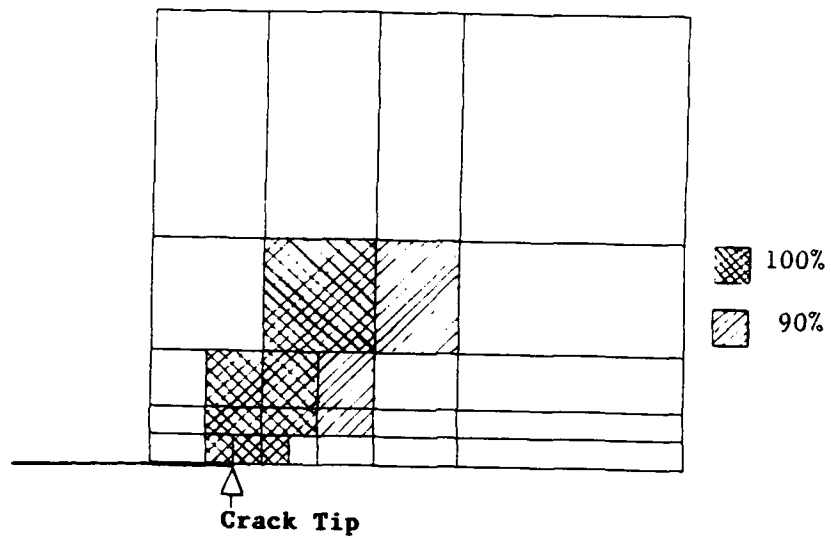
Figure 54(a). Yielded Cells at Maximum Load
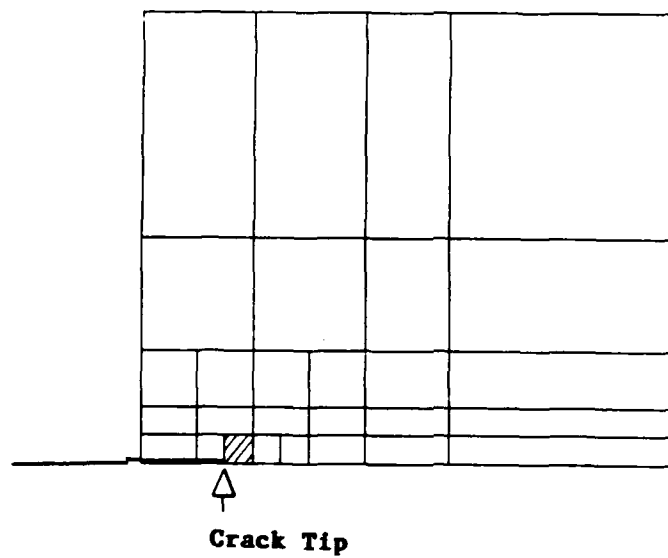
Figure 54(b). Yielded Cells at Minimum Load

CRACK OPENING DISPLACEMENT

at the center
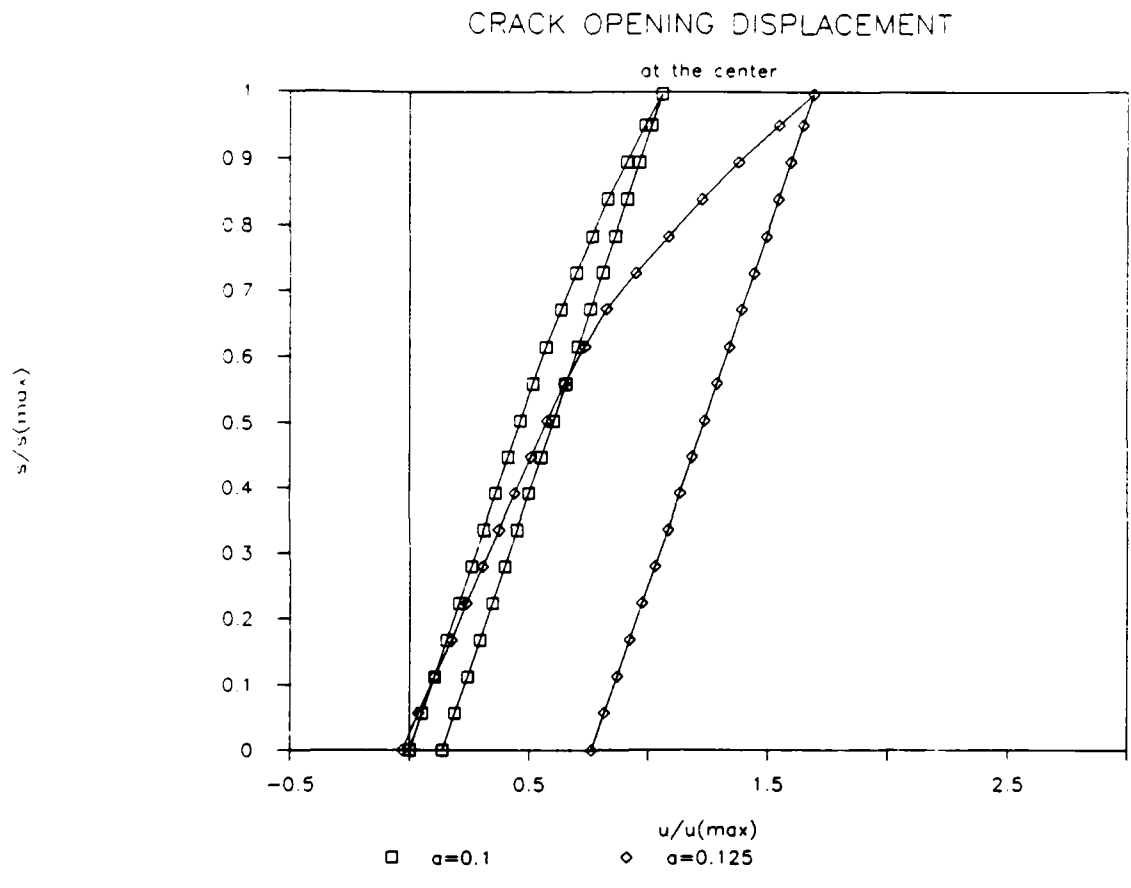
Figure 55. Load-Displacement Curve for Crack-Tip Node--y/a=10

CRACK OPENING DISPLACEMENT

at the free-surface
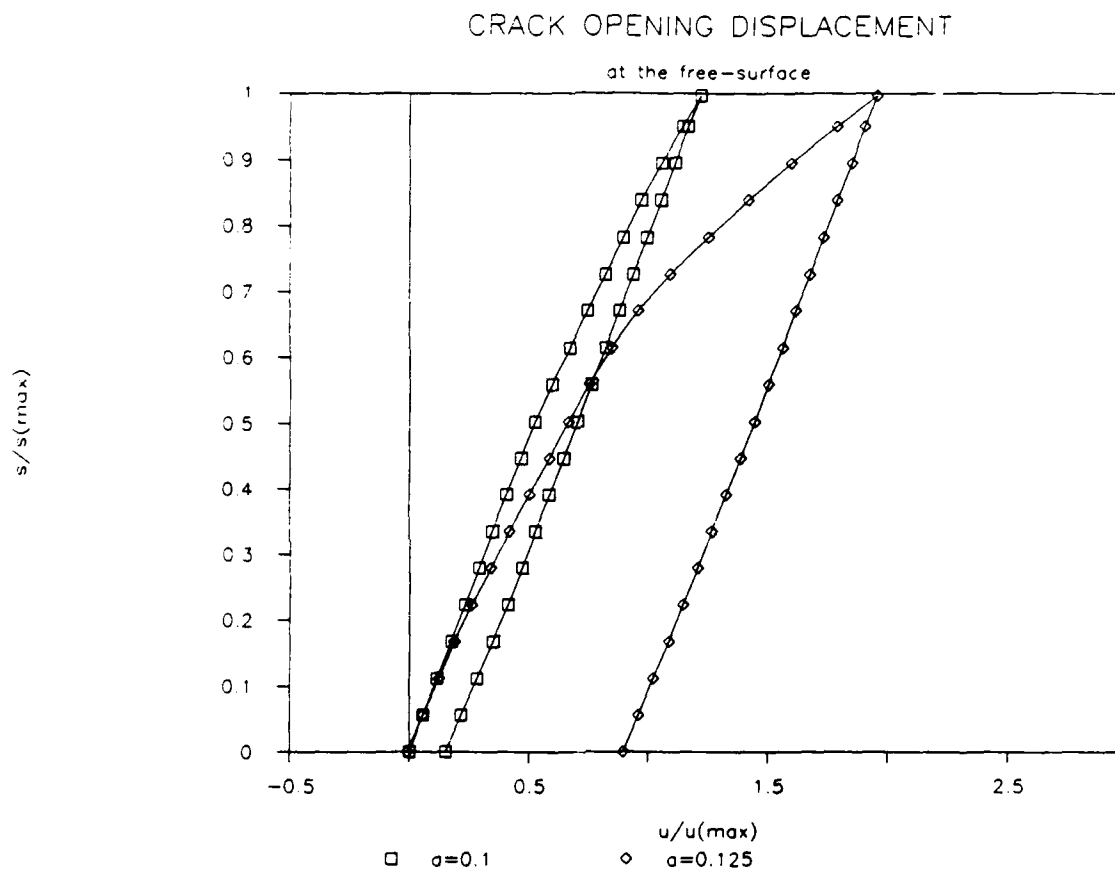
Figure 56. Load-Displacement Curve for Crack-Tip Node--y/a=0

CRACK OPENING DISPLACEMENT
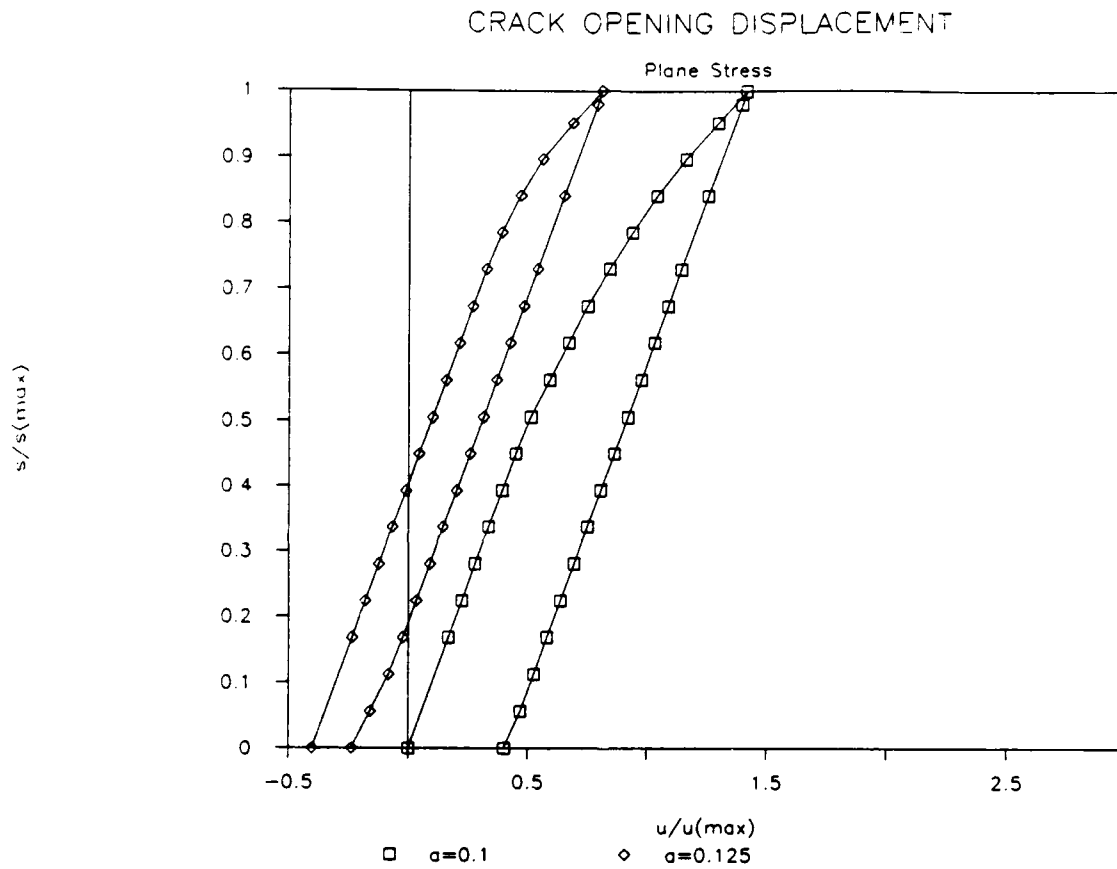
Plane Stress

Figure 57. Load-Displacement Curve for Crack-Tip Node--Plane Stress
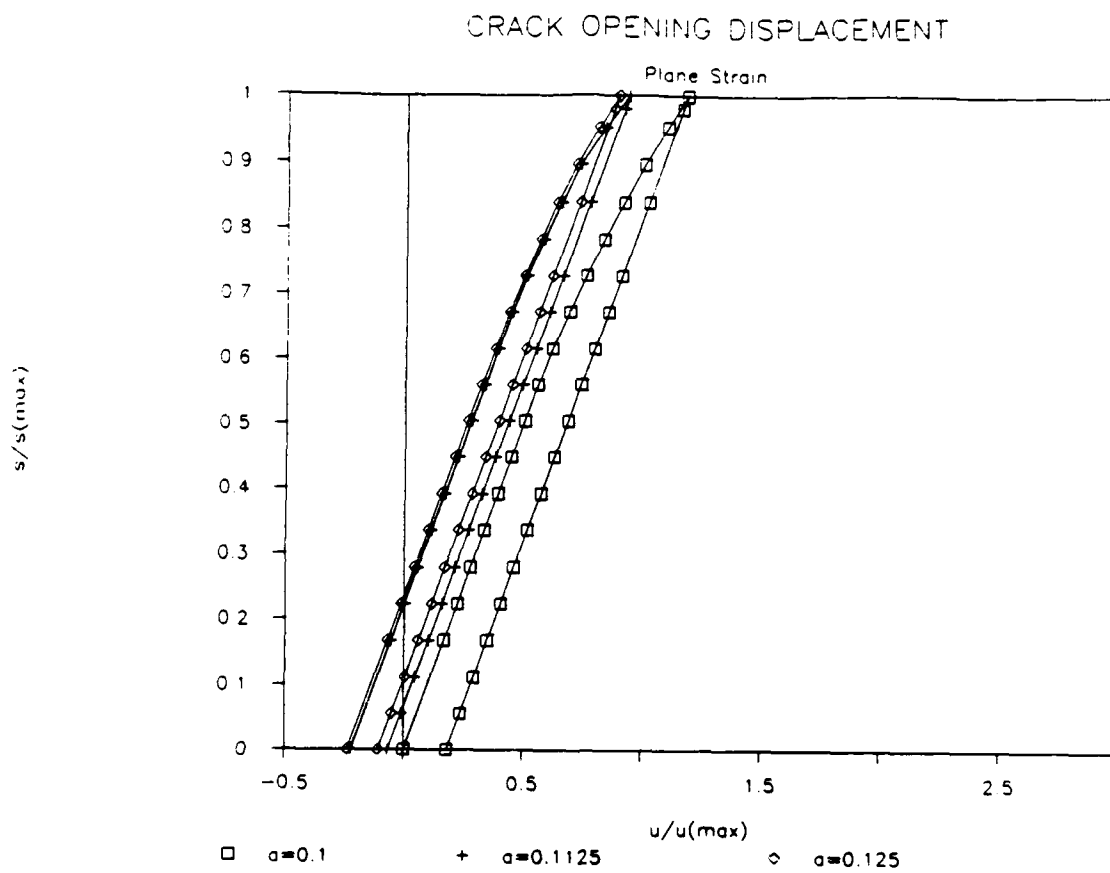
Figure 58. Load-Displacement for Crack-Tip Node--Plane Strain

In modeling the two-dimensional crack, the elastic solution to the crack problem is 'exact', and the only approximation is the domain discretization used for the plastic strain. In the three-dimensional case, however, both the elastic crack problem and the plastic strains are approximated. Further, the discretized integrals in the two-dimensional case were evaluated analytically, whereas, the three-dimensional integrals, except the volume integrals, were evaluated using approximate numerical procedures due to the use of higher order interpolation functions. While the use of higher interpolation functions for the surface modeling is known to give more accurate results, as evidenced in Section 3.2, the need to compute the burdensome near singular hyper-singular integrals accurately for displacement gradient appears to be the cause for the inconsistencies of the results. It is believed that the discrepancies between the two- and three-dimensional results are mainly a numerical problem, rather than a difference in the mechanics of the problems. Further research is required to refine the three-dimensional modeling problem to complete the analysis.

4.0 PROGRAM ACCOMPLISHMENTS AND CONCLUSIONS

The principal accomplishment of the project is the development of a boundary element method analysis to investigate the effect of plasticity on fatigue crack propagation of two- and three-dimensional cracks. The two-dimensional approach, based on the use of a special fundamental solution which explicitly accounts for the presence of stress-free crack, was developed in a previously sponsored AFOSR contract. The approach is extended for the investigation of crack tip behavior during crack propagation under cyclic loading. For the three-dimensional case, a previously developed computer program was modified to model fracture mechanics problems, this includes the use of substructuring for non-symmetric cracks and the use of special crack-tip elements. The elastoplastic analysis uses volume discretization and the volume contribution of the plastic strain is computed using an analytical solution of a rectilinear cell that contains plasticity embedded in an infinite body. The major findings of the project are as follows:

(1) The plastic zone/residual plastic zone size for stationary and propagating cracks is estimated by a new indirect method. This is, by computing the elastic stress intensity factor, due to crack extension into prior plasticity, the influence region of residual plasticity is estimated. This gives an unambiguous estimate of the plastic zone and compares favorably with the Dugdale model prediction for small plastic zones.

(2) It is established that the effect of the plastic wake on the stress intensity factor for crack opening (closure) is identical to the effect of the residual stress of crack on the retardation of the stress intensity factor. This is, crack retardation and closure are seen as identical manifestation of the same plasticity process for both stationary and propagating cracks. Further, the BIE formulation gives insight to the mathematical equivalence of these two effects.

(3) It is proposed plastic stretch rather than crack closure is the cause of increased fatigue crack damage of small cracks. The loss of constraint going from long crack to short crack which is further diminished going from plane strain to plane stress causes increase in plastic stretch and, therefore, invalidity of LEFM. Nevertheless, the amount of closure is an indication of the excess crack tip plastic damage and, thus, may serve in a secondary manner as a correlating parameter for short crack fatigue growth rate data.

(4) Three-dimensional elastoplastic problem imposes high requirement on finding efficient means for the accurate evaluation of integrals and also the size of the problem makes it computationally burdensome for any numerical solution procedure.

(5) The results establish BEM as a very attractive solution tool for the elastic and elastoplastic fracture mechanics analysis, especially for the two-dimensional case. Since only the plastic strain around the crack tip, rather than the entire field, as is the case in finite element method, is approximated in the boundary element method, the results are, generally, more accurate. Even though the domain modeling required for the elastoplastic solution may appear to make the method inefficient, the fact is that only the yielded region around the crack needs domain modeling and, therefore, compared to the overall problem the domain modeling is not substantial.

(6) Finally, the research results have been presented in a variety of technical symposia and will result in archival articles. The list of articles and presentations resulted form the research is as follows:

1. "A Comparison of Long and Short Crack Elastoplastic Response Using the Boundary Element Method," T.A. Cruse and S.T. Raveendra, _Engineering Fracture Mechanics_, to be published.

2.   "BEM Analysis of Problems of Fracture Mechanics," S.T. Raveendra and T.A. Cruse, (Editors P.K. Banerjee and R.B. Wilson) Developments in Boundary Element Methods -5, to be published.

3.   "Application of the Boundary Element Method to Inelastic Fracture Mechanics," T.A. Cruse and S.T. Raveendra, (Proceedings of the International Conference on Computational Engineering Science, Atlanta, Georgia, April 10-14, 1988).

4.   "Some Elastoplastic Fracture Mechanics Results Using Boundary Integral Equations," presented at First World Congress on Computational Mechanics, University of Texas at Austin, September 22-26, 1986.

5.   "Boundary Element Fracture Mechanics Modeling," presented at the Fourth International Conference on Numerial Methods in Fracture Mechanics, San Antonio, Texas, March 23-27, 1987.

6.   "Application of the Boundary Element Method to Nonlinear Stress Analysis," presented at ASCE Engineering Mechanics Division Specialty Conference, State University of New York at Buffalo, New York, May 20-22, 1987.

7.   "Boundary Element Fracture Mechanics Modelling," presented at the IUTAM Symposium on Advanced Boundary Element Methods: Applications in Solid and Fluid Mechanics, San Antonio, TX, April 13-16, 1987.

5.0 REFERENCES

[1] Elber, W., "Fatigue Crack Closure Under Cyclic Tension," _Engineering Fracture Mechanics_, Vol. 2, No. 1, July 1970. pp. 37-45.

[2] Elber, W., "The Significance of Fatigue Crack Closure," _Damage Tolerance in Aircraft Structures_, ASTM STP 486, American Society for Testing and Materials, 1971, pp. 230-242.

[3] Chermahini, R.G., "Three-Dimensional Elastic-Plastic Finite Element Analysis of Fatigue Crack Growth and Closure," Ph.D. Thesis, Old Dominion University, 1986.

[4] Leis, B.N., Hopper, A.T., Ahmad J., Broek, D., and Kanninen, M.F., "Critical Review of the Fatigue Growth of Short Cracks," _Engineering Fracture Mechanics_, Vol. 23, _5_, pp. 883-893, 1986.

[5] Hudak, S.J., Jr., "Small Crack Behavior and the Prediction of Fatigue Life," _Transactions of the ASME_, Vol. 103, 1981.

[6] Kanninen, M.F., and Popelar, C.H., "Advanced Fracture Mechanics," Oxford Science Series 15, Oxford University Press, New York, 1985.

[7] Newman, J.C., Jr., "A Nonlinear Fracture Mechanics Approach to the Growth of Small Cracks," Presented at the AGARD Specialists Meeting on Behavior of Short Cracks in Airframe Components, September 20-21, 1982, Toronto, Canada.

[8] Gray, T.D., and Gallagher, J.P., "Predicting Fatigue Crack Retardation Following a Single Overload Using a Modified Wheeler Model," _Mechanics of Crack Growth_, ASTM STP 590, American Society for Testing and Materials, pp. 331-344, 1976.

[9] Budianski, B., and Hutchinson, J.W. "Analysis of Closure in Fatigue Crack Growth," _Journal of Applied Mechanics_, Vol. 45, pp. 267-276, 1978.

[10] Dill, H.D., and Saff, C.R., "Spectrum Crack Growth Prediction Method Based on Crack Surface Displacement and Contact Analyses," _Fatigue Crack Growth Under Spectrum Loads_, ASTM STP 595, American Society for Testing and Materials, pp. 306-319, 1976.

[11] Lankford, J., and Davidson, D.L., "Near-Threshold Crack Tip Strain and Crack Opening for Large and Small Fatigue Cracks," _Proceedings of the International Symposium of Fatigue Crack Growth Threshold Concepts_, October 3-5, 1983, Philadelphia, Pennsylvania, pp. 447-463.

[12] Cruse, T.A., "Two-Dimensional BIE Fracture Mechanics Analysis," _Applied Mathematical Modelling_, Vol. 2, pp. 287-293, 1978.

[13] Cruse, T.A., and Polch, E.Z., "Ealstoplastic BIE Analysis of Cracked Plates and Related Problems, Part 1: Formulation," _International Journal for Numerical Methods in Engineering_, Vol. 23, pp. 429-437, 1986.

[14] Cruse, T.A., and Polch, E.Z., "Elastoplastic BIE Analysis of Cracked Plates and Related Problems, Part 2: Numerical Results," _International Journal for Numerical Methods in Engineering_, Vol. 23, pp. 439-452, 1986.

[15] Cruse, T.A., and Polch, E.Z., "Application an Elastoplastic Boundary Element Method to Some Fracture Mechanics Problems," _Engineering Fracture Mechanics_, Vol. 23, _6_, 1085-1096, 1986.

[16] Swedlow, J.L., and Cruse, T.A., "Formulation of Boundary Integral Equations for Three-Dimensional Elastoplastic Flow," *International Journal of Solids and Structures*, 7, pp. 1637-1684, 1972.

[17] Paris, P.C., Gomez, M.P., Anderson, W.E., "A Rational Analytical Theory of Fatigue," *The Trend in Engineering*, Vol. 13, University of Washington, pp. 9-14, January 1961.

[18] Paris, P.C., "The Fracture Mechanics Approach to Fatigue," *Fatigue - An Interdisciplinary Approach*, Tenth Sagamore Army Materials Research Conference, Aug. 1963, Syracuse University Press, pp. 107-132, 1964.

[19] Boettner, R.C., Laird, C., and McEvily, A.J., Jr., "Crack Nucleation and Growth in High Strain-Low Cycle Fatigue," *Trans. Met. Soc. AIME*, Vol. 233, Feb. 1965, pp. 279-387.

[20] McEvily, A.J., "Fatigue Crack Growth and the Strain Intensity Factor," Air Force Conf. on Fatigue and Fracture of Aircraft Structrues and Materials, Miami Beach, AFFDL-TR-70-144, pp. 451-458, Dec. 1969.

[21] Tomkins, B., "Fatigue Crack Propagation--An Analysis," *Philosophical Magazine*, Eighth Series, Vol. 18, 155, pp. 1041-1066, 1968.

[22] Tomkins, B., "Fatigue Failure in High Strength Metals," *Philosophical Magazine*, Eighth Series, Vol. 23, 183, pp. 687-703, 1971.

[23] Donahue, R.J., Clark, H. McI., Atanmo, P., Kumble, R., and McEvily, A.J., "Crack Opening Displacement and the Rate of Fatigue Crack Growth," *Int. J. Fracture Mechanics*, Vol. 8, 2, pp. 209-219, 1972.

[24] Lardner, R.W., "A Dislocation Model for Fatigue Crack Growth in Metals," *Philosophical Magazine*, Eight Series, Vol. 17, 145, pp. 71-82, 1968.

[25] Gowda, C.V.B., and Topper, THE, "Crack Propagation in Notched Mild Steel Plates Subjected to Cyclic Inelastic Strains," *Cyclic Stress-Strain Behavior--Analysis, Experimentation, and Failure Prediction*, ASTM STP 519, American Society for Testing and Materials, pp. 170-184, 1973.

[26] Neuber, J., "A Physically Nonlinear Notch and Crack Model," *J. Mech. Phys.Solids*, Vol. 16, pp. 289-294, 1968.

[27] Bhanderi, S., Charif D'Ouazzane, S., and Faidy, C., "Establishment of Governing Parameters for Fatigue Crack Growth Analysis in Areas of High Nominal Strain," ASME Paper 84-PVP-20, 1984.

[28] Dowling, N.E., "Crack Growth During Low-Cycl Fatigue of Smooth Axial Specimens," *Cyclic Stress-Strain and Plastic Deformation Aspects of Fatigue Crack Growth*, ASTM STP 637, American Society for Testing and Materials, pp. 97-121, 1977.

[29] Shih, C.F., and Hutchinson, J.W., "Fully Plastic Solutions and Large Scale Yielding Estimates for Plane Stress Crack Problems," *J .Eng. Materials and Technology*, Trans. ASME, Vol. 98, 4, pp. 289-295, 1976.

[30] McClung, R.C., "Fatigue Crack Closure and Crack Growth Outside the Small Scale Yielding Regime," Report No. 139, UILU-ENG 87-3605, College of Engineering, University of Illinois at Urbana-Champaign, 1987.

[31] Iyyer, N.S., and Dowling, N.E., "Opening and Closing of Cracks at High Cyclic Strains," *Small Fatigue Cracks*, Engineering Foundation Int. Conf., Met. Society of AIME, pp. 213-223, 1986.

[32] Iyyer, N.S., and Dowling, N.E., "Closure of Fatigue Cracks at High Strains," NASA CR-175021, Dec. 1985.

[33] Ogura, K., Miyoshi, Y., and Nishikawa, I., "Fatigue Crack Growth and Closure of Small Cracks at the Notch Root," Current Research on Fatigue Cracks, MRS Vol. 1, Society of Materials Science, Japan, pp. 57-78, 1985.

[34] Banerjee, P.K. and Butterfield, R., Boundary Element Methods in Engineering Science, McGraw-Hill Ltd., London, 1981.

[35] Banerjee, P.K. and Raveendra, S.T., "Advanced Boundary Element Analysis of Two- and Three-Dimensional Problems of Elastoplasticity," International Journal for Numerical Methods in Engineering, 23, pp. 985-1002, 1986.

[36] Barsoum, R.S., "On the Use of Isoparametric Finite Elements in Linear Fracture Mechanics, International Journal for Numerical Methods in Engineering, 10, pp. 25-37, 1976.

[37] Blandford, G.E., Ingraffea, A.R., and Liggett, J.A., "Two-Dimensional Stress Intensity Factor Computations Using the Boundary Element Method," International Journal for Numerical Methods in Engineering, 17, pp. 387-404, 1981.

[38] Bui, H.D., "An Integral Equation Method for Solving the Problem of a Plane Crack of Arbitrary Shape," Journal of the Mechanics and Physics of Solids, 25, pp. 29-37, 1977.

[39] Cherepanov, G.P., Mechanics of Brittle Fracture, McGraw-Hill, New York, 1979.

[40] Cruse, T.A. and VanBuren, W., Three Dimensional Elastic Stress Analysis of a Fracture Specimen with an Edge Crack," International Journal of Fracture Mechanics, 7, pp. 1-15, 1971.

[41] Cruse, T.A., "Numerical Evaluation of Elastic Stress Intensity Factors by the Boundary-Integral Equation Method," in The Surface Crack: Physical Problems and Computational Solutions," ASME, pp. 153-170, 1972.

[42] Cruse, T.A., "Boundary-Integral Equation Method for Three-Dimensional Elastic Fracture Mechanics Analysis," AFOSR-TR-75-0813, 1975.

[43] Cruse, T.A., and Wilson, R.B., "Boundary-Integral Equation Method for Elastic Fracture Mechanics Analysis," AFOSR-TR-0355, 1977.

[44] Cruse, T.A. and Meyers, G.J., "Three-Dimensional Fracture Mechanics Analysis," Journal of the Structural Division, 103, ASCE, pp. 309-320, 1977.

[45] Guidera, T.J., and Lardner, R.W., Penny-shaped Cracks, Journal of Elasticity, 5, pp. 59-73, 1975.

[46] Lachat, J.C., and Watson, J.O., "Effective Numerical Treatment of Boundary Integral Equations," International Journal for Numerical Methods in Engineering, 10, pp. 991-1005, 1976.

[47] Newman, J.C., and Raju, I.S., "An Empirical Stress-Intensity Factor Equation for the Surface Crack," Engineering Fracture Mechanics, 15, pp. 185-192, 1981.

[48] Polch, E.Z., Cruse, T.A., and Huang, C.-J., "Traction BIE Solutions for Flat Cracks," Computational Mechanics (to be published).

[49] Weaver, J., "Three-Dimensional Crack Analysis," _International Journal for Solids and Structures_, 13, pp. 321-330, 1977.